https://doi.org/10.59761/RCR5095

Triarylphosphonium compounds as effective vectors for mitochondria-targeted delivery systems: decoration strategies and prospects for clinical application

Tatiana N. Pashirova,[a] Andrey V. Nemtarev,[a] Eliana B. Souto,[b,c] Vladimir F. Mironov[a]

[a] *Arbuzov Institute of Organic and Physical Chemistry, Federal Research Center, Kazan Scientific Center, Russian Academy of Sciences, ul. Arbuzova 8, 420088 Kazan, Russian Federation*
[b] *UCIBIO — Applied Molecular Biosciences Unit, MEDTECH, Laboratory of Pharmaceutical Technology, Department of Drug Sciences, Faculty of Pharmacy, University of Porto, 4050-313 Porto, Portugal*
[c] *Associate Laboratory i4HB — Institute for Health and Bioeconomy, Faculty of Pharmacy, University of Porto, 4050-313 Porto, Portugal*

Mitochondrial dysfunctions lead to the emergence and development of a large number of diseases. The present review gives the first systematic survey of various aspects of studies of mitochondria-targeted nanosystems that contain triphenylphosphonium vector groups providing targeted delivery of drug substances to these organelles. Approaches to the design of components and various nanoparticles bearing these groups are summarized and analyzed. The relationship between the key parameters of triphenylphosphonium nanoparticles (chemical composition, size, shape, ζ-potential, drug loading, drug encapsulation efficiency, *etc*.) and the biological action is discussed; in some cases, the mechanism of mitochondria targeting is given. The design principles and preparation methods for mitochondria-targeted triphenylphosphonium delivery nanosystems are of interest to researchers in the field of nanomaterials, nanotechnology, molecular biology, biotechnology and pharmaceutical chemistry.

The bibliography includes 243 references.

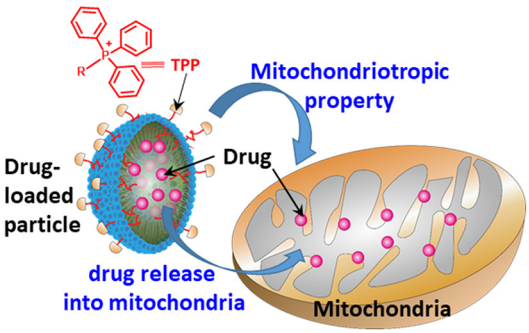

Keywords: mitochondria-targeted nanoparticles; functionalization of nanoparticles; triphenylphosphonium; triphenylphosphonium nanoparticles; mitochondrial dysfunction.

Contents

1. Introduction 2
2. Synthetic strategies towards triphenylphosphonium derivatives as vectors for mitochondria-targeted delivery systems 3
3. Liposomes decorated with triphenylphosphonium derivatives 4
3.1. Alkyltriphenylphosphonium salts. Targeted drug delivery 4
3.2. Conjugates of triphenylphosphonium with phospholipids 5
3.3. Triphenylphosphonio-containing cholesterol 6
3.4. Conjugates of triphenylphosphonium with poly(ethylene glycol) 9
3.5. Prodrugs containing a triphenylphosphonium group 11
4. Solid lipid nanoparticles and nanoemulsions decorated with triphenylphosphonium 13
5. Mitochondriotropic dendritic and polymer nanoparticles 14
5.1. Synthetic polymer systems modified with triphenylphosphonium 15
5.1.1. Mitochondria-targeted dendritic systems 15
5.1.2. Poly(ε-caprolactone) nanoparticles 18
5.1.3. Polyanhydride-based nanoparticles 19
5.2. Natural polymers (biopolymers) modified with triphenylphosphonium 19
5.2.1. Polydopamine-based nanoparticles 19
5.2.2. Nanoparticles based on the copolymer of lactic and glycolic acids 20
5.2.3. Chitosan-based polymer systems 21
5.2.4. Hyaluronic acid-based nanoparticles 23
5.3. Polymer micelles with triphenylphosphonium 23
6. Self-assembled amphiphilic triphenylphosphonium ligands 24
6.1. Amphiphilic polymer triphenylphosphonium conjugates 26
6.2. Functionalized triphenylphosphonium micelles based on prodrugs 31
7. Functionalized triphenylphosphonium inorganic nanosystems 34
7.1. Mesoporous silica nanoparticles 34
7.2. Metal nanoparticles 36

Received 7 July 2023

7.3. Carbon nanomaterials 37
7.4. Quantum dots 38
8. Other types of functionalized triphenylphosphonium nanoparticles and strategies for their use 38
9. Synergistic nanosystems for photodynamic and photothermal therapy 42
10. Conclusion 45
11. List of abbreviations and symbols 46
12. References 50

1. Introduction

Mitochondria are important organelles of eukaryotic cells. Being energy stations of the cell, they perform oxidative phosphorylation with subsequent accumulation of energy as adenosine triphosphate (ATP)[1] and enzymatic oxidation of various substances. Mitochondria are also involved in many other important metabolic processes in the cell, in particular, in the pyruvate conversion to acetyl-CoA catalyzed by the pyruvate dehydrogenase complex, degradation of fatty acids *via* β-oxidation, urea cycle,[2,3] calcium accumulation,[4,5] the synthesis of steroid hormone precursors[6–9] and biosynthesis of pyrimidine nucleotides.[10,11] In addition, mitochondria play a key role in the initiation and regulation of apoptosis (programmed cell death)[12–15] and ferroptosis.[16] Mitochondria form an integrated network that is important for maintaining cellular homeostasis.[17,18] In view of the interrelated functions of mitochondria, any mitochondrial dysfunction can disrupt the homeostasis,[19] which eventually creates conditions for various diseases, including neurological[20–24] and cardiovascular pathologies,[25–29] metabolism disorders,[30,31] diabetes mellitus,[32–37] cancer[38–47] and others.

Despite the modern achievements in the development of drugs for targeted therapy and immunotherapy, the use of chemical compounds is still the major approach to the clinical therapy of malignant neoplasms, including severe types of cancer such as triple-negative breast cancer[48,49] and pancreatic cancer.[50] Due to the lack of specificity of traditional anticancer drugs, the side effects of chemotherapy are often grave.

Nanotechnological approaches based on methods and techniques of colloidal chemistry and nanochemistry help to overcome a number of major limitations of chemotherapy as well as photodynamic and photothermal therapy. The effect is attained by targeting a drug to damaged (transformed) cells, controlled drug release into specific subcellular organelles or long-term action in the bloodstream.[51–57] Considering the critical role of mitochondria in the support of vital functions of cells, the development of mitochondria-targeted dosage forms is an important scientific challenge brought about by the needs of clinical medicine. A way to address this task is to use compounds containing a triarylphosphonium cation, most often, triphenylphosphonium cation (TPP),[a] which easily penetrate biological membranes.[58]

It is known that mitochondria of cancer cells have a higher membrane potential than normal cell mitochondria,[59] and high hydrophobicity and delocalized positive charge of the lipophilic triphenylphosphonium cation promote its penetration through the mitochondrial membrane and accumulation in the mitochondrial matrix. The covalent conjugation of an antitumor drug with triphenylphosphonium cations not only increases its activity, but also improves the targeted delivery to mitochondria of tumor cells, which has been demonstrated for quite a few drugs.[60–67] The efficiency of this approach gave rise to mitochondrial medicine as a new area of biomedical research.[68–70]

Compounds used for targeted delivery to mitochondria are called mitochondriotropic agents, or mitochondriotropics. Usually these are amphiphilic molecules with delocalized charge of the cationic moiety. Relatively high lipophilicity in combination with positive charge delocalization decrease the change in their Gibbs energy on moving from an aqueous solution to a hydrophobic medium. Presumably, this decrease is a prerequisite for the accumulation of these compounds in mitochondria, owing to the presence of mitochondrial membrane potential.[71] Currently, more than a hundred mitochondriotropics are known; data on these compounds have been analyzed using physicochemical classification and various theoretical models to predict their behaviour.[72] Some mitochondriotropics such as mitoquinone mesylate (MitoQ) have successfully passed clinical trials.[73,74] It was shown that taking MitoQ (20 mg per day for 6 weeks or a single dose of 80 mg) is safe and is well tolerated by middle-aged or elder adults; it improves vascular endothelial function, reduces aortic stiffness and lowers blood levels of low-density lipoproteins and oxidative stress markers.

However, often the conjugation of a TPP group with a pharmaceutical agent may alter the therapeutic properties of the agent. In addition, this strategy is inapplicable for the delivery of large biomolecules as their covalent conjugation with the TPP cation is sometimes problematic due to their polyfunctional

[a] Here TPP stands for any moiety containing a triphenylphosphonium cation.

T.N.Pashirova. PhD in Chemistry, Senior Researcher at the Laboratory of Phosphorus-Containing Analogues of Natural Compounds, IOPC.
E-mail: tatyana_pashirova@mail.ru
Current research interests: supramolecular chemistry, colloid chemistry, medicinal chemistry, targeted drug delivery systems, solid lipid nanoparticles, liposomes, nanoreactors, surfactants, micellar catalysis.
A.V.Nemtarev. PhD in Chemistry, Senior Researcher at the same Laboratory.
E-mail: a.nemtarev@mail.ru
Current research interests: chemistry of organophosphorus compounds, chemistry of natural and physiologically active compounds, medicinal chemistry.
E.B.Souto. Habilitation Professor, Faculty of Pharmacy, University of Porto. E-mail: ebsouto@ff.up.pt
Current research interests: nanomedicine, drug delivery, drug targeting, active pharmaceutical ingredients, volatile compounds, encapsulation.
V.F.Mironov. Corresponding member of RAS, Doctor of Chemical Sciences, Professor, Head of the Laboratory of Phosphorus-Containing Analogues of Natural Compounds, IOPC.
E-mail: mironov@iopc.ru
Current research interests: chemistry of organophosphorus compounds, chemistry of natural and physiologically active compounds, medicinal chemistry.

Translation: Z.P.Svitanko

nature. Therefore, in recent years, to attain high efficacy of the existing and prospective mitochondrial therapeutic agents, considerable attention has been paid to the development of nanoparticles, which are called colloidal vectors. Colloidal vectors represent a type of delivery nanosystems capable of performing the following functions:

(1) selective transport of biologically active molecules to mitochondria;[75]

(2) overcoming a few biological barriers;

(3) protecting biologically active agents from premature deactivation.

Modification of the nanoparticle surface with various mitochondriotropic ligands endows them with the above properties.[76] Nanoparticles targeting particular organelles are promising second-generation drug delivery systems.[55,77] Nanotechnology-based approaches in combination with the mitochondria-targeting strategies can substantially improve the clinical results and efficacy of mitochondrial medicine. Mitochondrial drug delivery systems meant for therapeutic applications can be designed using lipids (*e.g.*, liposomes, micelles, solid lipid particles, nanoemulsions), natural and synthetic polymer conjugates, dendritic carbon nanosystems or inorganic and hybrid templates.

Quite a few recent reviews (*e.g.*, Refs 78–82) are devoted to the development of strategies for rational design of nanocarriers for mitochondria-targeted therapeutic agents. A trend of nanomedicine research is surface functionalization of drug delivery nanosystems.[70] For example, the most readily available and often used conjugation of an active drug substance with polyethylene glycol (PEG), called PEGylation, is a routine procedure meant for decreasing the immunogenicity of a drug system and reducing the immune recognition and clearance. The surface of nanocarriers is functionalized, most often, by installing ligands such as peptides, antibodies and compounds that interact with receptors in order to improve the delivery of a drug to target tissues. In addition, functionalization serves to enhance internalization (*i.e.*, trapping *via* adsorption or adhesion followed by uptake) of nanocarriers by the target cells, which increases the accuracy and efficacy.[83] Nanoparticles can be accumulated in the damaged tissues and tumors, owing to the enhanced vascular permeability. The accumulation of nanoparticles is also increased because of poor lymphatic drainage and the enhanced permeability and retention (EPR) effect.[84] Many of these systems have already been recommended for clinical trials.[70]

Generally, the use of nanoforms of pharmaceuticals is currently at an early stage of development. To attain their clinical efficacy, it is necessary to solve a number of fundamental issues concerning not only the detailed procedure for their preparation and modification, but also the mechanisms of cellular and subcellular targeting.[85] Among all available mitochondriotropics, the TPP group is used most often as the vector ligand on the surface of nanocarriers. A review of Zielonka *et al.*[86] covers not only relevant original papers, but also a number of patents demonstrating various applications of mitochondria-targeted TPP agents. However, there are still no reviews considering the problems of design of delivery systems involving triarylphosphonium cations (in particular, TPP derivatives).

The purpose of the present review is to systematize and integrate published data on the preparation and modification methods for various nanoparticles intended for targeted delivery of drug substances (DS) functionalized with vector TPP groups to mitochondria. The primary attention is focused on delivery systems, especially for anticancer agents, used in preclinical trials or applicable for clinical therapy. Data on DS containing covalently bound TPP groups capable of self-assembly into nanosystems are also presented. The biological effects induced by the use of both TPP-modified nanocarriers of drug substances and self-assembling systems involving agents containing covalently bound TPP groups are analyzed. The review gives a detailed account of approaches based on the rational design of initial TPP components for the delivery systems as a tool for fine tuning of physicochemical characteristics of the target therapeutic molecules and for optimization of biological effects caused by using these nanoparticles.

2. Synthetic strategies towards triphenylphosphonium derivatives as vectors for mitochondria-targeted delivery systems

Functional materials containing TPP groups are obtained using two approaches (Fig. 1).

One approach is based on the treatment of the pre-assembled functional structure with triarylphosphines. This process has a limited scope of applicability, since it implies conduction of the reaction by heating in an organic solvent (acetonitrile, haloalkanes, *etc.*). This is not always possible when the substrate contains a large number of reactive groups capable of reacting with triphenylphosphine.

The other approach implies the conjugation of two substrates, one of which contains TPP groups. The possible TPP substrates are ω-phosphonioalkyl halides, carboxylic acids, amines or thiols with an oligomethylene (see structure **A** in Fig. 1), oxoalkylene (**B**), aminoalkylene (**C**) or thioalkylene (**D**) linkers, respectively. In the rational design of TPP components for delivery systems, the choice of the linker is a tool for fine tuning of the physicochemical characteristics of the target molecule, for example, lipophilicity.

Analysis of the published data covered in this review shows that most of the currently known methods for the preparation of TPP derivatives are based on conjugation of phosphonio-alkylcarboxylates with amines or alcohols in the presence of carbodiimides [*e.g.*, 1-(3-dimethylaminopropyl)-3-ethyl-

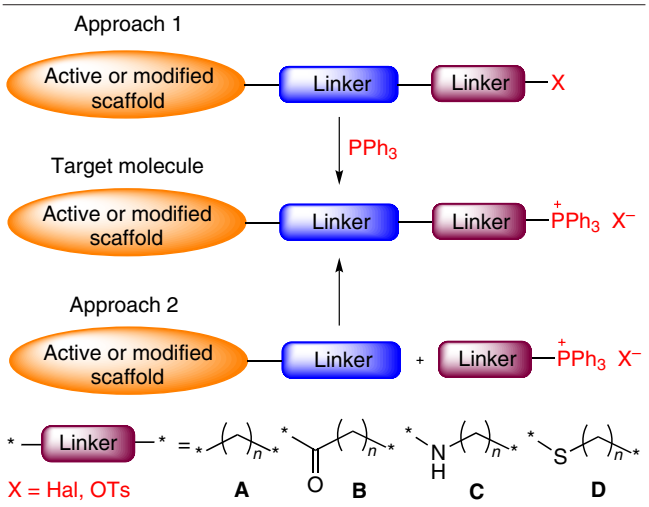

Figure 1. Approaches to the synthesis of functional compounds containing triphenylphosphonium cations. The asterisk indicates continuation of the polymer chain, Ts is *p*-toluenesulfonyl (tosyl).

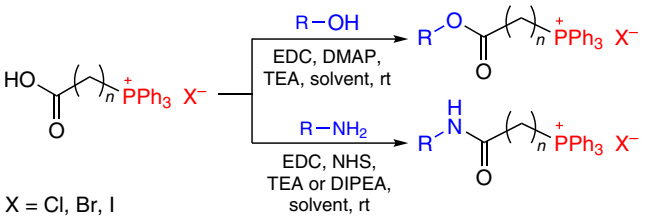

Figure 2. Scheme of conjugation of ω-phosphonioalkylcarboxylates with alcohols and amines.

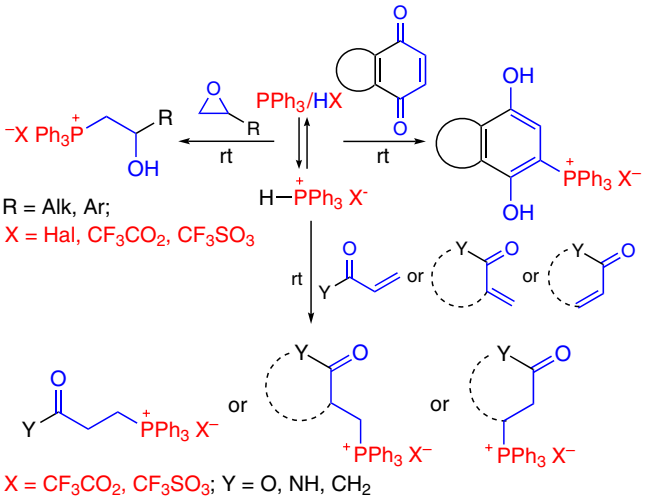

Figure 3. Synthetic routes to compounds with a TPP moiety.

carbodiimide (EDC)], *N*-hydroxysuccinimide (NHS) or 4-dimethylaminopyridine (DMAP) and tertiary amine [triethylamine (TEA), diisopropylethylamine (DIPEA)]. The process is performed at room temperature (rt), which is fairly important if thermally labile compounds are used (Fig. 2).

Methods based on the reactions of stabilized P–H phosphonium salts with compounds containing activated multiple bonds[87–90] or strained heterocycles[61] are also of obvious interest for the synthesis of TPP components of delivery systems (Fig. 3). These reactions proceed quantitatively at room temperature and do not require purification to remove by-products, and the formed compounds contain functional groups convenient for further use (hydroxyl or carbonyl group).

3. Liposomes decorated with triphenylphosphonium derivatives

Liposomes can improve the pharmaceutical properties and decrease the toxicity of drugs. Liposomes are mainly formed from phosphatidylcholine (PC) and cholesterol (Chol). Since the diameter of liposomes is ~100 nm, they can be selectively accumulated in the tumor due to the EPR effect. Liposomes carrying encapsulated water-soluble molecules are usually taken up by cells *via* endocytosis. Conventional liposomes devoid of surface-grafted groups specific to organelles cannot selectively target mitochondria. Thus, subcellular (*i.e.*, organelle-specific) targeting was a major breakthrough in the development of targeted drug delivery systems.[91,92] The mitochondriotropic liposomes bearing triphenylphosphonium cations on the surface were described for the first time[93] as mitochondria-targeting ligands in 2005, while their efficacy in drug delivery to mitochondria *in vitro* and *in vivo* was demonstrated[94] in 2008.

3.1. Alkyltriphenylphosphonium salts. Targeted drug delivery

D'Souza *et al.*[93–96] synthesized stearyltriphenylphosphonium bromide (STPPB) and for the first time prepared liposomes consisting of phosphatidylcholine, cholesterol and STPPB at a PC : Chol : STPPB molar ratio of 65 : 15 : 20 (the total content of the lipid was 25 mg mL^{-1}). These liposomes had surface TPP cations specific to mitochondria. The specificity was attained owing to the lipophilic stearyl chain, which served as the lipid anchor for TPP derivatives in the liposome bilayer membranes (Fig. 4, $n = 17$ for STPPB). The average diameter of STPP liposomes was ~130 nm, while the ζ-potential linearly increased with increasing content of incorporated STPP and reached a stationary value between STPP concentrations of 15 and 20 mol.%. Subsequently, liposomes containing 20 mol.% STPP were used in all *in vitro* investigations.

It is reasonable to assume that a nanosystem decorated with the TPP groups will be accumulated in mitochondria, while the biological molecules loaded (encapsulated) into this nanocarrier may become mitochondriotropic without any covalent chemical modification.

It is known[97] that ceramides participate in various signal transduction processes in cells, including programmed cell death. Ceramide targeting to mitochondria may enhance apoptosis in comparison with the usual way of introduction of this sphingolipid into a cell. It was shown[94] that ceramide delivery by STPP liposomes was favorable for the inhibition of tumor growth and improved the survival rate of animals. In order to eliminate the influence of charge-mediated cellular association, the authors synthesized liposomes containing another cationic lipid, *N*-[1-(2,3-dioleoyloxy)propyl]-*N*,*N*,*N*-trimethylammonium chloride (DOTAPC) in an amount of 1.5 mol.%, which had the surface charge identical to that of STPP liposomes (+30 ± 12 mV). Treatment with 'empty' nanocarriers modified with STPPB did not result in a noticeable decrease in the tumor growth rate, that is, these nanocarriers did not show an antitumor action. However, when the content of ceramide in liposomal systems was 6 mg kg^{-1} (which is 6 times lower than effective doses, which were 36 to 72 mg kg^{-1}), the tumor growth rate significantly decreased. Hence, the enhanced activity of ceramide was related to the delivery into particularly cancer cell mitochondria.

It was shown[96] by confocal microscopy that the anticancer drug paclitaxel (PTX) extracted from the bark of *Taxus chinensis*,

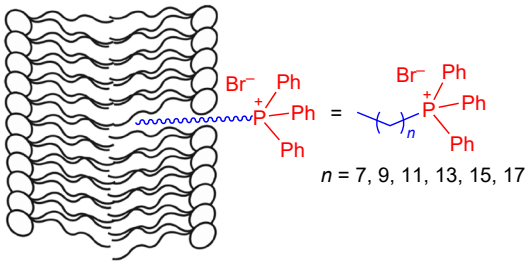

Figure 4. Structure of liposomes with incorporated alkyltriphenylphosphonium cation. The oval denotes the polar part of the bilayer membrane and tails are hydrophobic groups. The Figure was created by the authors using published data.[93–96]

when loaded in STPP liposomes, was accumulated in mitochondria and decreased the viability of paclitaxel-resistant cells. Paclitaxel-loaded STPP liposomes showed a higher toxicity against human ovarian cancer cells (Ovcar-3) than conventional non-modified PTX liposomes containing only the drug. Since no significant difference in cytotoxicity was found between PTX–STPP and PTX liposomes, the authors concluded that the enhanced efficacy was due to both location of paclitaxel in mitochondria and their toxicity.[96] Subsequently, STPP liposome systems with an improved composition were obtained. They consisted of egg phosphatidylcholine, dipalmitoyl phosphatidylcholine (DPPC), stearyltriphenylphosphonium chloride (STPPC) and sclareol, a labdane diterpene, in 8.87:0.1:0.136:5 molar ratio.[95] The results of experiments demonstrated significantly improved apoptotic and cytotoxic effect of sclareol incorporated into liposomes compared to the conventional drug. An increase in the activity of caspase-9 compared to caspase-8 in the presence of these liposomes attested the enhanced induction of mitochondrial-mediated apoptosis.

Kuznetsova *et al.*[98] decorated liposomes with TPP derivatives with different alkyl chain lengths (see Fig. 4, for $n = 6, 8, 9, 11, 13, 15$). Liposomes were prepared using DPPC with various molar ratios of the components. It was found that elongation of the alkyl chain up to 14 methylene units (TPP–C14 compound) increased the positive charge of the liposome; however, no explanation to this fact was given in the study. The authors found that the decorated TPP–C14/DPPC liposomes were better taken up in the mitochondria of pancreatic carcinoma cells (PANC-1)[96] and lung adenocarcinoma cells (A-549)[99] than non-modified DPPC liposomes. The cytotoxicity[b] of doxorubicin (DOX) ($IC_{50} = 3.2 \pm 0.2$ μM) against the PANC-1 cell line (ductal carcinoma of the pancreas) decreased twofold in comparison with the cytotoxicity of DOX encapsulated into TPP–C14 liposomes in 0.029:1 molar ratio. This was accompanied by a decrease in the toxicity against the Chang Liver normal cells ($IC_{50} = 2 \pm 0.1$ μM) in comparison with non-encapsulated doxorubicin.

Thus, STPP-decorated liposomes can efficiently deliver drug substances to mitochondria. However, it is noteworthy that the toxicity of STPP liposomes is non-specific. When liposomes are modified with cationic groups, a considerable positive charge is formed on the surface, and non-specific toxicity becomes a great concern.[100]

Shah *et al.*[101] investigated the toxicity of STPP liposomes against several cell lines, including drug-resistant ones. The authors showed that high toxicity of STPP liposomes against cancer cell lines compared to a solution of STPPB is attributable to uncoupling of mitochondrial respiration and oxidative phosphorylation (OXPHOS) processes. Phosphatidylcholine–cholesterol (PC–Chol) liposomes decorated with STPPB [PC:Chol:STPPB molar ratio of 68:30:2] with a diameter (d) of 107±4 nm, polydispersity index (PDI) of 0.28±0.002 and ζ-potential of +28±3 mV were prepared by thin-film hydration method. Unlike a solution of STPPB in DMSO, the liposomes show high toxicity against both highly drug-resistant cancer cells (H69AR lung cancer and Ovcar 3 ovarian cancer) and non-resistant cells (A549 lung cancer and A2780 ovarian cancer). Dye accumulation assay (using 5,5,6,60-tetrachloro-1,10,3,30-tetraethylbenzimidazolylcarbocy anine iodide) confirmed that the dye accumulation was much higher in the drug-resistant cell lines containing mitochondria with a higher negative potential than in the drug non-resistant cell lines. Apparently, the higher toxicity of PC–Chol–STPP particles against drug-resistant cells is due particularly to the presence of liposomal lipids. Meanwhile, the toxicity of STPPB is comparable with that of carbonyl cyanide-*p*-trifluoromethoxy phenylhydrazone, a known uncoupling agent for the mitochondrial respiration and OXPHOS. Hence, STPPB is more toxic for the resistant cell lines, which, as noted above, require a higher mitochondrial membrane potential and higher OXPHOS levels for the cellular activity to be manifested.[102]

In order to overcome the non-specific cytotoxicity of STPP-modified liposomes and the limited applicability of cationic liposomes for *in vivo* mitochondria-targeted drug delivery, TPP-modified phospholipid conjugates and polymer–liposomal complexes were proposed. They are described in the following Sections.

3.2. Conjugates of triphenylphosphonium with phospholipids

An approach consisting in the conjugation of triphenylphosphonium salts with commercially available phospholipids was proposed to ensure the flexibility of the lipid composition of liposomes and to study the effect of the lipid anchor on the mitochondrial compatibility of the liposomal platform.[103] TPP-Modified phospholipids were synthesized using phosphatidylethanolamine (PE) derivatives with dioleoyl (DOPE), dimyristoyl (DMPE) or dipalmitoyl (DPPE) moieties (Fig. 5). Liposomes decorated with TPP phospholipids were prepared by lipid-film hydration. These liposomes had the same mitochondriotropic properties as STPP liposomes, but had a better biocompatibility. Thus, incubation of BT-20 breast cancer cells with STPP liposomes resulted in a dose-dependent decrease

[b] For quantitative evaluation of the cytotoxicity, the half-maximal inhibitory concentration (IC_{50}) is used.

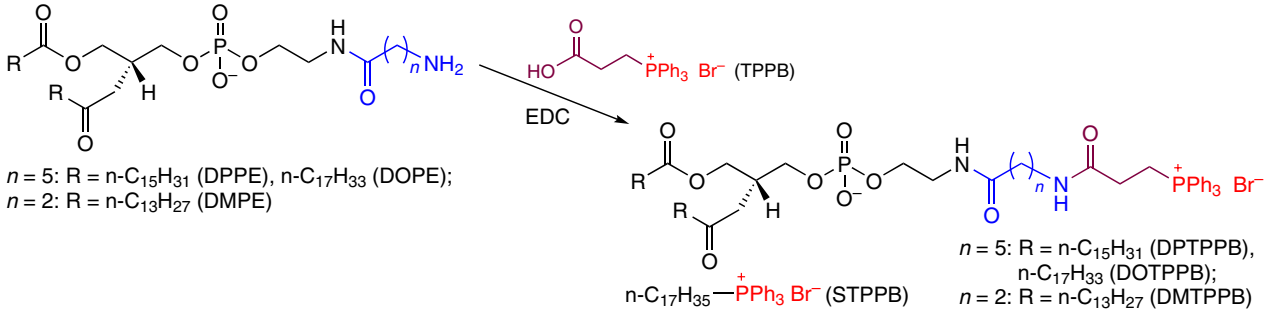

Figure 5. Scheme of preparation and structure of TPP-modified phospholipids.

in the cell viability, whereas DOTPP, DMTPP and DPTPP liposomes did not significantly change this characteristic. When the concentration of STPP liposomes was 2.5 mg mL^{-1}, a 35% loss of membrane integrity of BT-20 cells took place. Conversely, in the presence of PE-based liposomes, the cell membrane remained intact.[104]

Jiang *et al.*[105] compared the specificity and mitochondria targeting efficacy for liposomes modified with dendrite amino acids (G2R-DA) or TPP conjugate, 2-distearoyl-*sn*-glycero-3-phosphatidylethanolamine-3-carboxypropyltriphenylphosphonium bromide (DTPPB) (Fig. 6).

The composition of G2R-DA-modified liposomes was as follows: dendritic lipopeptides, soy phosphatidylcholine (SPC), Chol, PEGylated distearoyl phosphatidylethanolamine ($DSPE–PEG_{2000}$) and indocyanine green (ICG) as a photosensitizer. TPP-Modified liposomes that comprised SPC, Chol, DSPE–PEG, DTPPB and indocyanine green in 5 : 1 : 0.35 : 2.4 : 1.3 molar ratio had the following characteristics: $d = 139.4 \pm 2.5$ nm, PDI = 0.24±0.02, ζ-potential +23.67±0.12 mV (Fig. 7*a*). Experiments showed a 3.7 times higher mitochondria-targeting level upon intravenous injection

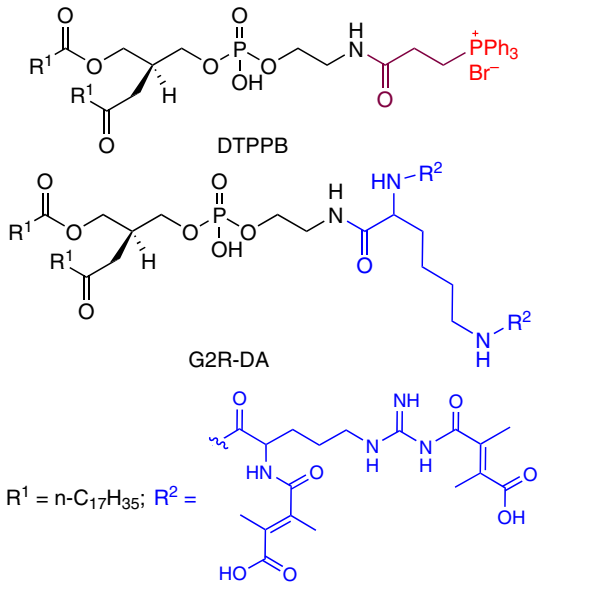

Figure 6. Structures of components of mitochondria-targeted liposomes — DTPP and G2R-DA.

for G2R-DA liposomes compared to TPP liposomes and complete disappearance of the tumor in mice (4T1 breast cancer). The authors proposed a probable mechanism for mitochondria targeting of the G2R-DA liposomes, which included the following steps (see Fig. 7*b*):

(1) G2R-DA liposomes enter the cells *via* macropinocytosis and then they are released from endosomes to the cytoplasm;

(2) in the cytoplasm, G2R-DA liposomes are transported to the mitochondrial matrix by TOM- and TIM23-mediated pathway[c] due to the selective adsorption by mitochondrial membrane translocases, unlike liposomes without an amino acid component.

The antidiabetic drug metformin (MET, used as a hydrochloride) is effective for the treatment of some types of cancer, first of all, *via* the action on mitochondria.[106] For the targeted delivery of MET to mitochondria, mito-liposomes of the following composition were designed: Tween 80 polysorbate, Chol, phospholipid lipoid S-100 and TPP–DPPE conjugate (Fig. 8); they had $d = 85.28 \pm 0.86$ nm and ζ-potential of +29.8±1.47 mV. Evaluation of the antitumor activity (MTT assay) against HeLa cell line gave half-maximal inhibition concentrations (IC_{50}) of 19.4±1.9, 10.4±0.5 and 1.3±0.1 μM for free MET and liposomal and mito-liposomal forms, respectively. The experiment clearly demonstrated a 15-fold increase in the drug activity when loaded into mito-liposomes in comparison with the usual form. The authors believe that the enhanced efficacy of MET was due to selective delivery of the mito-liposomes directly to the mitochondria.

3.3. Triphenylphosphonio-containing cholesterol

Celastrol-loaded cationic liposomes Cela–TL/HA (TL stands for mitochondria-targeted liposomes) were developed for the targeted delivery of celastrol (Cela)[d] to the mitochondria of tumor cells and for increasing the Cela anticancer activity. These particles consisted of soy phosphatidylcholine (SPC), cholesterol modified with TPP cations (TPP–Chol), and hyaluronic acid (HA) residues, which provided for the electrostatic binding of

[c] TOM/TIM is the translocase of the mitochondrial outer/inner membrane complex.

[d] Celastrol is a quinomethide, which belongs to friedelane type triterpenoids and was isolated from root extracts of *Tripterygium wilfordii* and *Tripterygium regelii*.

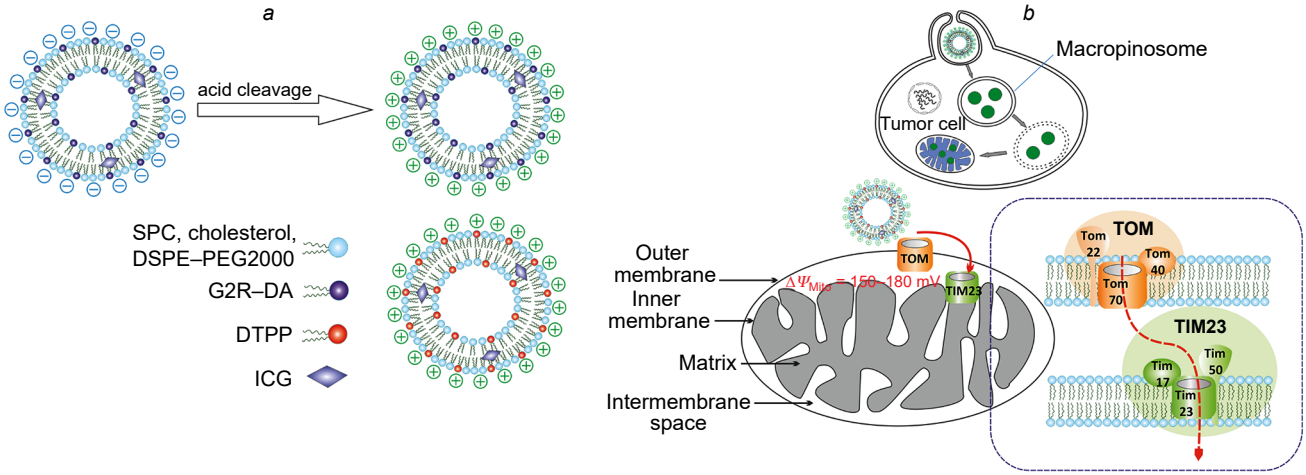

Figure 7. Structures of mitochondria-targeted liposomes modified with dendrite amino acids (above) and DTPP (below) (*a*) and the possible mechanism of mitochondria targeting of liposomes (*b*). The Figure was created by the authors using published data.[105]

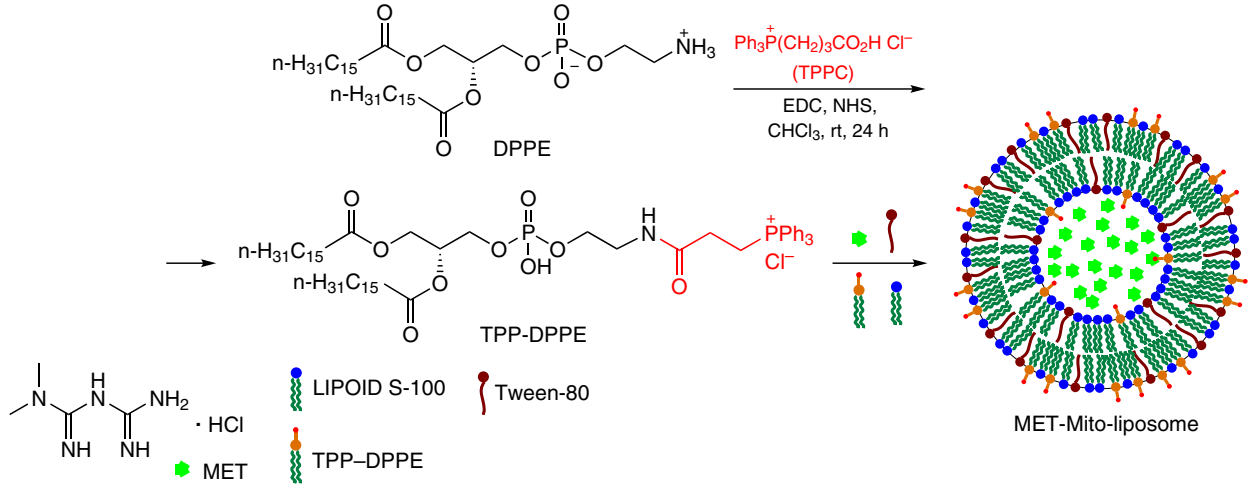

Figure 8. Preparation and structure of MET-containing liposomes. The Figure was created by the authors using published data.[106]

the components.[107] The synthetic routes to TPP–Chol (abbreviated as CT) and to Cela–TL/HA nanoparticles are depicted in Fig. 9.

The Cela–TL particles were prepared by lipid-film hydration, with the CT and SPC component ratio being optimized. For the optimal ratio of 1 : 10 (w/w), the efficacy of Cela encapsulation reached 99%, the particle size was less than 100 nm (83.77 ± 1.04 nm), and the ζ-potential was +28.57 ± 0.53 mV, *i.e.*, the particles were able to target the mitochondrial membrane. The efficiency of celastrol encapsulation into Cela–TL/HA

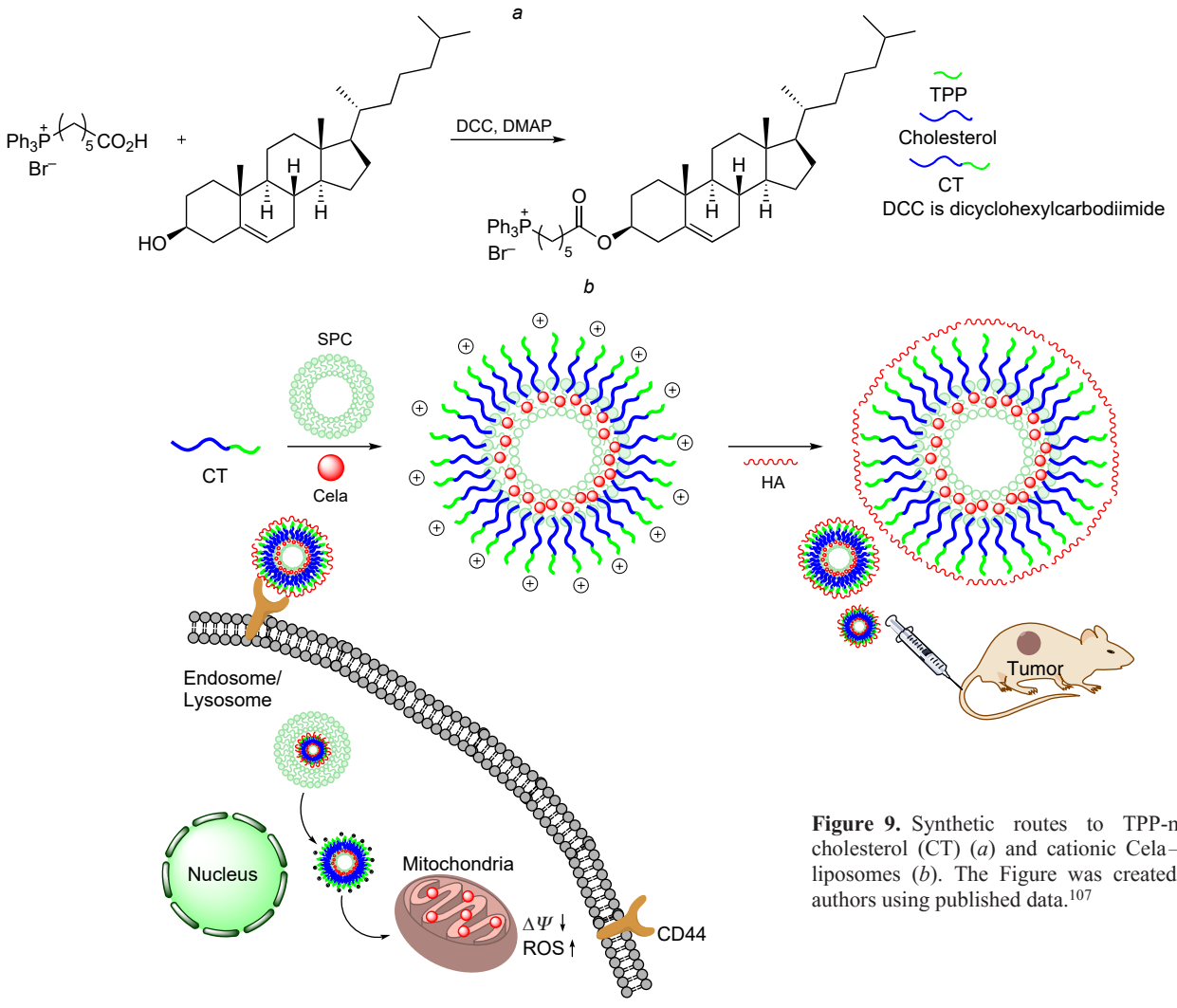

Figure 9. Synthetic routes to TPP-modified cholesterol (CT) (*a*) and cationic Cela–TL/HA liposomes (*b*). The Figure was created by the authors using published data.[107]

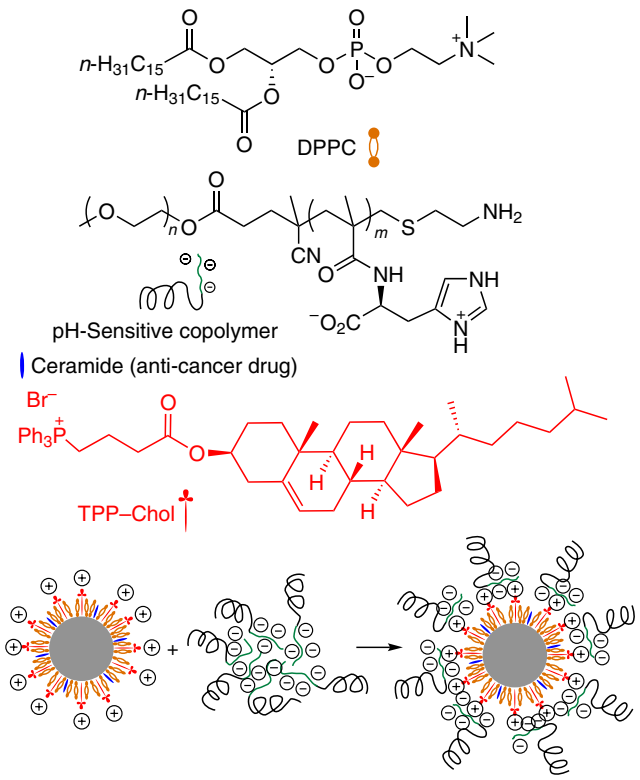

Figure 10. Preparation of pH-sensitive polymer–liposome complexes. The Figure was created by the authors using published data.[108]

particles was approximately the same, but they were somewhat larger in size (88.97±1.27 nm), but still smaller than 100 nm, which promoted their accumulation near the tumor cells because of the EPR effect. Hyaluronic acid was applied onto the outer layer of the Cela–TL particles; therefore, it successfully quenched the TL positive charge, and the ζ-potential of the particles became negative (−23.43±2.20 mV). The results indicated that Cela–TL/HA liposomes successfully transported celastrol into mitochondria, where it effectively initiated apoptosis *via* mitochondrial pathway and more actively inhibited the tumor growth and had less toxic side effects than the free drug. What is even more important, HA coating not only provided this delivery system with high stability and biosafety *in vivo*, but also improved drug uptake by the tumor *via* recognition of the CD44 receptors expressed on the surface of tumor cells.

For the targeted delivery of ceramide, possessing an antitumor action, to the mitochondria of cancer cells, pH-sensitive polymer–liposome complexes were prepared.[108] The cited study describes the synthesis of a mitochondriotropic agent, TPP–Chol, for the fabrication of cationic liposomes containing DPPC, ceramide and TPP–Chol conjugate in the 4:0.75:1 (w/w) ratio. An anionic block copolymer, methoxypoly(ethylene glycol)-*block*-poly(methacrylic acid–histidine) was adsorbed on the liposomes for shielding the positive charge at pH 7.4 (Fig. 10).

After cancer cells have internalized the polymer–liposome complexes *via* endocytosis, the copolymers become neutral and are desorbed from the surface of cationic liposomes, thus inducing the destruction of the endosomal membrane due to the

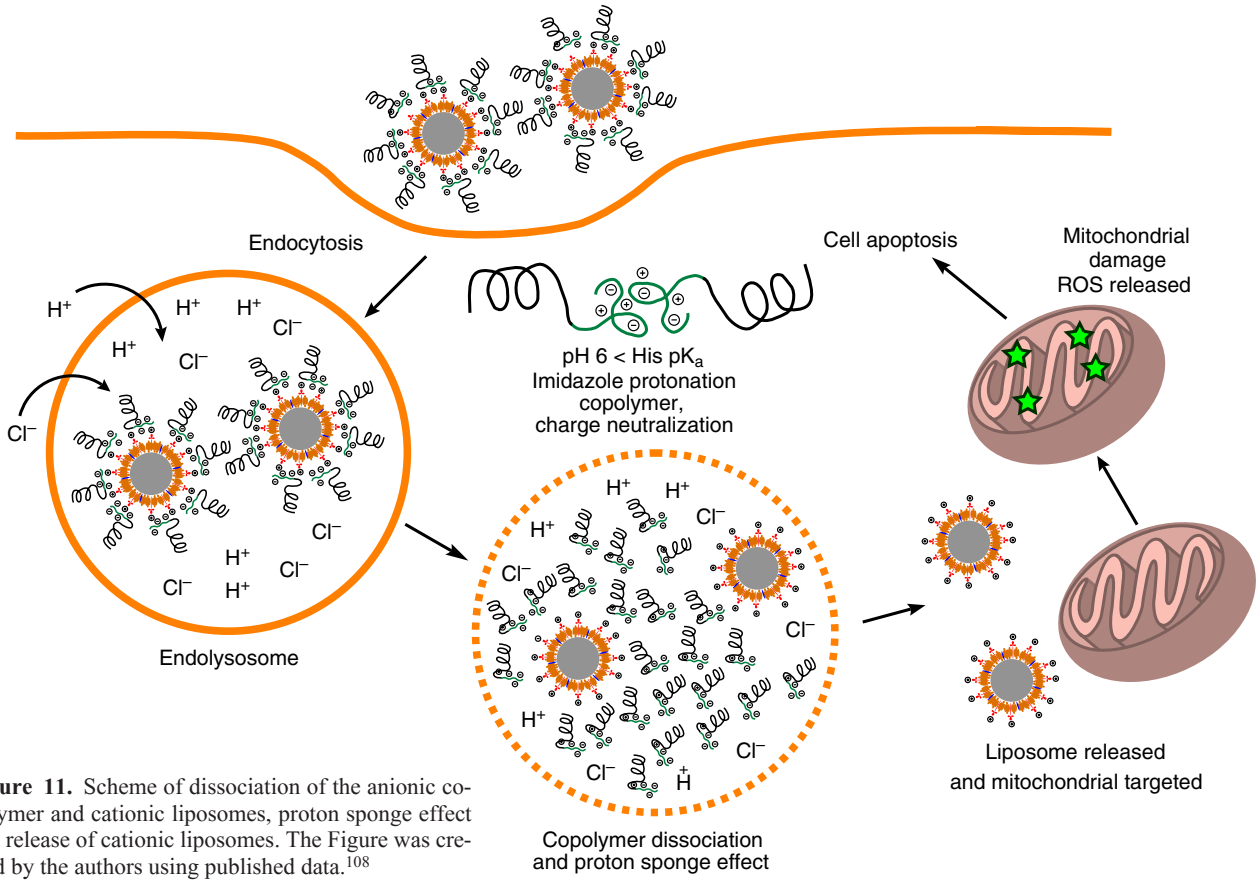

Figure 11. Scheme of dissociation of the anionic copolymer and cationic liposomes, proton sponge effect and release of cationic liposomes. The Figure was created by the authors using published data.[108]

proton sponge effect and promoting the release of cationic liposomes into the cell cytosol (Fig. 11).[108] The pH-sensitive polymer–liposome complexes rapidly (within 3 h) migrate from the endosomes of MCF-7 (breast cancer) cells to mitochondria, giving rise to reactive oxygen species (ROS) and triggering apoptosis of cancer cells.

3.4. Conjugates of triphenylphosphonium with poly(ethylene glycol)

Most often, TPP liposomes are positively charged; this increases their toxicity against both normal and cancer cells; also, they are readily recognized and captured from the bloodstream with the reticuloendothelial system. One strategy for masking positively charged TPP liposomes is based on the use of PEG. Poly(ethylene glycol)-stabilized liposomes (*e.g.*, Doxil®) are successfully used in clinics for the targeted delivery of therapeutic agents. Biswas *et al.*[109] used TPP–PEG_{2000}–PE particles, comprising a copolymer of poly(ethylene glycol) and phosphatidylethanolamine (PEG–PE) with a TPP moiety, for the inclusion into the liposomal bilayer (Fig. 12).

Liposomes decorated with the TPP–PEG_{2000}–PE polymer were investigated for the toxicity, mitochondrial targeting and possibility of PTX drug delivery to tumor cells *in vitro* and *in vivo*. These liposomes proved to be less cytotoxic than STPP or PEG–STPP liposomes and demonstrated effective uptake in the tumor cell mitochondria. Paclitaxel encapsulated into TPP–PEG_{2000}–PE liposomes exhibited higher PTX-induced cytotoxicity and anticancer activity in assays using cell cultures and mice than PTX encapsulated into unmodified liposomes.[109]

An identical conjugate synthesized by Kang *et al.*[110] was used to modify liposomes and deliver resveratrol (RES) to the tumor. Mitochondria-targeted liposomes for the delivery of RES were prepared by thin-film hydration of a mixture of 1-palmitoyl-2-oleoyl-*sn*-glycero-3-phosphatidylcholine, Chol and PEG_{2000}–PE (or TPP–PEG_{2000}–PE) in 7 : 3 : 0.15 molar ratio. The RES–TPP–PEG2000–PE liposomes had a positive surface charge (+10.46 mV), which confirmed the presence of TPP cations on the surface, as the charge of RES–PEG_{2000} liposomes was close to zero (–1.68 mV). The TPP–PEG_{2000}–PE liposomes were tested *in vitro* against the B16F10 melanoma cell line. Enhanced accumulation of the liposomes in the mitochondria, anticancer activity and ROS generation were observed.

Yue *et al.*[111] reported an example of synthesis of one more TPP–PEG conjugate involved in the development of mitochondria-targeted liposomes for the delivery of the IR-780 photosensitizer and the anticancer drug lonidamine [1-(2,4-dichlorobenzyl)-1*H*-indazole-3-carboxylic acid; LND]. Liposomes consisting of DPPC, 1,2-distearoyl-*sn*-glycero-3-phosphatidylcholine (DSPC), Chol, TPP–PEG, IR-780 and LND in 10 : 2 : 3 : 5 : 1 : 3 mass ratio were prepared by lipid-film hydration. The liposome size was 125.0 ± 63.3 nm, the ζ-potential was +23.5 ± 3.1 mV, PDI = 0.294, and the encapsulation efficiency was 83.6 and 85.4% for IR-780 and LND, respectively. The presence of the dye in the lipid bilayer endowed the liposome membrane with the susceptibility to laser radiation, leading to its destruction, which facilitated drug release from the liposome. The fluorescence analysis of the biodistribution of IR-780 showed that liposomes were efficiently accumulated in the tumor, most likely, due to the EPR effect. Liposomes loaded with a combination of two compounds (IR-780 and LND) exhibited an excellent synergistic therapeutic effect in LL/2 mice bearing subcutaneous tumor xenografts.

Acute myocardial infarction (AMI) is one of the most common causes of disability and mortality in the world. Patients diagnosed with AMI usually undergo early reperfusion using percutaneous coronary intervention to timely restore oxygen supply of the blocked blood vessels. However, coronary reperfusion may induce myocardial ischemia/reperfusion injury (MI/RI). Although the exact mechanism of MI/RI has not been clarified, it is believed to include continuous release of ROS, calcium escape from mitochondria and continuous opening of mitochondrial permeability transition pores (mPTP), which changes the mitochondrial permeability, *i.e.*, this can induce mitochondrial dysfunction. When cardiomyocytes are damaged or necrotized by infarction, cells secrete large amounts of inflammatory cytokines and matrix metalloproteinases (MMP), which infiltrate the area of ischemic myocardium, thus leading to a significant increase in the level of these enzymes.[112] The mitochondrial dysfunction allows cytochrome *c* (Cyt *c*) to be released from mitochondria to the cytosol, thus inducing the caspase cascade and triggering apoptosis in cardiomyocytes. Thus, mitochondria are key regulators of the survival of cardiomyocytes, and mitochondria-targeted therapeutic strategies may be promising for preventing MI/RI.

Puerarin [8-(β-*D*-glucopyranosyl)-4′,7-dihydroxyisoflavone, PUE], the major biologically active component of the root of *Pueraria lobata* (Willd.) Ohwi, inhibits opening of mPTP and thus mitigate the MI/RI symptoms. However, free PUE can hardly get into mitochondria. Le *et al.*[113] designed PUE@T/M–L liposomes[e] which could bind to MMP by means of the MMP–TP peptide (amino acid sequence: GGGGCTTHWGFTLC) and were modified with a TPP group with encapsulated PUE for its delivery to mitochondria

[e] In the notation for complex systems in this review, the components are separated by characters '–', '/' and '@', most often, taken from original publications.

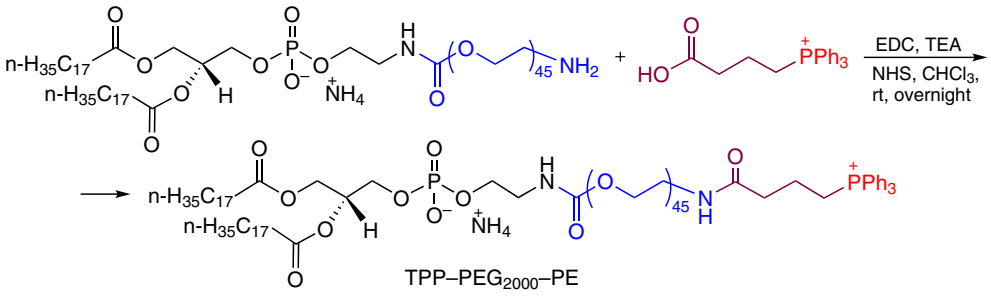

Figure 12. Synthesis of the TPP–PEG2000–PE conjugate.

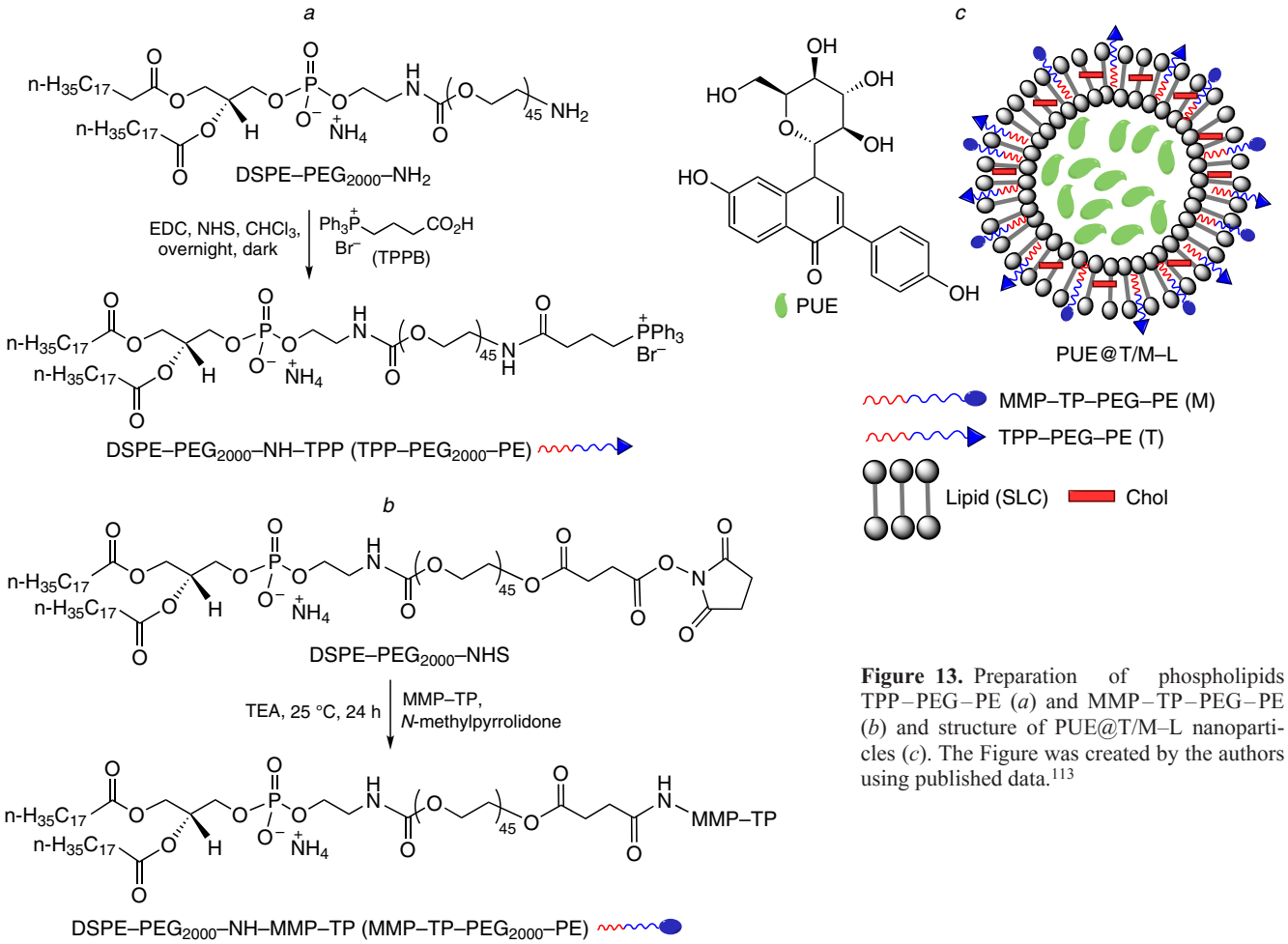

Figure 13. Preparation of phospholipids TPP–PEG–PE (*a*) and MMP–TP–PEG–PE (*b*) and structure of PUE@T/M–L nanoparticles (*c*). The Figure was created by the authors using published data.[113]

(Fig. 13). The starting polymers (TPP–PEG–PE and MMP–TP–PEG–PE, abbreviated as T and M) were obtained from the ammonium salt of 1,2-distearoyl-*sn*-glycero-3-phosphoethanolamino-*N*-[amino(polyethylene glycol)$_{2000}$] (DSPE–PEG$_{2000}$–NH$_2$) and (3-carboxypropyl) triphenylphosphonium bromide in the presence of coupling agents (EDC and NHS) (see Fig. 13 *a*) and from 1,2-distearoyl-*sn*-glycero-3-phosphoethanolamino-*N*-[(polyethylene glycol)$_{2000}$, succinimidylsuccinate ether] (DSPE–PEG$_{2000}$–NHS) and MMP–TP peptide (see Fig. 13 *b*). The PUE@T/M–L liposomes had the following characteristics: d = 144.9±0.8 nm, ζ-potential of 19.4±0.5 mV, drug loading capacity of 6.2±0.1% and encapsulation efficiency of 78.9±0.6%. They remained stable after the release of PUE. These particles were obtained by hydration of a lipid film containing soy lecithin (SLC), Chol, TPP–PEG–PE and MMP–TP–PEG–PE in 52:26:11:11 molar ratio in the presence of PUE in methanol (see Fig. 13 *c*). The dried lipid film was hydrated with distilled water or phosphate buffered saline (PBS), treated and extruded by passing through a polycarbonate membrane with a pore size of 100 nm. The results of the cytofluorimetric experiments showed that PUE@T/M–L liposomes enhanced the cellular uptake of the drug, escaped lysosomal capture and promoted PUE targeting into mitochondria. Furthermore, these liposomes increased the viability of hypoxia–reoxygenation (H/R) damaged H9c2 cells (myoblasts used as a cell model of cardiomyocytes) by inhibiting mPTP opening and ROS production and a change in the expression of apoptosis markers: a decrease for the Bax protein and increase for the Bcl-2 protein.

It is known that the concentration of glutathione (GSH) is substantially (~100 times) higher in tumor cells that in normal cells and that disulfide bonds are sensitive to the redox potential and acidity of the medium.[114] Peng *et al.*[115] developed polyfunctional liposomes for the delivery of anticancer drugs DOX and LND for the synergistic treatment of glioma. The following conjugates were prepared for the decoration of liposomes: PEGylated cholesterol modified with glucose and containing bridging disulfide bonds (Chol–SPG; SPG means sulfur, PEG, glucose) and PEGylated cholesterol with triphenylphosphonium groups (TPP–Chol) (Fig. 14). The Lip–SPG liposomal system, which was a combination of Chol–SPG and TPP–Chol conjugates (SPC : cholesterol : Chol–SPG : Chol–TPP = 60 : 34 : 3 : 3 by mass) and a combination of drugs (lipid : DOX : LND = 40 : 1 : 1 by mass), inhibited proliferation of cancer cells and induced apoptosis *in vitro*. In addition, this system markedly affected mitochondria, in particular, it reduced intracellular ATP production, enhanced the formation of ROS and promoted mitochondrial membrane depolarization. It was found that Lip–SPG liposomes had a low toxicity against normal tissues and a high inhibitory activity against glioma in *in vivo* assays where they increased the survival time of mice from 19 to 39 days (*in situ* glioma model).[115]

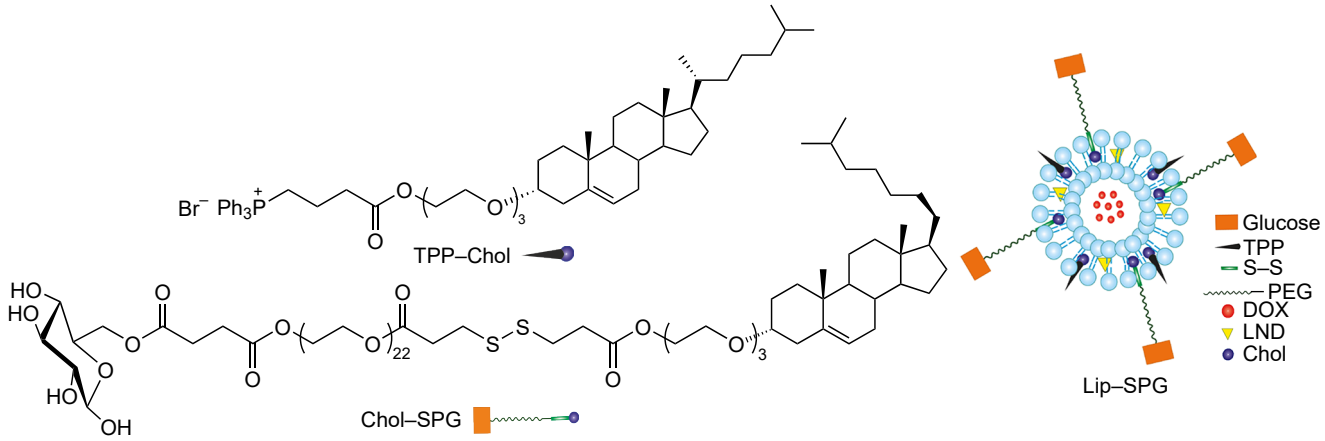

Figure 14. Structure of conjugates based on cholesterol for the decoration of liposomes. The Figure was created by the authors using published data.[115]

3.5. Prodrugs containing a triphenylphosphonium group

The covalent bonding of a drug to a lipid moiety in the same molecule makes it amphiphilic. Prodrug-loaded[f] liposomes possess a high therapeutic efficacy: they virtually prevent leakage of the drug and cause its rapid release in the cell.[116] It is known that MitoQ (Fig. 15) obtained by combining triphenylphosphonium cation and ubiquinone moiety in the same molecule can be selectively taken up by mitochondria.[117] This type of drug is safe for long-term oral administration,[118] improves vascular endothelial function,[73] activates superoxide dismutase[74] and has antioxidant properties.[119] The derivative MitoPBN (see Fig. 15) is a free-radical scavenger, which has a protective action on the liver mitochondria.[120] Liposomes decorated with MitoPBN (lecithin : Chol : MitoPBN = 50 : 25 : 5 by mass) were mainly accumulated in liver, thus reducing the cellular oxidative stress and increasing ATP synthesis, *i.e.*, they alleviated the mitochondrial dysfunction. Finally, this increased the intensity of glycolysis and tricarboxylic acid cycle. Furthermore, acceleration of glucose breakdown led to faster glucose utilization and, hence, decreased the blood level of glucose in diabetic rodents.[121]

Zhou *et al.*[122] synthesized the TPP–$TPGS_{1000}$ conjugate from D-α-tocopherol poly(ethylene glycol) succinate (TPGS) and triphenylphosphonium salt and used it to prepare liposomes for the targeted delivery of paclitaxel into mitochondria (see Fig. 15). These liposomes had the following composition: egg phosphatidylcholine, Chol and TPP–$TPGS_{1000}$ in 88 : 3.5 : 8.5 molar ratio; the particle size was 80 nm; they were characterized with high encapsulation efficiency (>85%) and a small positive ζ-potential (+1.93 ± 0.56 mV). The liposomal PTX was efficiently taken up by drug resistant tumor cells and induced apoptosis through the release of Cyt C; it also initiated a cascade of biochemical reactions involving caspases-9 and -3 (Cas-9/3) *via* activating the proapoptotic Bax and Bid proteins and inhibiting the anti-apoptotic Bcl-2 protein.

Docetaxel (DTX) derivative with a TPP group at the periphery (see Fig. 15) was synthesized[123] with the goal of targeted delivery to mitochondria and overcoming non-specific cytotoxicity caused by the positive charge of triphenyl-

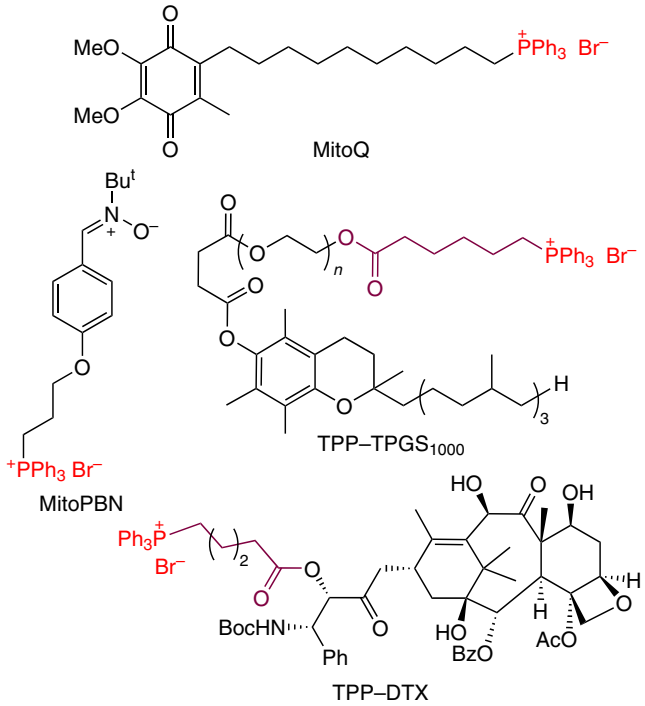

Figure 15. Structure of TPP prodrugs meant for the decoration of liposomes.

phosphonium. The thin-film hydration of a mixture of TPP–DTX, SPC, dioleoylphosphatidylethanolamine, Chol and SPC–Mal (copolymer of PEG, Schiff base, Chol and NH-maleimide) in 4 : 40 : 40 : 5 : 5 mass ratio (20 mg mL^{-1}) total lipid content) was used to obtain pH-sensitive liposomes; the size of the resulting liposomes was 110 nm. After incorporation of TPP-containing docetaxel into liposomes, ζ-potential of the particles changed from negative to positive (up to +9 mV). In order to shield the positive charge and decrease the toxicity, the liposomes were PEGylated and modified by Eph tyrosine kinase receptor (EphA). As a result, the ζ-potential decreased to neutral and negative values. The resulting liposomes were accumulated in MCF-7 cells *via* receptor-mediated endocytosis and efficiently delivered TPP–DTX into mitochondria; they decreased the mitochondrial membrane potential, increased the release of Cyt C into cytosol and activated Cas-9/3, which induced tumor cell apoptosis. It was found that liposomes specifically accumulated in the tumor and showed an excellent activity *in vivo* against

[f] By prodrug is usually meant a chemically modified form of a drug substance that is converted to a pharmacologically active compound *via* metabolic processes in biological media.

MCF-7 tumor in immunodeficient mice. In addition, they exhibited antiangiogenic and antiproliferative effects *in vivo* and caused apoptosis of tumor cells.[123]

Lung cancer is the most frequently encountered lethal malignant neoplasm. Unfortunately, most advanced stages of lung cancer are not curable, but worsen with time. A key method improving the prognosis of this disease is radiation therapy (RT), although currently it has limited use in clinical practice. This is due to the consequences of RT, namely, a decrease in the DNA damage under hypoxia and acquired immunity due to enhanced expression of programmed death ligand-1 (PD-L1). The major function of PD-L1 located on the cell membrane is to inhibit the anticancer action of activated immune T-cells. Blocking the PD-L1/PD-1 membrane axis (PD-1 is programmed cell death receptor) is considered to be an ideal target for the immunotherapy of lung cancer. The inhibition of the intracellular expression of PD-L1 improves the sensitivity of tumors to RT as a result of inhibition of the DNA damage repair. Simultaneous inhibition of membrane and intracellular PD-L1 may improve the efficacy of RT in the treatment of lung cancer.

In order to address this problem, mitochondria-targeted liposomes based on hydrogenated soy phosphatidylcholine (HSPC) and cholesterol and containing an anticancer drug, lonidamine, bound to the TPP groups were prepared[124] using the thin-film hydration method. The TPP–LND@Lip liposomes (143.4±2.8 nm size and ζ-potential of +19.9±1.6 mV) efficiently

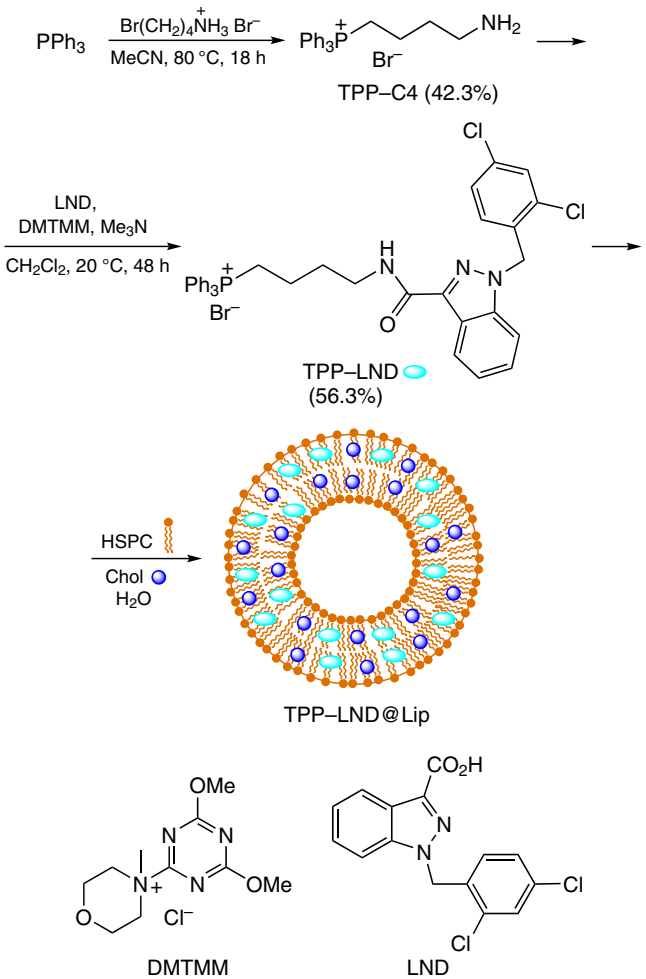

Figure 16. Preparation of TPP–LND@Lip liposomes. The Figure was created by the authors using published data.[124]

inhibited OXPHOS by acting on mitochondrial complexes I and II. The TPP–LND derivative was synthesized by the reaction of triphenylphosphine with 4-bromobutylammonium bromide followed by condensation of the TPP–C4 salt with LND in the presence of 4-(4,6-dimethoxy-1,3,5-triazin-2-yl)-4-(*N*-methylmorpholinium) (DMTMM) chloride (Fig. 16).

The content of the TPP–LND hybrid compound in the TPP–LND@Lip liposomes was 87.2%, as found by HPLC and UV spectroscopy. Owing to the presence of TPP groups, these liposomes selectively transported the antitumor agent into the mitochondria of cancer cells. The modified TPP–LND agent inhibited the OXPHOS process approximately 50 times more efficiently than the LND@Lip liposomes containing only LND. As regards the regulation of PD-L1 expression, the TPP–LND@Lip particles decreased the expression when present in a relatively low concentration (2 μM). Meanwhile, LND alone was effective only in the concentration of 300 μM. In addition, the TPP–LND@Lip liposomes in combination with RT blocked the action of intracellular PD-L1, were able to reverse the tumor hypoxia and induced a greater generation of ROS. Thus, the synergistic effect of the TPP–LND@Lip liposomes led to a substantial inhibition of the growth of lung cancer cells *in vitro* and *in vivo*.

Multiple drug resistance (MDR) is a severe problem responsible for the lack of efficacy of chemotherapy in patients with non-small cell lung cancer. Currently, cancer cell mitochondria are considered to be a promising target for overcoming MDR, as they play a crucial role in the intrinsic apoptosis pathway and in the energy metabolism in the cell. An ATP-binding cassette transporter is P-glycoprotein, which is overexpressed in MDR cells and promotes the subsequent expulsion of chemotherapeutic drugs from the cell. This energy-dependent process is the most important mechanism of drug resistance.

Paclitaxel is often used as a first-line chemotherapeutic agent for the treatment of non-small cell lung cancer, ovarian cancer and breast cancer; however, the PTX resistance develops rapidly. To overcome this problem, Wang *et al.*[125] proposed a two-stage targeted liposome. The two-step preparation process of the liposome started with the design of the PTX-loaded cationic TT–LP/PTX liposome (Fig. 17). The TPP–TPGS conjugate (see Fig. 15; for brevity, designated by TT) can overcome MDR by targeting liposomes to mitochondria and destroying the mitochondria. For increasing the selectivity to tumor cells and stability in the bloodstream, the TT-modified cationic nanoparticles were coated by an anionic polysaccharide (hyaluronic acid). This modification provided the nanoparticles with the ability to actively target mitochondria *via* specific recognition of the CD44 receptors overexpressed in tumor cells. The TT–LP/PTX liposomes were prepared by the hydration method, in particular, an SPC+Chol mixture and PTX-loaded TT nanoparticles (TT/PTX) were dissolved in chloroform, then the solution was concentrated until a thin lipid film formed, which was then hydrated with a 5% glucose solution followed by ultrasonic treatment. For the optimal TT to SPC mass ratio of 1:10, a high drug encapsulation efficiency of approximately 91.6% was attained. The TT–LP/PTX particles were then treated with a solution of HA under sonication, which resulted in the formation of the target HA/TT–LP/PTX particles. The optimal composition of the HA/TT–LP/PTX liposomes was as follows: Chol:SPC = 1:10, PTX:SPC = 1:15, TT:SPC = 1:10 and HA:TT = 1:1 (mass ratios); the SPC concentration was 5 mg mL^{-1}. The LP/PTX, TT–LP/PTX and HA/TT–LP/PTX particles had a spherical shape and sizes of 107, 92 and 153 nm,

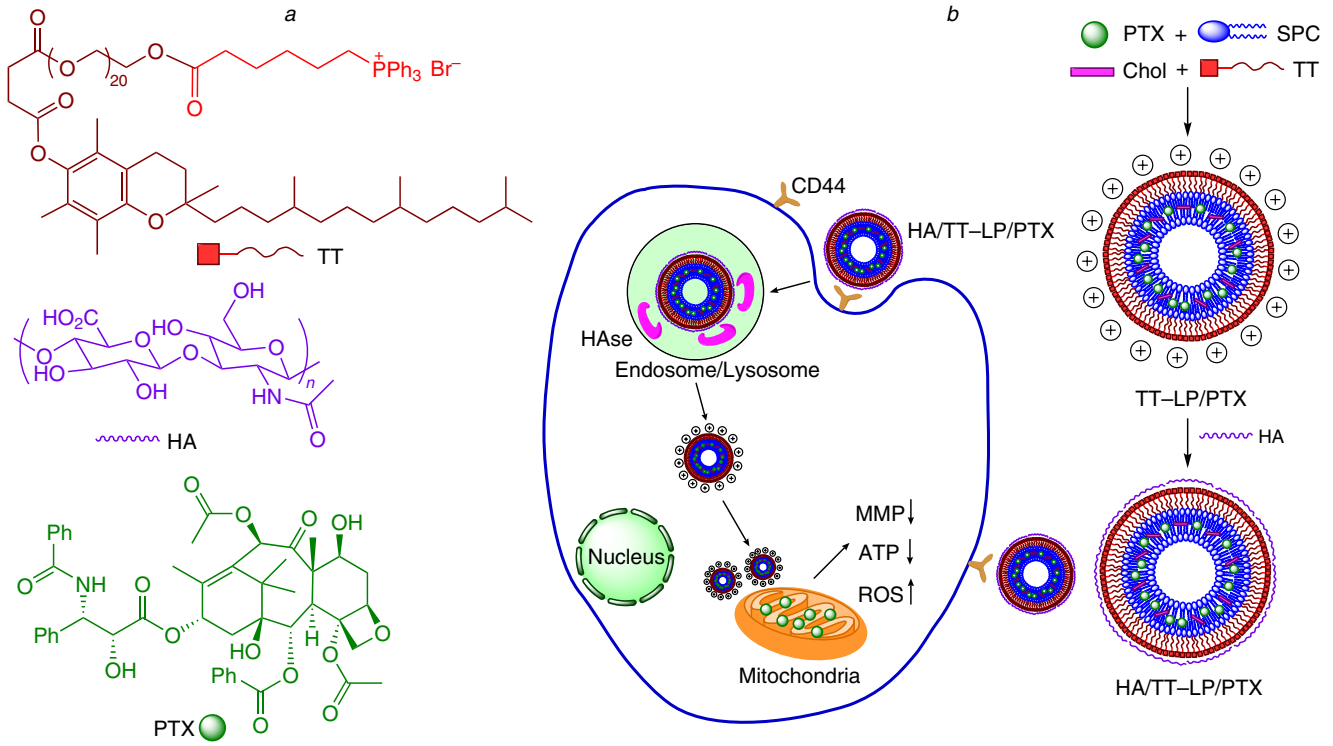

Figure 17. Composition of (*a*) HA/TT–LP/PTX nanoparticles and (*b*) mechanism of their action on mitochondria. The Figure was created by the authors using published data.[125]

respectively; ζ-potentials were +5.5, +39.7 and –30.3 mV. Both empty and PTX-loaded liposomes demonstrated good biocompatibility (the hemolysis was <5%). It was shown that hyaluronic acid improves the cellular uptake of PTX in drug-resistant A549/T cells through CD44 receptor-mediated endocytosis followed by degradation by hyaluronidase (HAse) in endosomes and promotes drug accumulation within the mitochondria (see Fig. 17). As a result, the mitochondrial function in A549/T cells is disturbed, which increases ROS level, decreases ATP level, decreases MMP and enhances the cell cycle arrest in the G2/M phase. In other words, paclitaxel loaded in liposomes exhibits higher antitumor activity than the free drug. The IC_{50} values for LP/PTX, TT–LP/PTX and HA/TT–LP/PTX particles in the A549 cells were 17.4, 8.9 and 7.1 μg mL^{-1}, respectively; in the case of A549/T cells, these values were 57.7, 29.4 and 28.3 μg mL^{-1}, respectively.

4. Solid lipid nanoparticles and nanoemulsions decorated with triphenylphosphonium

Solid lipid nanoparticles (SLNs) are obtained from natural lipids that are solid at room temperature and the degradation products of which cannot affect extra- or intracellular medium. The preparation of SLNs does not require an organic solvent, which makes such drug delivery systems in demand for the treatment of complex disorders. Han *et al.*[126] achieved an increase in the efficiency of targeted drug delivery by modifying SLNs with two conjugates: DSPE–PEG_{2000}–RVG29 (RVG29 is rabies virus glycoprotein) and TPP–DSPE–PEG (Fig. 18). The latter compound was also synthesized in other studies[109–111] with a minor change in the reaction conditions. Nanoparticles were coated by a macrophage (MA) membrane prepared from mouse-derived peritoneal macrophages with high expression of F4/80 and CD11b cells.

Modification with the above conjugates promoted internalization of TPP–MA–SLN–Cou6 [Cou6 is 3-(2-benzothiazolyl)-7-(diethylamino)coumarin], RVG/MA–SLN–Cou6 and RVG/TPP–MA–SLN/Cou6 particles into differentiated HT22 neurons compared to MA–SLN–Cou6 particles. The introduction of a TPP group into biomimetic nanosystems changed the surface charge of nanoparticles, thus increasing their association and cellular uptake. The targeted delivery of genistein (GS) with RVG/TPP–MA–SLN–GS particles alleviated the symptoms of Alzheimer's disease in mice in *in vivo* experiments and changed the biochemical indicators of glial cell functioning in *in vitro* assays. A combination of RVG29 and TPP moieties synergistically improved the nanoparticle transport through the blood–brain barrier into the target neurons, thus promoting the genistein delivery to the neuronal mitochondria *in vivo*.

Karunanidhi *et al.*[127] developed SLNs containing TPP groups and the extract of *Ficus religiosa* L with the goal to normalize the mitochondrial function in oxidative stress-induced diabetes. The particle surface treated with this extract was modified by incubation in a solution of the TPP salt [1 mass (or volume) %][g] for 12 h at room temperature. The ζ-potential of the TPP–SLN particles was +53.1±3.4 mV, which confirms the presence of TPP groups on the SLN surface. The nanoparticles had a spherical shape and ~200 nm size. The oral administration of these nanoparticles to rats with induced diabetes resulted in improvement of the mitochondrial function by normalizing the mitochondrial morphology, intracellular concentration of calcium ions, activity of respiratory complexes I, II, IV and V, the mitochondrial membrane potential and the level of antioxidants. Low contents of apoptosis markers, that is, cytochrome *c*, caspase-3 and caspase-9, were observed. In

[g] The amount of the extract was calculated in wt.% and introduced into a solution of a TPP salt.

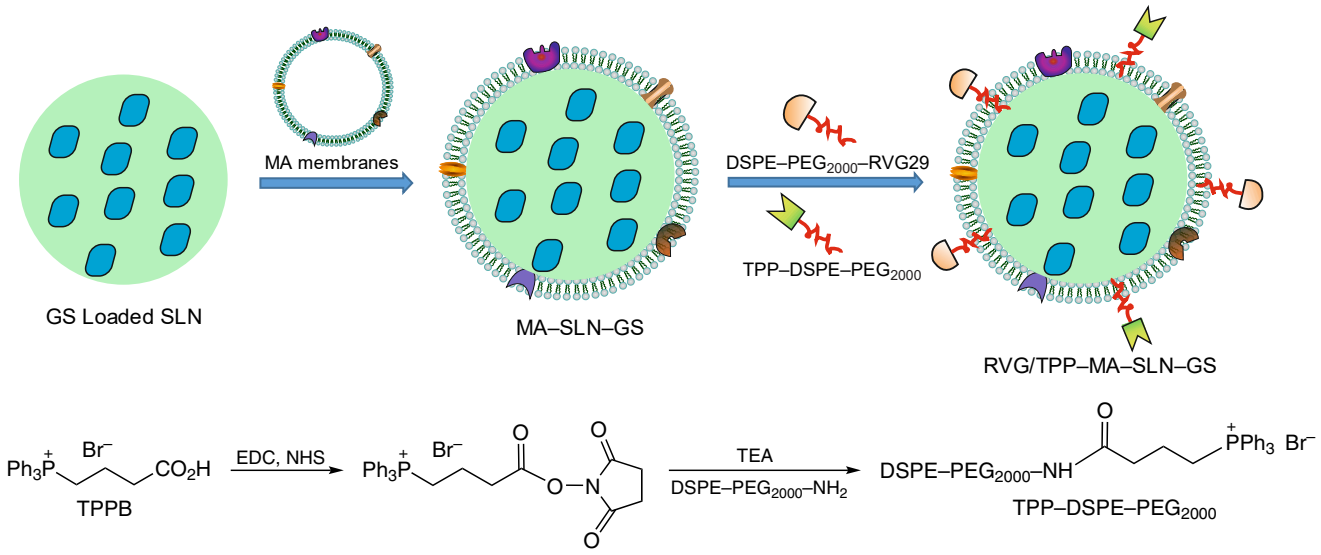

Figure 18. Preparation of lipid nanoparticles modified with DSPE–PEG–RVG29 and TPP–DSPE–PEG conjugates. The Figure was created by the authors using published data.[126]

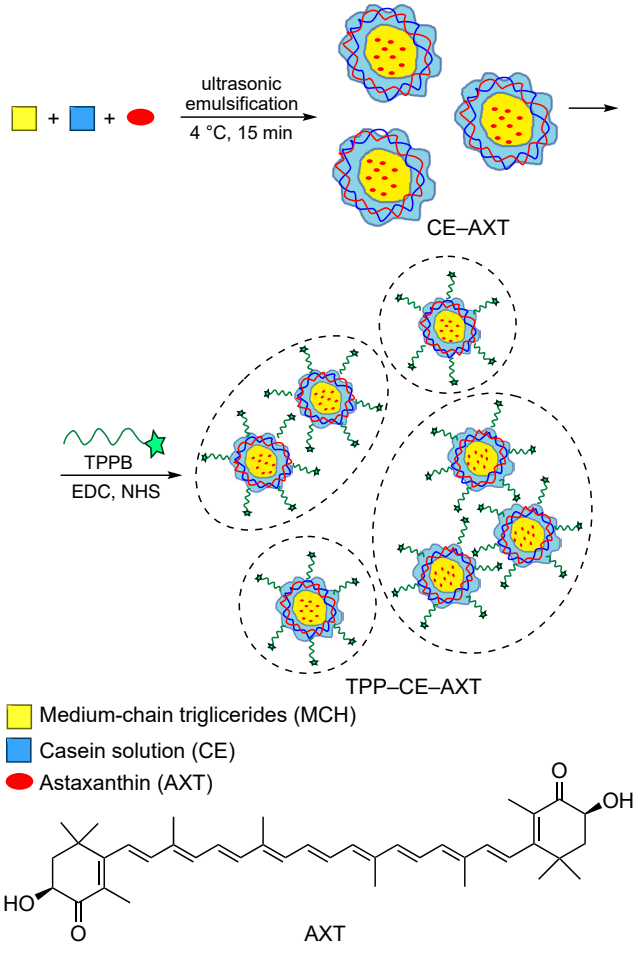

Figure 19. Preparation of TPP–CE–AXT nanoparticles. The Figure was created by the authors using published data.[128]

addition, a considerable decrease in the blood glucose level and glycosylated hemoglobin level was found in rats after the therapy, with a noticeable increase in the amount of insulin in plasma in comparison with these characteristics in the group of untreated diabetic animals.

Astaxanthin (AXT) is a xanthophyll carotenoid with an extended polyunsaturated chain, which has excellent antioxidant activity. This compound was isolated from crustaceans, in particular from shrimps, and was also detected in algae and yeast (Fig. 19). However, AXT is poorly soluble in water, unstable and readily degrades under the action of light, high temperature and oxygen during some treatment or storage. In order to increase the drug bioavailability, stability and efficiency of delivery to the cell, Zhang *et al.*[128] prepared oil-in-water (O/W) emulsions by ultrasonic treatment of medium-length triglycerides (C6–C12), regular casein (CE) and casein modified with (3-carboxypropyl) triphenylphosphonium (TPP–CE).[128] The modification of the casein emulsion with TPP groups was accompanied by increase in the droplet size from 183 (CE) to 535 nm (TPP–CE with 12.5 : 1 component ratio). The hydrodynamic diameter of TPP–CE emulsions with encapsulated astaxanthin (TPP–CE–AXT) was 543 nm, while the ζ-potential was –38.1 mV. According to scanning electron microscopy data, the TPP–CE–AXT particles had a spherical shape. The CE–AXT nanoparticles had a smaller hydrodynamic diameter (227 nm) and ζ-potential of –47.93 mV. The encapsulation efficiency for the CE–AXT and TPP–CE–AXT agents was 88.51 ± 1.85 and 80.51 ± 6.29%, respectively. After encapsulation, the thermal stability and UV stability of AXT were markedly improved. Astaxanthin encapsulated into the TPP-modified nanocarriers protected the mitochondrial membrane from depolarization in normal rat kidney (NRK) cells after their oxidative damage. Analysis of the cell viability showed that TPP–CE–AXT accelerated the growth of the NRK and RAW264.7 cells (leukemia virus-transformed murine macrophages) with respect to astaxanthin encapsulated in a regular casein emulsion.

5. Mitochondriotropic dendritic and polymer nanoparticles

Targeted drug delivery systems based on polymer nanoparticles have their own features, including perfect biocompatibility, flexible design and specific preparation techniques.[129]

5.1. Synthetic polymer systems modified with triphenylphosphonium

5.1.1. Mitochondria-targeted dendritic systems

5.1.1.1. Dendrimers based on polyamidoamines

The conjugation of drugs with polyamidoamine (PAMAM) dendrimers is used to increase drug solubility and improve delivery within the body. Unlike the self-assembling nanocarriers, the stability of which depends on the concentration, dendrimers retain their structural integrity in biologic media. PAMAM dendrimers are widely used as non-viral gene delivery vectors. The PAMAM–nucleic acid complexes with an overall positive charge can leave endosomes and ensure effective transfection. Since PAMAM dendrimers with generation number > 5 (abbreviated as G5D) have a high positive surface charge, they can spontaneously bind nucleic acids through electrostatic interaction.[130] Functionalization of dendritic polymers with TPP groups gave targeted systems, which efficiently delivered DS to the cell mitochondria *in vitro*.[77]

Biswas *et al.*[131] synthesized a TPP-conjugated fluorescence-labelled acetylated PAMAM dendrimer and performed its targeted delivery to mitochondria (Fig. 20).[h] The charge of the initial G5D dendrimer was higher than the charge of the product, and it was more efficiently associated with anionic cell membranes and surface membrane proteins.

Bielski *et al.*[132] investigated the effect of the type of conjugation between the TPP group and PAMAM fourth generation dendrimer (G4D) modified with amino groups and fluorescein moieties, *i.e.*, whether it is direct binding (TPP–G4D) or binding *via* a flexible PEG linker (TPP–PEG–G4D) (Fig. 21). In the former case, no significant dependence of the particle characteristics on the concentration of TPP groups was found: their size was always ~6–7 nm. As the number of TPP groups on the nanoparticle surface increased, the dendrimer surface charge increased to +43 mV (for TPP–PEG–G4D–NH_2–FITC) and +34 mV (for TPP–G4D–NH_2–FITC).[132]

Both types of PAMAM dendrimers provided a pronounced increase in the mitochondria targeting compared to the non-conjugated control.[132] Whereas in the case of direct conjugation, the degree of mitochondria targeting was directly correlated with the number of TPP groups, the conjugation through a PEG linker resulted in a high level of mitochondria targeting for any content of TPP cations; no effect of the degree of PEGylation on the targeting was detected either. In addition, the presence of PEG reduced the toxicity of nanocarriers, while preserving the mitochondrial targeting.

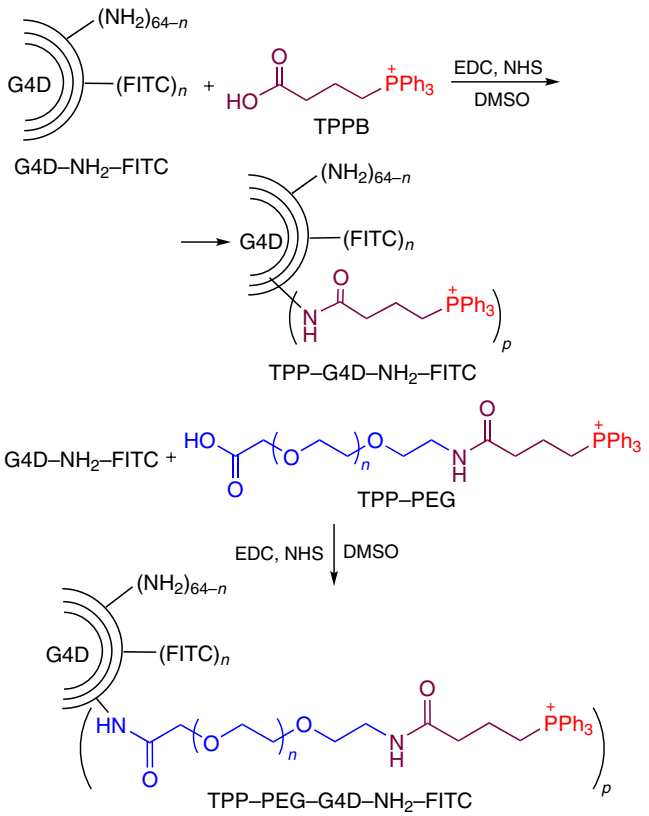

Figure 21. Preparation of TPP-modified PAMAM dendrimers containing a fluorescein moiety. The Figure was created by the authors using published data.[132]

Sharma *et al.*[133] described a PAMAM dendrimer (designated by D in Fig. 22) with peripheral OH groups containing

[h] MWCO means molecular weight cut-off: the lowest molecular weight at which 90% of the molecules are retained by the membrane.

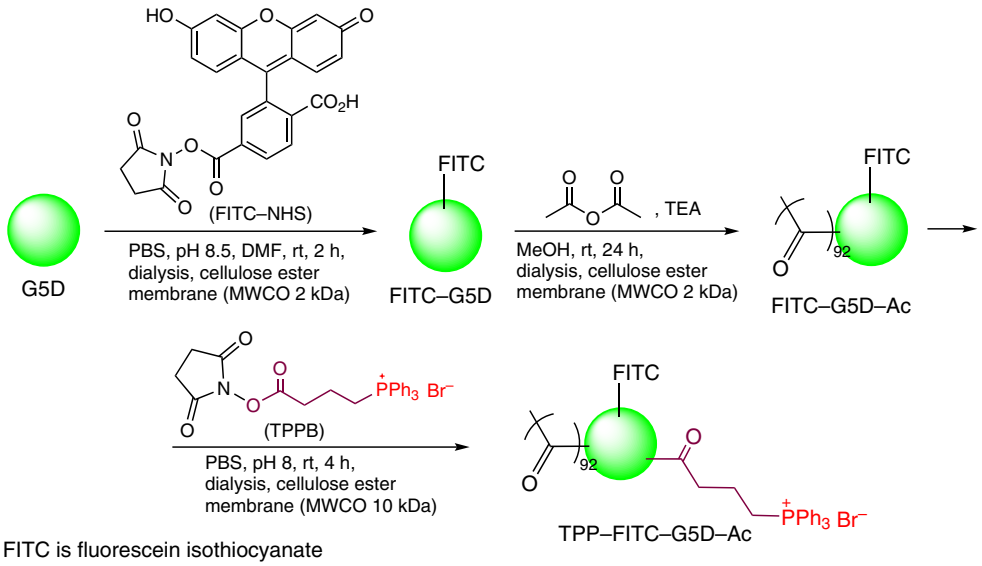

Figure 20. Preparation of TPP-conjugated fluorescence-labelled acetylated PAMAM dendrimer. The Figure was created by the authors using published data.[131]

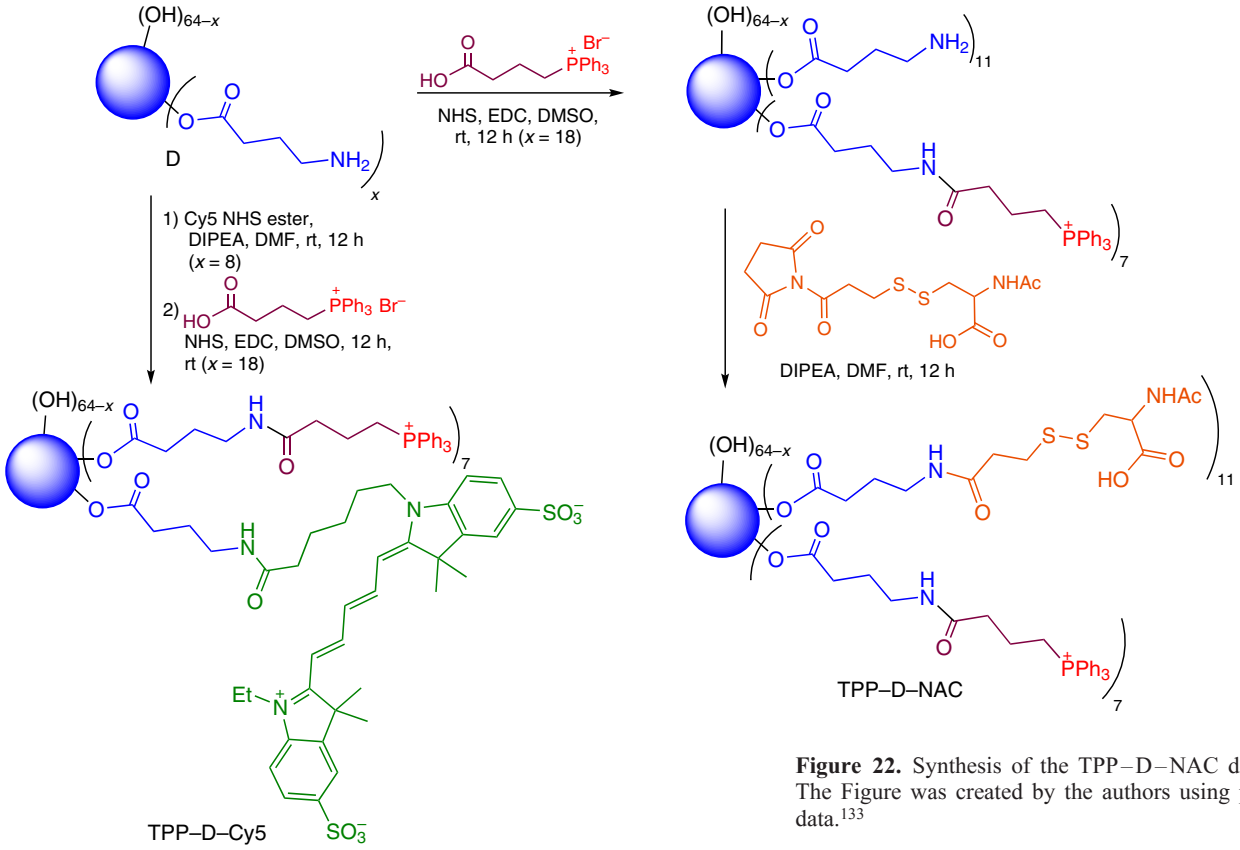

Figure 22. Synthesis of the TPP–D–NAC dendrimer. The Figure was created by the authors using published data.[133]

γ-aminobutyric acid residues, which were modified with TPP groups. This dendrimer was used to synthesize mitochondria-targeted TPP–D–NAC system with a disulfide linker meant for the delivery of *N*-acetylcysteine (NAC). This drug is used in clinical practice as an antioxidant and anti-inflammatory agent. Systemic administration of NAC to laboratory rats resulted in its localization, together with mitochondria, in activated mi/ma cells in the white matter of ipsilateral brain injury [traumatic brain injury (TBI) model]. The targeted delivery of this drug as a part of TPP–D–NAC particles resulted in a considerable decrease in the oxidative stress compared to that for NAC-loaded dendrimer or free NAC. The TPP–D–Cy5 dendrimer containing the cyanine dye Cy5 was also prepared for visualization of the mitochondrial targeting. Successive grafting of the cyanine dye and a 3-(carboxypropyl)triphenylphosphonium moiety to the dendrimer D was performed *via* coupling reactions. Like the TPP–D–NAC system, the TPP–D–Cy5 system exhibited similar properties, indicating high potential for the therapy of oxidative stress at the site of injury *in vivo*.

5.1.1.2. Oligolysine-based nanosystems

It is known that linear, branched and dendritic systems based on polyethylenimine and poly(L-lysine) (PL) are widely used for the targeted delivery of nucleic acids within the body.[134,135] The TPP moiety was attached to the primary amino groups of the biodegradable oligo(L-lysine) through a lipophilic spacer; this gave the modified TPP–PL polymer.[136] In the next stage, for the mitochondrial delivery of D-luciferin (Luc), the firefly luciferase substrate, D-luciferin was covalently bound to the TPP–PL

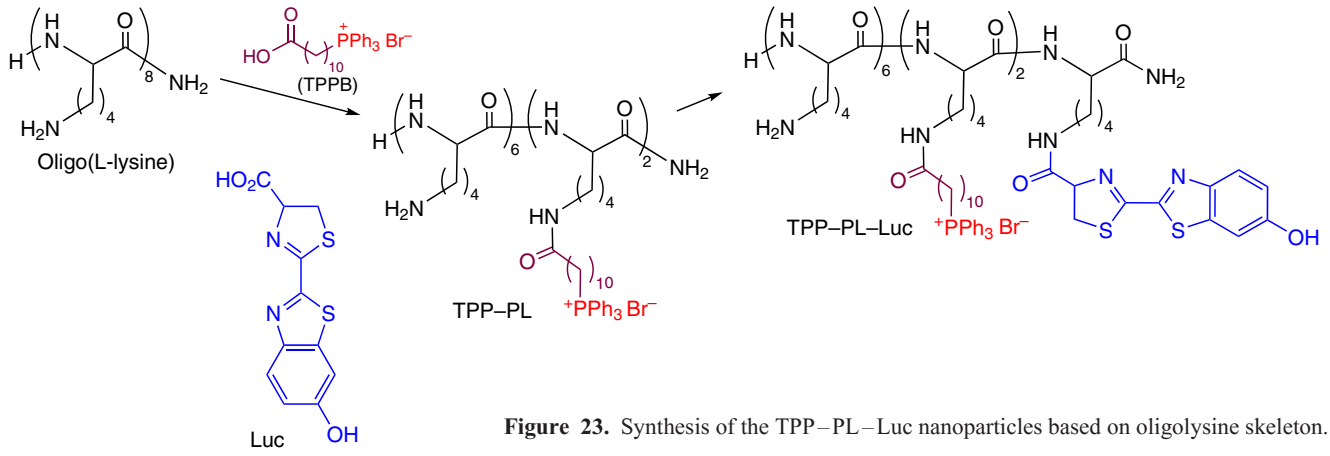

Figure 23. Synthesis of the TPP–PL–Luc nanoparticles based on oligolysine skeleton.

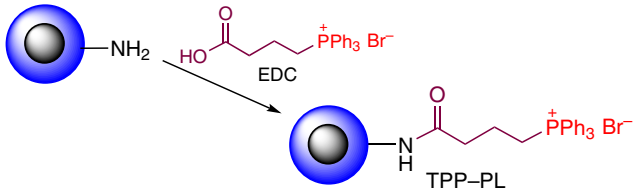

Figure 24. Synthesis of TPP–PL nanoparticles.

polymer, which gave the TPP–PL–Luc nanoparticles (Fig. 23). The TPP–PL–Luc system provided a highly efficient delivery of the covalently bound D-luciferin to the mitochondria of human prostatic carcinoma (DU145) cells.

Wang *et al.*[137] introduced a TPP moiety to the nanoparticle surface *via* carbodiimide reactions of TPPB with the polylysine amino groups (Fig. 24). This was done using four types of PL with different molecular weights (MW = 1.5–3, 4–15, 30–70 and 150–300 kDa), which influenced the size and morphology of the resulting nanoparticles. All TPP–PL nanoparticles had a high ζ-potential (>+45 mV). However, their cytotoxic effect proved to be relatively low, although efficient cellular uptake and free release from endosomes were established for these polymers using the Cou6 fluorescence probe and confocal laser scanning microscopy.

5.1.1.3. Branched polyethyleneimines

Hyperbranched polyethyleneimine (PEI) was functionalized with a TPP moiety (Fig. 25) using *N*,*N*,*N*′,*N*′-tetramethyl-*O*-(1*H*-benzotriazol-1-yl)uronium (HBTU) hexafluorophosphate, 1-hydroxybenzotriazole (HOBt) and diisopropylethyamine.[138] The TPP–PEI polymer was insoluble in water, but was able to form nanoparticles of ~100 nm diameter in a phosphate buffered saline. These nanoparticles were loaded with doxorubicin, and then the resulting TPP–PEI–DOX system was injected into DU145 cells.

The ζ-potentials of TPP–PEI and TPP–PEI–DOX nanoparticles were +14±1 and +40±1 mV, respectively. The toxicity of the TPP–PEI carrier was found to increase with time, being <25% depending on the concentration (in the 1–5 μM range), whereas the PEI–TPP–DOX system had a ~100% toxicity in the same concentration range at any time point (24, 48 and 72 h). It is evident that the delivery of the therapeutic agent directly into the mitochondria of cells significantly increased its antitumor activity. In addition, it was shown that the mechanism of cell death changed from slow apoptosis in the case of free DOX to fast necrosis when modified nanoparticles were used.[138] The authors noted that acute necrotic process induced by the TPP–PEI–DOX nanoparticles had certain advantages, for example, the potential for activation of the inflammatory response. Unlike apoptosis in which cells die 'quietly', necrosis can act as a 'loud' immune distress signal.

Doxorubicin or the chloroquine (CQ) chemosensitizer were encapsulated into the TPP–PEI nanoparticles obtained from hyperbranched PEI (MW = 1300 Da) as depicted in Fig. 25. Chloroquine efficiently acts on the response of malignant tumors to the cellular stress.[139] The TPP–PEI–DOX nanoparticles in an aqueous dispersion had a hydrodynamic radius of 30–35 nm, and the amount of encapsulated DOX was 50 μM for a content of the starting nanoparticles in the dispersion of 1 mg mL^{-1} with a loading capacity of 3 mass%. The TPP–PEI–CQ nanoparticles obtained in the same way had a hydrodynamic radius of 50–55 nm and a concentration of 300 μM in a dispersion containing 1 mg mL^{-1} of TPP–PEI nanoparticles (9% loading). The authors evaluated the anticancer activity of both types of nanoparticles *in vivo* against two DOX-resistant aggressive cell lines, DU145 and PC3 (prostate cancer). The co-administration of encapsulated DOX and CQ gave rise to enhanced inhibition of cell proliferation at extremely low concentrations of the former (0.25 μM). Experiments *in vivo* with DU145 cells grafted on immunodeficient SCID mice resulted in arrest of the tumor growth during a three-week administration period. In addition, the combined use of the TPP–PEI–DOX and PEI–TPP–CQ particles was not accompanied by side effects frequently observed upon the use of either free DOX or the TPP–PEI–DOX system.

It is known that cancer stem cells (CSC) play a key role in the appearance and progression of tumors and in the development of drug resistance. The viability of such cells is affected by impaired autophagy. Stagni *et al.*[140] studied the effect of the mitochondriotropic TPP–PEI nanocarrier ($d \approx 35$ nm) and the chloroquine-containing TPP–PEI–CQ particles ($d \approx 60$ nm) on breast cancer cell lines (MCF-7, MDA-MB-231 and SK-BR-3), which were grown as either adherent cells or as mammospheres mimicking a stem-like phenotype. In addition, TPP–PEI–Rhd nanoparticles were obtained by the reaction of TPP–PEI with rhodamine B isothiocyanate (Rhd) in 3:1 molar ratio. Using a similar procedure, the nanoparticles were converted to chloroquine-containing TPP–PEI–Rhd–CQ systems. These systems provided reliable evidence for the mitochondrial

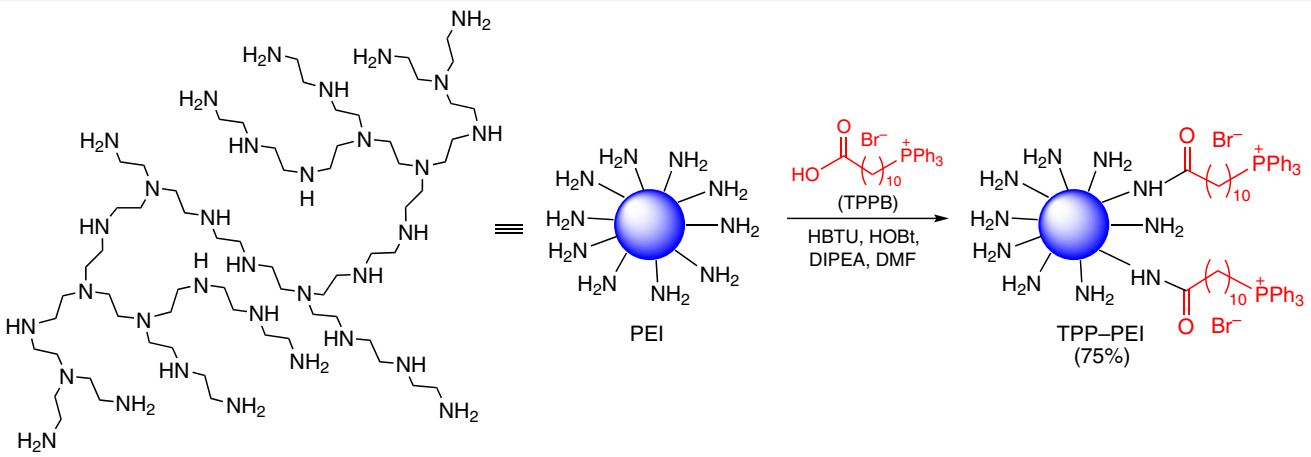

Figure 25. Synthesis of TPP–PEI nanoparticles. The Figure was created by the authors using published data.[138]

localization of this agent. The TPP–PEI nanocarrier exhibited a fairly high cytotoxicity both directly and after encapsulation of CQ, a known inhibitor of autophagy. The TPP–PEI and TPP–PEI–CQ nanoparticles were found to induce to equal extents the formation of mitochondrial superoxide (indicator of mitochondrial stress) in adherent MCF-7 cells. The authors noted a greater selective sensitivity of mammospheres to chloroquine encapsulated in the TPP–PEI carrier (~40–80% decrease in cell viability) compared to adherent MCF-7 cells (~20–40%), which is associated with the expression of ATM-kinase[i] in mammospheres and does not depend on the status of the p53 tumor suppressor gene.

ATM kinase is a key protein mediating the DNA damage, which binds to the damaged site and phosphorylates various target proteins that induce a cellular response. Hence, inhibition of this enzyme has become an attractive concept for the treatment of cancer, since it increases the sensitivity of tumor cells to chemotherapeutic agents. The action of ATM is associated with regulation of mitochondrial functions, including mitophagy. It is known that 2-(morpholin-4-yl)-6-(thianthren-1-yl)pyran-4-one (commercial code KU-55933, KU) is an ATM inhibitor, reducing the mitochondrial membrane potential and disrupting the tricarboxylic acid cycle and OXPHOS.[141] The KU agent loaded into TPP–PEI nanoparticles endows them with solubilizing properties, despite the lipophilic nature of phosphonium substituents. Stagni *et al.*[142] demonstrated the potential of TPP–PEI particles (see Fig. 25) in which KU was encapsulated for mitochondria targeting and for sensitization of mammospheres considered as a model system for breast cancer stem cells. The drug content in TPP–PEI–KU nanoparticles ($d \approx 60$ nm) was 28.3 mass%, which corresponded to a concentration of 1 μM for a solution of 1 mg mL of empty TPP–PEI nanoparticles ($d \approx 55$ nm) formed under the same conditions. The authors showed that encapsulated KU was effective against chemotherapy-resistant mammospheres of MCF-7 breast cancer cells, while possessing comparatively lower cytotoxicity against adherent cells grown as monolayers. It was also noted that the encapsulated drug significantly increased the sensitivity of mammospheres to DOX, but had only a slight effect on MCF-7 adherent cells. The co-administration of TPP–PEI–KU nanoparticles and DOX considerably decreased the viability of cancer cells (by 50% when DOX concentration was 1 μM and by 80% when the DOX concentration was 10 μM). Thus, triphenylphosphonium-functionalized drug delivery systems containing encapsulated KU form a useful addition to chemotherapeutic protocols for the treatment of proliferative cancer.

[i] ATM (ataxia telangiectasia-mutated serine threonine protein kinase) is an enzyme functioning as an important signaling mediator that provides growth of cancer stem cells through regulation of autophagy.

5.1.2. Poly(ε-caprolactone) nanoparticles

Cho *et al.*[143] reported covalent binding of two 3-carboxybutylphosphonium bromide molecules to biocompatible and biodegradable poly(ε-caprolactone) (PCL); this gave amphiphilic polymer TPP–*b*–PCL–*b*–TPP (abbreviated as TPCL) (Fig. 26).

The morphology of TPCL nanoparticles depended on the method of preparation: dispersion in a solvent or film hydration. The former method gave nanofiberes of 8–9 nm size, while in the latter case, nanovesicles of 50–200 nm size were obtained. The nanoparticle ζ-potential was +40 mV. Both hydrophobic DOX and the hydrophilic form DOX·HCl were encapsulated in TPCL; the concentration of the drug was ~2–10 mass%. The nanoparticles containing doxorubicin hydrochloride showed higher mitochondrial uptake (2–7-fold) and enhanced antitumor activity (7.5–18 times lower IC_{50}) than the free drug.[143]

Micelles of star-like PCL polymer with a PEG corona, with TPP groups incorporated in the molecule (Fig. 27) were used to deliver coenzyme Q10 (CoQ10) to mitochondria.[144]

The TPP–PEG–PCL micelles with a diameter of 51.7±7.6 nm and ζ-potential of +12.1 mV were obtained by evaporation of the co-solvent (acetone). The polymer and the coenzyme were dissolved in acetone, and this solution was added dropwise with stirring to deionized water. Then the mixture was stirred in the dark for 24 h for acetone evaporation and micelle formation. The particle diameter increased when CoQ10 was incorporated into the micelle core. The accumulation of coenzyme-bearing micelles in mitochondria was observed by confocal microscopy using a FITC probe. An effective antioxidant action of these micelles on hippocampal neuron and glial cell cultures was observed.[144]

Micelles based on the TPP–PEG–PCL polymer (Fig. 28) intended for the mitochondria-targeted delivery of gambogic acid were obtained by analogous evaporation of the co-solvent.[145] Characteristics of these micelles were as follows: $d = 150$ nm, ζ-potential of +11.8 mV and encapsulation efficiency of 8%. The gambogic acid-loaded TPP–PEG–PCL micelles were selectively accumulated in mitochondria, thus

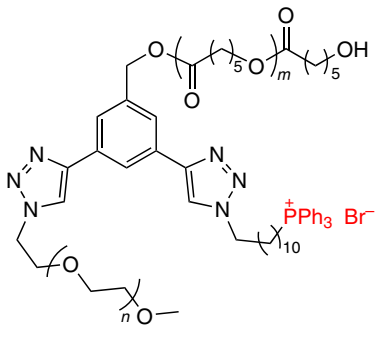

Figure 27. Structure of star-like copolymer of PEG and PCL containing TPP group.

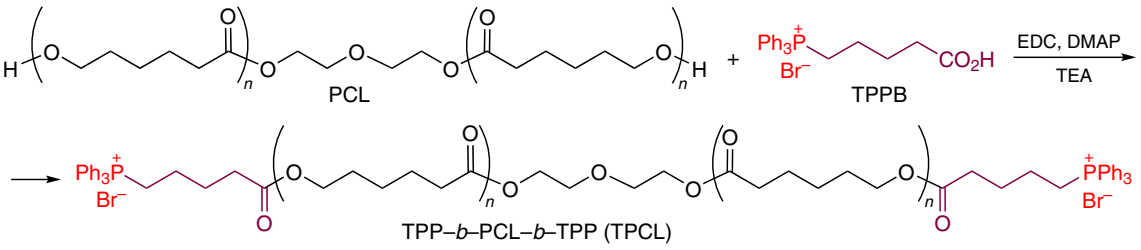

Figure 26. Synthesis of block copolymer with poly(ε-caprolactone) decorated with the TPP groups.

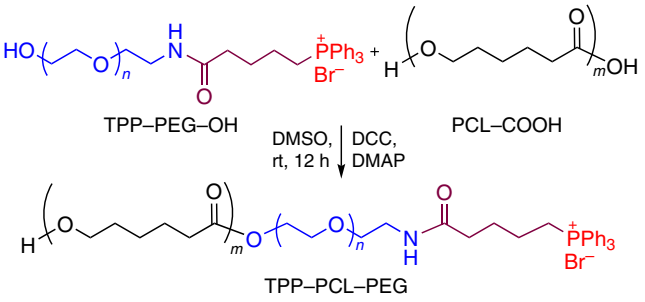

Figure 28. Synthesis of the TPP–PEG–PCL polymer.

decreasing the mitochondrial membrane potential and inducing release of cytochrome *c*. The enhancement of their antioxidant effect on cells was attained by induction of apoptosis *via* the mitochondrial signaling pathway.[145]

5.1.3. Polyanhydride-based nanoparticles

Polyanhydrides are biocompatible and biosafe materials serving for the delivery of drugs to various sites such as brain, bones, vessels and eyes. In the body, polyanhydrides decompose to form non-toxic analogues of dicarboxylic acids and are excreted as metabolites.[146,147]

Schlichtmann *et al.*[148] synthesized nanoparticles based on polyanhydride containing TPP group by nanoprecipitation (Fig. 29). First, the targeting ligand [(3-carboxypropyl)-triphenylphosphonium bromide] was acetylated with anhydride and then allowed to react with polyanhydride under standard conditions. Flash nanoprecipitation of this polymer afforded either non-functionalized nanoparticles (NPs) bearing COOH groups or nanoparticles with TPP-functionalized terminal groups.

The obtained particles were spherical and uniform and had a diameter in the range of 300–400 nm. When the nanoparticles were functionalized with TPP groups, the ζ-potential changed from negative values to zero. According to confocal microscopy data, the nanoparticles were internalized rather than were merely bound to the cell membrane of mesencephalic neurons of rats (N27). The treatment of cells with non-functionalized nanoparticles containing mitochondria-targeted metformin (Mito-MET) in 30 nm concentration, reduced the rotenone-induced toxicity, but did not lead to a noticeable decrease in cell death. However, the use of TPP-functionalized nanoparticles containing Mito-MET in the same concentration considerably improved protection of the cells from the rotenone-induced damage.[148]

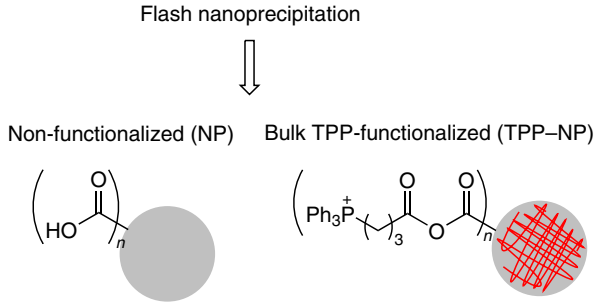

Figure 29. Synthesis of nanoparticles based on polyanhydride with (3-carboxypropyl)triphenylphosphonium. The Figure was created by the authors using published data.[148]

Apocynin conjugated with a TPP moiety (Mito-Apo) is an antioxidant that protects dopaminergic neurons both in the primary culture and in an animal model in the presence of a potent dopaminergic toxin.[149] This compound is of interest as a promising a neuroprotective drug for the treatment of Parkinson's disease.[149] Polyanhydride-based nanoparticles were loaded with 5 mass% Mito-Apo;[150] the resulting systems provided an excellent protection of neuronal cells (N27 rat mesencephalic neurons and primary cortical neurons) from the mitochondrial dysfunctions and damages induced by oxidative stress.

5.2. Natural polymers (biopolymers) modified with triphenylphosphonium

The preparation of DS-loaded capsules based on natural polymers is of considerable interest for biomedicine, because biomacromolecules are highly biocompatible and have excellent biodegradability.

5.2.1. Polydopamine-based nanoparticles

Polydopamine (PDA) is a major structural component of one of the melanin types present in the body (eumelanin). The design and use of biocompatible nanoparticles based on PDA is a vigorously developing trend of biomedical research.[151,152] The synthesis of TPP–PDA–PEG nanoparticles by ammonia-catalyzed polymerization in an oil-in-water microemulsion has been reported[153,154] (Fig. 30, ψ_m is the mitochondrial membrane potential).

The PDA–PEG nanoparticles and their TPP-modified analogues had a similar morphology and size (~28 nm), and the latter did not possess a significant cytotoxicity. The delivery of DOX by PDA-based nanoparticles to cell mitochondria depended on the nanoparticle type. The PDA–PEG–DOX particles were accumulated in lysosomes to a higher extent than their TPP derivatives. However, both the PDA–PEG–DOX and TPP–PDA–PEG–DOX systems induced apoptosis of breast cancer cells (MDA-MB-231) for 24 h to approximately equal

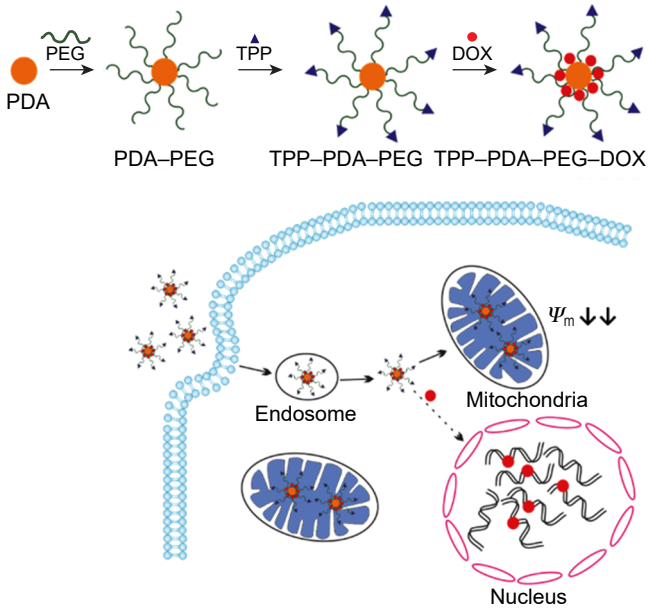

Figure 30. Preparation of TPP–PDA–PEG nanoparticles and delivery of DOX to mitochondria. The Figure was created by the authors using published data.[153,154]

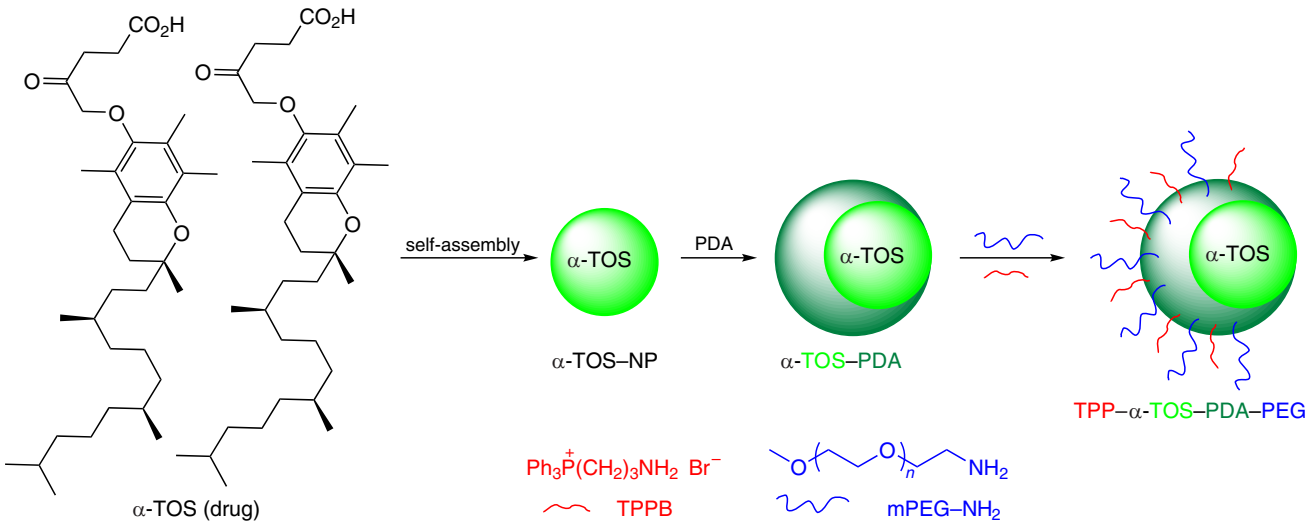

Figure 31. Synthesis of the TPP–α-TOS–PDA–PEG nanoparticles. The Figure was created by the authors using published data.[155]

extents. To mimic the clinical therapy with anticancer drugs, Li *et al.*[153] repeatedly treated the MDA-MB-231 cancer cells with doxorubicin encapsulated into PDA–PEG and TPP–PDA–PEG carriers for 48 h. It was found that the mitochondrial membrane of the cells was destroyed by both the former and the latter. However, the TPP–PDA–PEG–DOX particles caused more severe damage to the mitochondrial membrane in the mentioned cells and, hence, they had a higher potential for overcoming the drug resistance to doxorubicin.

Meng *et al.*[155] proposed TPP-functionalized α-TOS–PDA–PEG nanoparticles (α-TOS is α-tocopheryl succinate) for the delivery of PDA as a photothermal agent and α-TOS as a chemotherapeutic agent to the cancer cell mitochondria. The authors expected a synergistic effect of chemotherapy and photothermal therapy (PTT) for tumor growth inhibition. First, PDA was deposited on the surface of α-TOS nanoparticles formed upon self-assembly (Fig. 31), and then the resulting particle surface was treated with PEG to increase the blood circulation time. In *in vitro* assays, the TPP–α-TOS–PDA–PEG nanoparticles were efficiently taken up by tumor cells and accumulated in mitochondria, which induced apoptosis and synergistic inhibition of cell proliferation. *In vivo* experiments showed efficient accumulation of the same nanoparticles at the tumor location sites and the inhibition of tumor growth under irradiation in the near-IR (NIR) range without obvious toxicity.

5.2.2. Nanoparticles based on the copolymer of lactic and glycolic acids

Drug delivery systems based on the biodegradable copolymers of lactic and glycolic acids (PLGA) are well known; some carriers of this type are already used in clinical practice for the therapy of non-mitochondrial diseases.[156,157] The synthetic route to the PLGA–*b*–PEG copolymer modified with TPP groups is depicted in Fig. 32.[103,158] Nanoparticles based on PLGA–*b*–PEG–OH and TPP–PLGA–*b*–PEG copolymers with different size and surface charge were prepared by nanoprecipitation. As a rule, the preparation procedure of diblock copolymers such as PLGA–PEG includes the dissolution of the components in a solvent miscible with water (for example, acetonitrile) and the subsequent dropwise addition of this solution into an aqueous solution. The maximum mitochondrial uptake was observed for nanoparticles of 80 and 100 nm in diameter and was higher when positively charged samples were used. The cellular uptake increased as the surface charge of nanoparticles reached +1.3 mV and then remained constant up to +22 mV.

Other compounds such as curcumin, 2,4-dinitrophenol, LND and α-TOS were encapsulated into PLGA–*b*–PEG–OH and TPP–PLGA–*b*–PEG nanoparticles in a similar way.

The most pronounced neuroprotective action compared to the starting PLGA–*b*–PEG copolymer and free curcumin was observed in the case of curcumin encapsulated into TPP–PEG–*b*–PLGA nanoparticles. The IC_{50} value for the LND drug loaded in the TPP–PEG–*b*–PLGA nanoparticles was four times lower than that for the non-modified PLGA–*b*–PEG copolymer and 108 times lower than that for the free drug. The highest cytotoxic effect was detected for α-TOS encapsulated into the TPP–PEG–*b*–PLGA nanoparticles (IC_{50} = 75±2 nm). Similar particles loaded with 2,4-dinitrophenol inhibited the differentiation of the 3T3-L1

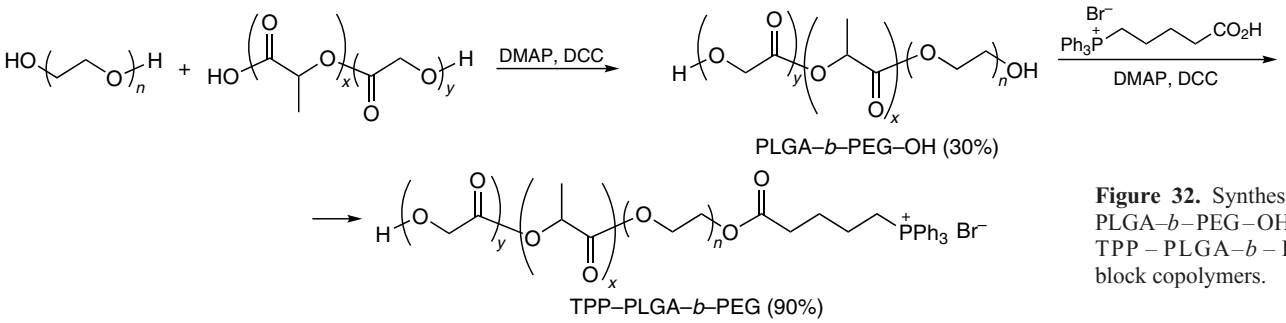

Figure 32. Synthesis of PLGA–*b*–PEG–OH and TPP – PLGA–*b* – PEG block copolymers.

cells to adipocytes at concentrations of 1 and 4 μM and did not exert a cytotoxic effect.[158] The same polymer systems with a photosensitizer, zinc phthalocyanine (ZnPhc), were used for *ex vivo* engineering of mitochondria-targeted nanoparticles for cancer immunotherapy, namely for the production of gamma-interferon. The ZnPhc complex was encapsulated into TPP–PEG–*b*–PLGA nanoparticles (65 to 75 nm size; ζ-potential of +24 to +34 mV) with a high efficiency. A more pronounced phototoxic effect and early apoptosis were observed for the TPP–*b*–PEG–PLGA–ZnPhc system against HeLa and MCF-7 cells.[159] Coenzyme Q10 was also efficiently delivered to mitochondria by the TPP–PEG–*b*–PLGA nanoparticles; this resulted in enhancement of the antioxidant protection of mitochondria in the body's cells upon long-term administration of antiretroviral drugs.[160]

The strategy of increasing the anticancer activity of paclitaxel by redox activation and mitochondria targeting using a lipid–polymer hybrid was reported by Zhou *et al*.[161] This hybrid consisted of PLGA, TPP-containing amphiphilic polymer TPP–C18–PEG_{2000} (abbreviated as CPT) and the DLPE–S–S–$mPEG_{4000}$ polymer (DSSP) sensitive to reduction, which contained 1,2-dilauroyl-*sn*-glycero-3-phosphoethanolamine (DLPE) and PEG linked by a disulfide bridge. Nanoparticles with a size from 150 to 180 nm were obtained from the PLGA–CPT–DSSP polymer by nanoprecipitation. The nanoparticles were nearly neutral (ζ-potential = +2.4 mV) as their surface was shielded by PEG.[162] After the nanoparticles were taken up by tumor cells under reductive conditions, their charge shifted towards positive values (+17.2 mV). The PTX–PLGA–CPT–DSSP system showed a high cytotoxicity *in vitro* (IC_{50} = 1.65 μg mL^{-1}) against MCF-7 cells, which was caused by apoptosis *via* the mitochondria-dependent pathway. It was found in *in vivo* experiments that the PTX concentration in the tumor and in the tumor cell mitochondria 24 h after intravenous administration was higher in the case of mitochondria-targeted nanoparticles than in the case of free PTX or PTX–PLGA–CPT delivery system.[161]

The lipid-based hybrid nanoparticles based on PLGA were obtained using a pH-sensitive hybrid containing anisamide (AA) and PEG as well as hydrated (hydChol) and TPP-modified cholesterols.[163] For the PLGA, AA–PEG–hydChol and TPP-Chol component ratio of 3 : 2 : 3, the greatest doxorubicin loading (5.4%) into 180-nm nanoparticles was observed. The ζ-potential of these particles was –25.3 mV at pH 7.4 and shifted towards positive values (up to +5.8 mV) at pH 5.0, which is attributable to cleavage of the hydrazone bond in the AA–PEG–hydChol conjugate and shedding of the PEG shell. The doxorubicin-loaded nanoparticles had a pronounced hemolytic action on red blood cells at pH 5.0. The cellular uptake of DOX was lower in the human hepatocellular carcinoma cells (HepG2) than in lung adenocarcinoma cells (A549). According to the results of *in vivo* experiments, the anticancer activity of DOX encapsulated in nanoparticles was higher than that of the free drug. In addition, in the latter case, the body weight of mice bearing the tumor considerably decreased, whereas DOX-loaded nanoparticles did not cause a noticeable change in the weight of animals and had a lower systemic toxicity.[163]

In the tumor cells, the outer PEG shell of the nanoparticles consisting of TTP–PLGA–PEG copolymers with encapsulated 10-hydroxycamptothecin (HCPT) was shed.[164] In this case, after opening of the heterocycle in PBS at pH 7.4, the TPP-modified inner shell was exposed. Subsequently, the TTP–PLGA nanoparticles were released from lysosomes, while closed-ring HCPT was delivered to both the nucleus and the mitochondria, which increased the therapeutic efficacy of this agent in the treatment of colorectal cancer.

Qin *et al*.[165] described multifunctional nanoparticles based on PLGA for encapsulation of celastrol, which is released in mitochondria in an alkaline medium. First, the authors reacted TPGS with 6-triphenylphosphoniovaleryl chloride to obtain mitochondria-targeted triphenylphosphonio-α-tocopherol-poly(ethylene glycol) succinate (designated by TT; see Fig. 17) (Scheme 1). Then TT–PLGA@Cela nanoparticles (ζ-potential of +22.3 mV) were prepared by emulsification with PLGA in the presence of celastrol followed by evaporation of the solvent. The positive charge on the TT–PLGA@Cela nanoparticle surface was then neutralized by tumor-targeted pH-sensitive SGP–FA conjugate obtained by the reaction of chondroitin sulfate (SGP) with folic acid (FA) in the NHS–EDC system (see Scheme 1).

The neutralization afforded SGP–FA/TT–PLGA@Cela nanoparticles, which were spherical, had a smooth surface (d = 100 nm, ζ-potential of –20 mV) and were stable at pH 7.4 (Fig. 33). The celastrol loading capacity and encapsulation efficiency were 36.1±2.1% and 75.4±2.8%, respectively. After SGP–FA/TT–PLGA@Cela nanoparticles were taken up by breast cancer cells (4T1), the SGP–FA conjugate degraded in lysosomes (pH 5.0), and the positively charged TT–PLGA@Cela nanoparticles entered mitochondria, and then the anticancer drug was released under the action of the alkaline medium in the mitochondria. Evaluation of the mitochondrial respiration and membrane potential showed that celastrol induced mitochondrial damage. Generally, the action of these nanoparticles on the 4T1 cells markedly increased the expression of the proapoptotic protein *in vitro* and induced stable anticancer effects *in vivo*. The whole set of results demonstrates a high potential of SGP–FA/TT–PLGA@Cela nanoparticles releasing Cela in the mitochondrial alkaline medium for the treatment of breast cancer.

5.2.3. Chitosan-based polymer systems

Chitosan (CS) is a promising biomedical material for chemotherapy.[166] The specificity of chitosan is related to its polycationic structure and the possibility of electrostatic interactions with negatively charged surfaces of infectious agents of the mucous membrane and macromolecules. The products of degradation of this amino carbohydrate are non-toxic, non-immunogenic and non-carcinogenic. Diverse methods for the preparation of CS-based nanoparticles, including the ionic cross-linking with polyanions, covalent conjugation, and emulsion and droplet formation and coalescence extend the scope of CS applicability in various fields. Chemical modification of CS gives rise to water-soluble forms and provides new opportunities for the use of its derivatives in biomedicine. The solubility in water is much higher for esters derived from chitosan, in particular, upon the introduction of the (3-carboxypropyl)triphenylphosphonium bromide substituent into this biopolymer.[167] TPP-grafted chitosan (TPP–g-CS) showed selective toxicity against different cell lines and arrested the migrations of HepG2 liver cancer cells, but did not affect their invasion. In addition, this complex inhibited the growth of H22 tumors *in vivo* in female BALB/c-nu mice and regulated the expression of key inflammatory cytokines VEGF and TNF-α.

Arafa *et al*.[168] proposed an approach to the rational design of mitochondria-targeted core–shell polymer nanoparticles for efficient delivery of doxorubicin (DOX) to HepG2 cell line. First, TPPB was conjugated with 89% deacetylated chitosan

Scheme 1

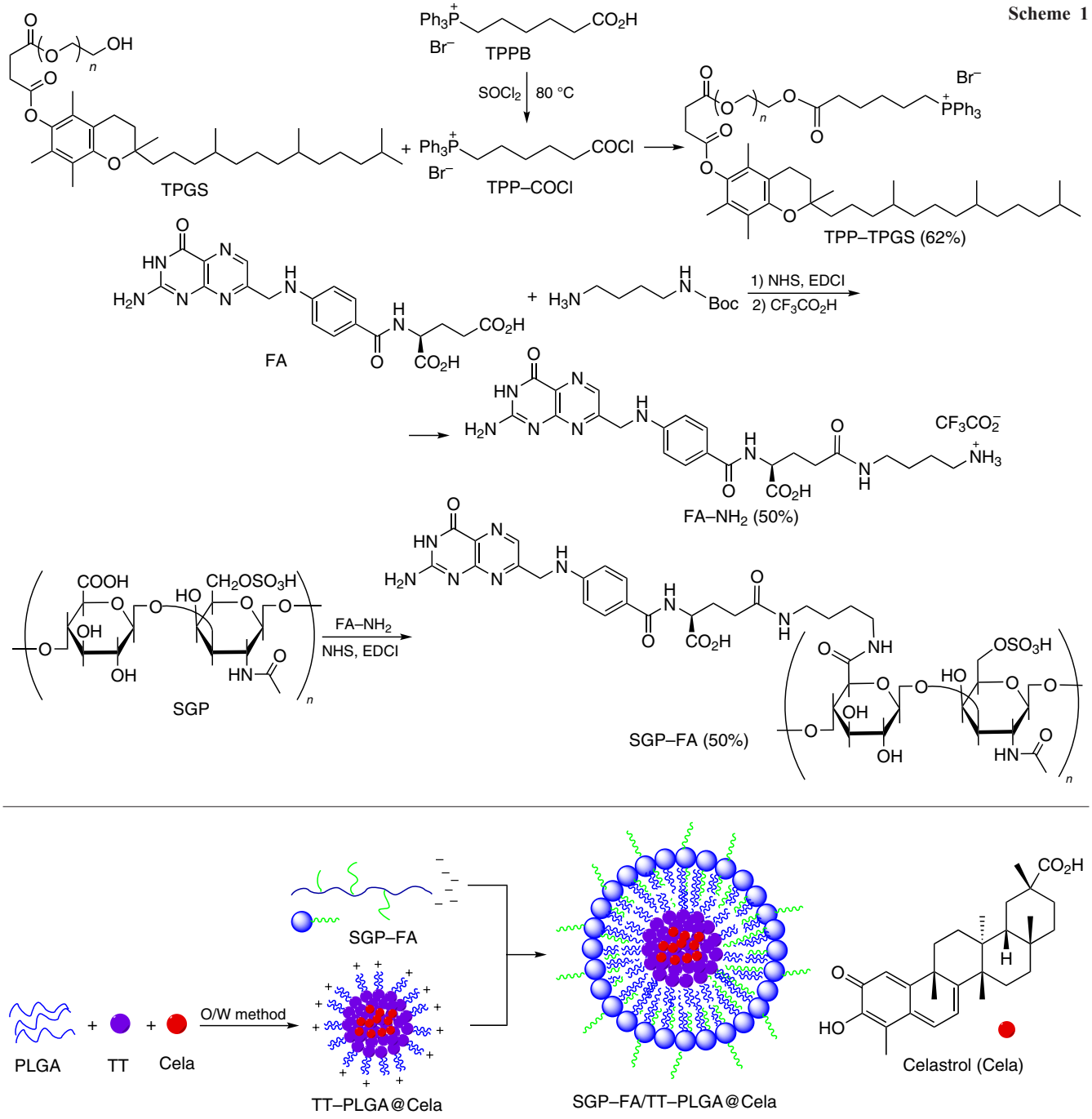

Figure 33. Scheme of formation of TT–PLGA@Cela and SGP–FA/TT–PLGA@Cela nanoparticles on the basis of delivery systems shown in Scheme 1. The Figure was created by the authors using published data.[165]

(MW = 100–300 kDa) to give the TPP–g-CS polymer (Fig. 34). The next step was the preparation of electrostatic complexes of DOX with sodium alginate (SA). Then solutions of the complex and TPP–g-CS polymer were mixed dropwise in 1 : 2 volume ratio and homogenized until the desired concentration of doxorubicin was attained. To increase the stability of nanoparticles, polyvinyl alcohol was added to the polymer solution. The optimal composition of the nanoparticles was as follows (mass% relative to chitosan): TPP–g-CS (0.05), DOX–SA (0.05), polyvinyl alcohol (0.2). The DOX–SA/TPP–g-CS nanoparticles of this composition had a spherical shape and a particle size of 70–110 nm and positive surface charge (the ζ-potential varied from +24 to +34 mV); the DOX encapsulation efficiency reached 63.33±10.18%. The *in vitro* experiments showed that these mitotropic nanoparticles had low IC_{50} equal to 3.86±0.20 μM (for DOX–SA/TPP–g-CS with the DOX : SA mass ratio of 1 : 1 where TPP–g-CS and DOX–SA concentrations were 0.05 mass% relative to chitosan), effectively induced apoptosis and arrested the cell cycle in the G2/M phase. In addition, *in vivo* studies in mice demonstrated high antitumor activity of these nanoparticles along with a reduced profile of biological toxicity.

Arafa *et al.*[169] used the reaction of a polyanion (hyaluronic acid) with the polycation (chitosan) to form nanoparticles for the treatment of cancer. The authors synthesized TPP derivative of doxorubicin, which was encapsulated into HA–CS nanoparticles

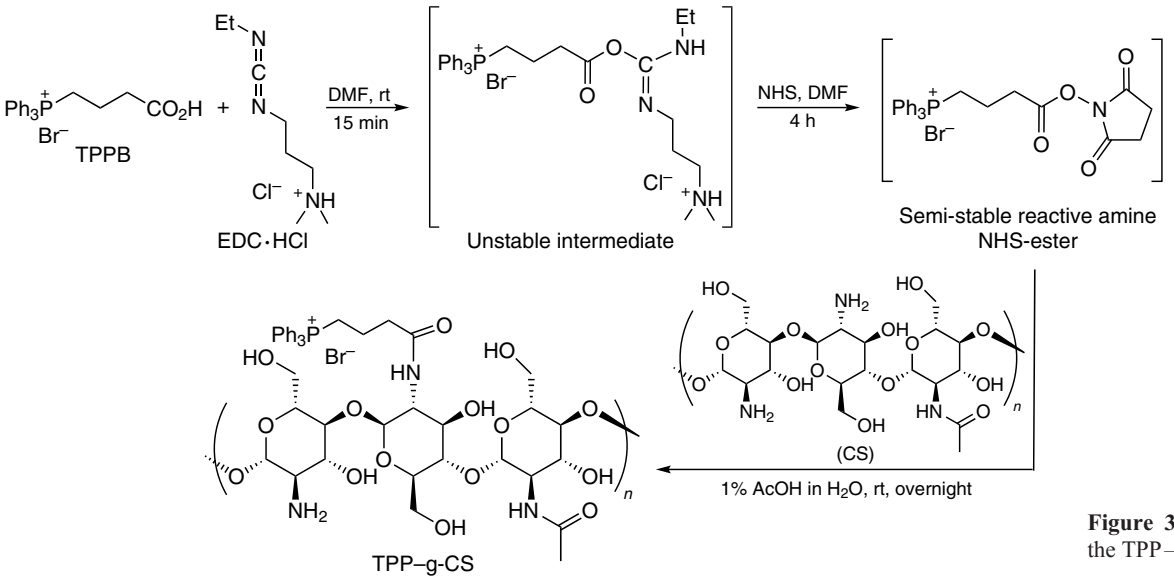

Figure 34. Synthesis of the TPP–g-CS conjugate.

with a size from 220 to 280 nm. The *in vitro* cytotoxicity assay for the resulting systems attested to the induction of apoptosis in the MCF-7 cells and cell cycle arrest. The *in vivo* experiments confirmed high antitumor activity of the TPP–DOX conjugate loaded into HA–CS nanoparticles; in particular, the tumor mass and volume considerably decreased compared to those for the group of mice that did not received the therapy.[169]

5.2.4. Hyaluronic acid-based nanoparticles

Liu *et al.*[170] described the supramolecular HA–*ionic*–TPP–DOX structures based on TPP–DOX derivative and hyaluronic acid, which were self-assembled through the formation of a new ionic bond (this is indicated by the word '*ionic*' in the designation of particles). These structures had a spherical shape with an average diameter of 257 nm (PDI = 0.096) and a ζ-potential of –24.1 mV. The HA–*ionic*–TPP–DOX nanoparticles provided a much higher cellular uptake of the drug, which was accumulated in mitochondria, compared with free DOX. This resulted in higher production of ROS, a minor decrease in the mitochondrial membrane potential and increase in the cytotoxicity against cells resistant to the antibiotic Adriamycin (MCF-7/ADR). In addition, it was found that the antitumor action of the HA–*ionic*–PP–DOX particles on the MCF-7/ADR cells was higher than that induced by the injection of TPP-modified doxorubicin. The HA–*ionic*–TPP–DOX nanoparticles demonstrated a good biocompatibility and a higher efficacy of the treatment of mice bearing MCF-7/ADR tumors than the TPP–DOX conjugate or free DOX.[170]

Hyaluronic acid and TPP–DOX were also conjugated *via* the hydrazone bond formation (the word '*hydra*' is added) using adipic acid dihydrazide (ADH) (Fig. 35).[171] The HA–*hydra*–TPP–DOX nanoparticles had a spherical shape and a size of 192 nm and ζ-potential of –28.8 mV.

The negative charge on the nanoparticle surface, as shown by *in vivo* experiments, promoted their long-term blood circulation and accumulation in the tumors due to the EPR effect. The hydrazone bond is sensitive to changes in the acidity of the medium; therefore, the release of HA–*hydra*–TPP–DOX nanoparticles *in vitro* took place at pH < 7. These nanoparticles were more efficiently accumulated in the tumor and had higher cytotoxic activity and a better safety profile than free DOX.[171]

Lee and Cho[172] prepared loaded HA–TPP–α-TOS nanoparticles based on hyaluronic acid, (4-carboxybutyl) triphenylphosphonium bromide and D-α-tocopherol succinate, meant for the delivery of lapatinib (LPT) to hyaluronic acid receptors (CD44) and to the mitochondria of triply negative breast cancer cells. The obtained particles had a spherical shape (d = 207 nm) and unimodal size distribution, negative ζ-potential and good stability. The ability of HA–TPP–α-TOS/LPT nanoparticles to reach the tumor *in vivo* was demonstrated *via* experiments in mice using real-time optical imaging. It is noteworthy that these nanoparticles demonstrated the best tumor growth inhibition profile in comparison with other agents.[172]

Wang *et al.*[173] described the TPP–HA–SS–Cur polymer based on HA oligomer covalently bound, at one end, directly to the (5-carboxypentyl)triphenylphosphonium bromide and, at the other end, to curcumin (Cur) through a bridge containing a disulfide bond (Fig. 36). On the basis of this polymer, spherical micelles were obtained by dialysis and were used to encapsulate free curcumin.

The size of the Cur/TPP–HA–SS–Cur micelles was 122 nm (PDI = 0.132), while the ζ-potential was −22 mV. The results of studies of these micelles for cellular uptake, localization in mitochondria and cytotoxicity demonstrated that they can interact with the CD44 receptor and are accumulated in mitochondria.[173]

5.3. Polymer micelles with triphenylphosphonium

Micelles based on block copolymers are spherical nano-sized core–shell supramolecular assemblies of amphiphilic macromolecules with a size from 10 to 100 nm.[174,175] The micelle core is a hydrophobic space, which usually accommodates hydrophobic drugs, while the shell is a brush-like protective corona, which provides for the micelle dispersibility in water. The advantages of block copolymer micelles include their relatively small size, high and controllable loading capacity and good biocompatibility. It is possible to prepare such micelles with a large number of functional groups on the surface, for example, TPP groups capable of conjugation with target ligands.

A successful example of using polymer micelles for the drug delivery to cancer cells was reported by Zhang *et al.*[176] A drawback of polymer micelles is the multistage procedure for

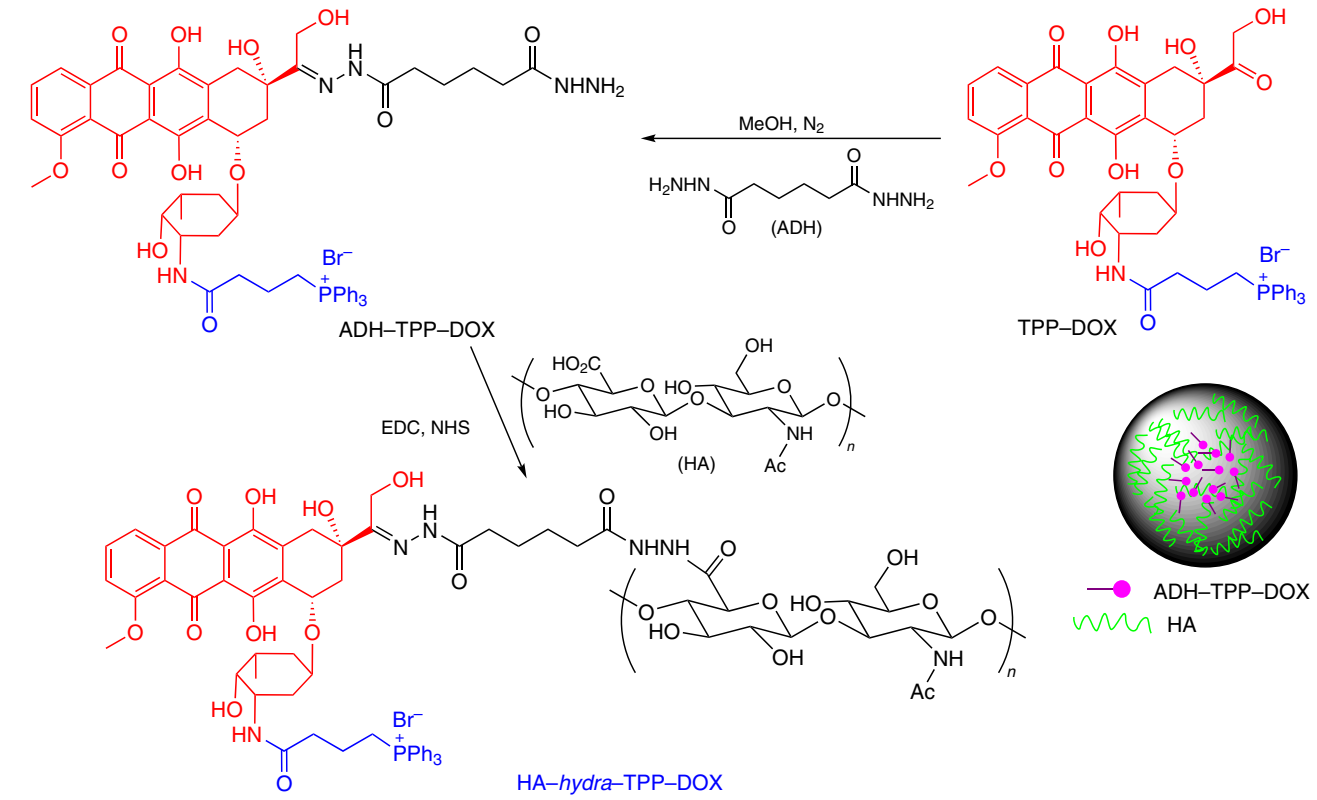

Figure 35. Synthesis of HA–*hydra*–TPP–DOX nanoparticles. The Figure was created by the authors using published data.[171]

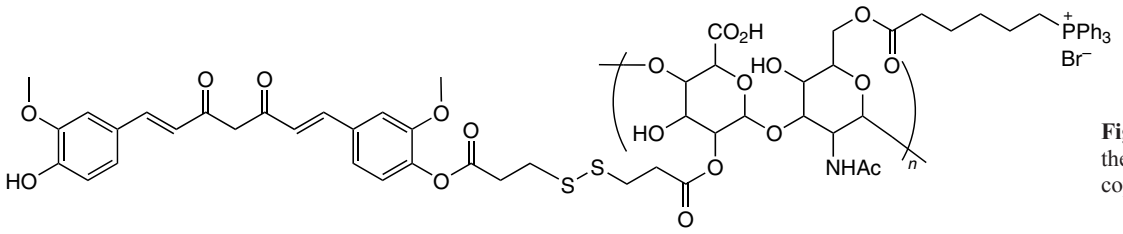

Figure 36. Structure of the TPP–HA–SS–Cur copolymer.

their preparation, starting with the synthesis of block copolymer and ending with self-assembly to micelles, which is inefficient in the case of high dilution. This problem is solved by using the polymerization-induced self-assembly (PISA) process.

The synthesis of nanoparticles decorated with the TPP groups by PISA process was reported by Noy *et al.*[177] (Fig. 37). The attachment of TPP groups to the PPM–NP4 and MPM–NP2 micelles obtained from As-containing copolymers (PP3 or MP2) and methyl methacrylate in the presence of V-501 (4,4′-azo-bis(4-cyanovaleric acid)) as the polymerization initiator was performed in the presence of EDC coupling agent. This modification increased the particle diameter from ~85 to 136 nm, PDI of the nanoparticles was <0.078, and the surface charge was negative: –4.7 and –5.1 mV for PPM–NP4–TPP and MPM–NP2–TPP micelles, respectively.

The presence of TPP groups on the nanoparticle surface facilitated their uptake by tumors and enhanced the cytotoxicity, whereas in the absence of the TPP groups, this effect was not observed.[177]

6. Self-assembled amphiphilic triphenylphosphonium ligands

The synthesis of single-chain bolaamphiphiles TPP1–TPP4 containing TPP cations as the head groups with the alkyl chain consisting of 12, 16, 20 and 30 carbon atoms, respectively, is depicted in Fig. 38.[178]

The TPP bolaamphiphiles are capable of spontaneously forming vesicles, the shape and size of which depend on the length of the oligomethylene chain. The compound with $n = 30$ forms monodisperse vesicles with a diameter of 190 nm, while lower homologues ($n = 12$, 16, 20) form two separate vesicle populations of 75–100 and 250–360 nm size.[179]

Also, TPP derivatives of alkylated cyanostilbenes were used as building blocks for the design of supramolecular assemblies for DOX delivery (Fig. 39).[180]

The N1 assemblies thus formed were spherical and had a diameter of 20 nm, a narrow size distribution and a surface potential of 10 mV. These systems exhibited a strong cytotoxic effect against tumor cell lines (HeLa, MCF-7, Hec-1A, KGN, HCT116 and A549) in concentrations ranging from 1 to 100 μg mL^{-1}, and their cytotoxicity increased in the presence of DOX. It was established that the N1–DOX assemblies were efficiently delivered to the mitochondrial membranes and induced a considerable activation of caspases 3 and 7 in cancer cells. The intravenous injections of N1 or N1–DOX particles to mice resulted in a 35 or 70% reduction in tumor volume, respectively, after two weeks of treatment compared to the control.[180]

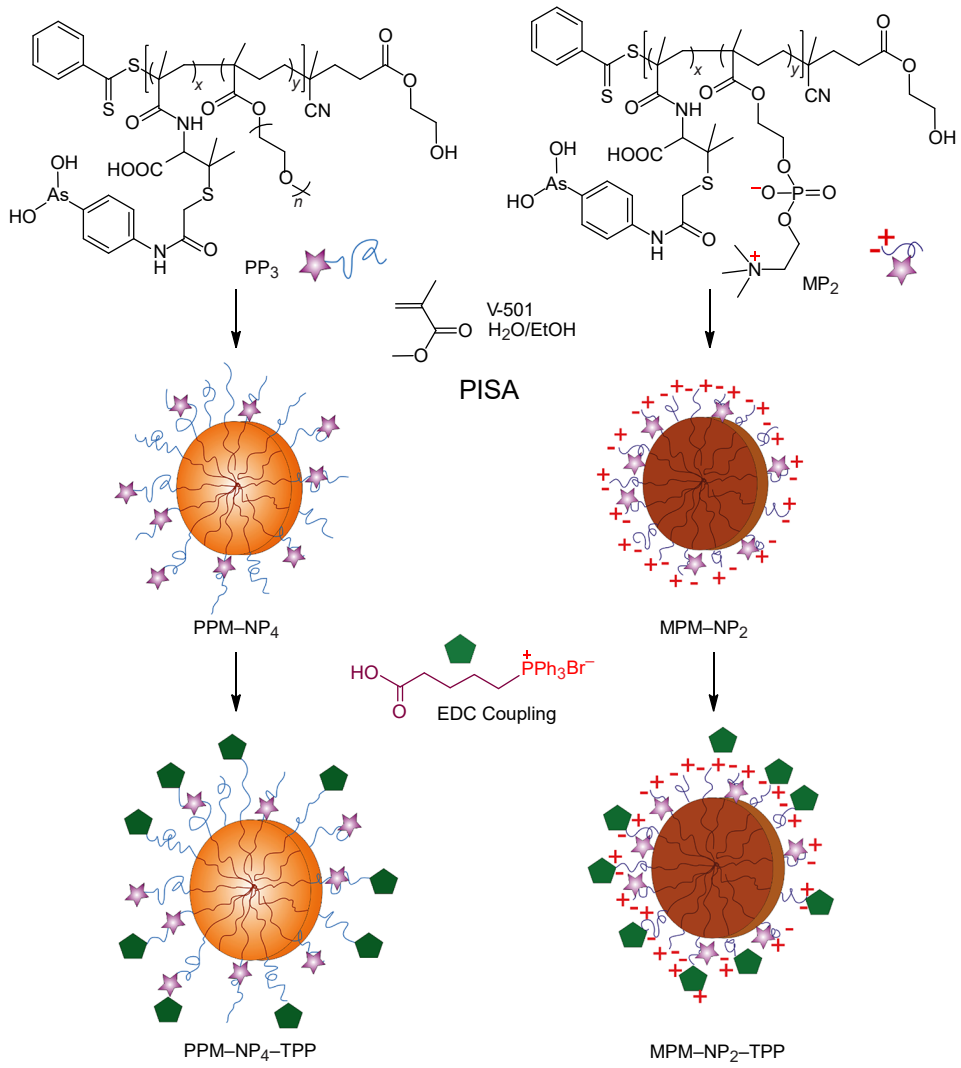

Figure 37. PISA synthesis of nanoparticles. The Figure was created by the authors using published data.[177] A star means the arsenic-containing group and a green pentagon stands for the TPP group. In the structures drawn on the right, the charges of only the starting zwitter-ion polymer are indicated. The positive charge acquired upon the addition of TPP-groups is not shown.

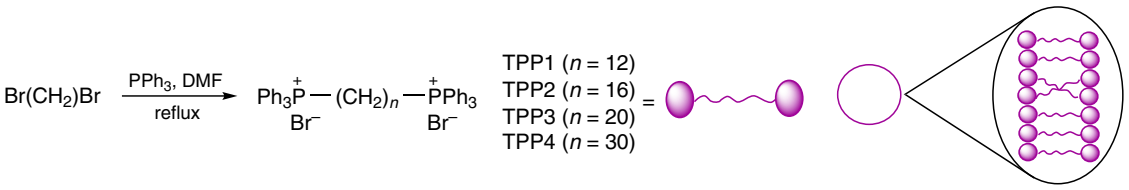

Figure 38. Synthesis of TPP-containing bolaamphiphiles. The Figure was created by the authors using published data.[178]

Battogtokh *et al.*[181] used the carbodiimide method to synthesize the TPP–DTX2 docetaxel conjugate (for its analogue, see Fig. 15) with an ester bond that was cleaved by esterases under physiological conditions; the conjugate was encapsulated into bovine serum albumin (BSA) nanoparticles (Fig. 40). The TPP–DTX2 derivative was loaded into a mixture of FA–Chol–BSA and Chol–BSA conjugates taken in 1:2 mass ratio; the loading capacity was 33.6%. Evaporation of the solvent from this mixture furnished TPP–DTX2@FA–Chol–BSA particles with a diameter of 135.7±18.2 nm (PDI = 0.32±0.11) and ζ-potential reaching –15.6±2.69 mV.[181]

The TPP–DTX2 and TPP–DTX2@FA–Chol–BSA nanoparticles produced a higher amount of ROS, they were better localized in mitochondria and better initiated apoptosis than free docetaxel. These particles showed high and moderate cytotoxicity (IC_{50} = 10 μM) against B16F10 (C57BL/6J murine melanoma) and MCF7 cells. The *in vivo* experiments with MCF7 xenograft tumor-bearing mice showed that TPP–DTX2@FA–Chol–BSA delivery systems inhibited the tumor growth during the first 14 days after the injection more efficiently than free DTX.

Liu *et al.*[182] found that the delivery of Pt to mitochondria led to reversal of cisplatin resistance of cells caused by impaired ability of the mitochondrial DNA to self-repair. They synthesized a Pt(IV) prodrug, TPP–Pt–*acetal*–CA, composed of cinnamaldehyde (CA), which induced the generation of reactive oxygen species, TPP-modified ligand able to damage the mitochondrial DNA, and a pH-cleavable acetal link (designated by '*acetal*') (Fig. 41). First, TPPB was reacted with cisplatin in the presence of 2-(1*H*-benzotriazol-1-yl)-1,1,3,3-tetramethyluronium tetrafluoroborate (TBTU) under sonication to give TPP–Pt complex, which was then treated with acetal–CA under the same conditions, giving rise to the final product. This product self-assembled to give TPP–Pt–*acetal*–CA nanoparticles under usual precipitation conditions in a DMF and water mixture. The nanoparticles had a regular spherical shape

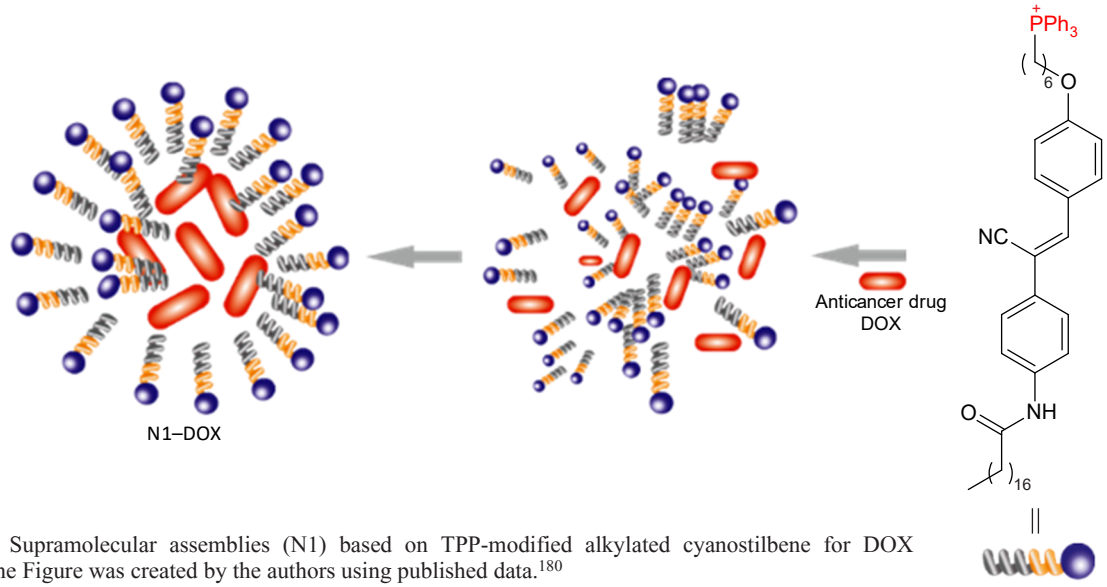

Figure 39. Supramolecular assemblies (N1) based on TPP-modified alkylated cyanostilbene for DOX delivery. The Figure was created by the authors using published data.[180]

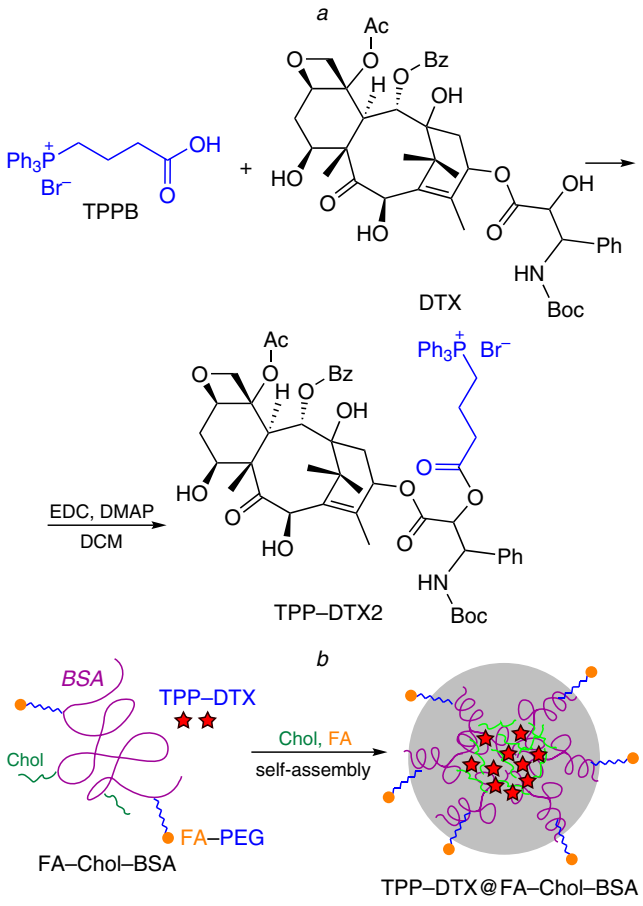

Figure 40. Preparation of TPP–DTX2 conjugate (*a*) and TPP–DTX2@FA–Chol–BSA nanoparticles (*b*). The Figure was created by the authors using published data.[181]

and the following characteristics: d = 109.8 nm, PDI = 0.06, ζ-potential of +8.4 mV. According to transmission electron microscopy data, these systems formed stable colloidal solutions at physiological pH, which were stable at 4°C for 6 months.

The cytotoxicity of the TPP–Pt–*acetal*–CA nanoparticles was assessed against two normal (HUVEC and HK-2) and three cancer (A549, MCF-7 and SMCC-7721) cell lines and also against cisplatin-resistant cancer cells–A549/DDP.[182] The inhibition of cancer cells by these nanoparticles was approximately equal to that of cisplatin, while the IC_{50} values for the cisplatin-resistant A549/DDP cells were six times lower (5.99±1.04 μM) than that for cisplatin. They were also an order of magnitude less toxic to normal cells than cisplatin. The *in vivo* studies carried out in BALB/c mice bearing the A549/DDP xenograft tumor demonstrated considerably higher concentrations of nanoparticles at the tumor sites compared to those in undamaged organs and a 3.6 times more pronounced decrease in the tumor weight compared to that for cisplatin. The authors concluded that the toxicity of the TPP–Pt–*acetal*–CA-NPs was due to synergistic mitochondrial dysfunction and to markedly enhanced oxidative stress.

6.1. Amphiphilic polymer triphenylphosphonium conjugates

Zhang *et al.*[183] described the synthesis of TPP-modified D-α-tocopherol poly(ethylene glycol) succinate TPP–TPGS (see Fig. 15). The nanomicelles for DOX delivery were obtained from this polymer and fluorescent carbon quantum dots (CQD), formed upon pyrolysis of citric acid, hexadecylamine (HDA) and octadec-1-ene (ODE), by emulsification and evaporation of the solvent from a hexane–water mixture. The TPP–TPGS–CQD/DOX had the following characteristics: d = 101.4 nm, ζ-potential of +21 mV and loading capacity of 3.4% (Fig. 42).

These micelles had a higher cytotoxicity against the Adriamycin-resistant breast cancer cells (MCF-7/ADR) than free DOX. During the treatment with TPP–TPGS–CQD/DOX nanomicelles, MDR reversal was more efficient for MCF-7/ADR spheroids than in the case of CQD–TPGS/DOX particles or free DOX.

Tan *et al.*[184] developed a polycationic C–P–CSOSA glycolipid polymer based on chitosan, MW = 19 kDa, modified with stearic acid, and TPP-containing PEG_{2000} conjugate (Fig. 43). First, (4-carboxybutyl)phosphonium salt (TTPB) was coupled with the polymeric diamine (NH_2–PEG_{2000}–NH_2) by the carbodiimide method. The resulting TPP derivative was then activated using *N*,*N*-disuccinimidyl carbonate (DSC). The final product, TTP–NH–PEG_{2000}–NH–C(O)SC, contained a succinyl urea moiety to which the CSOSA polymer obtained by

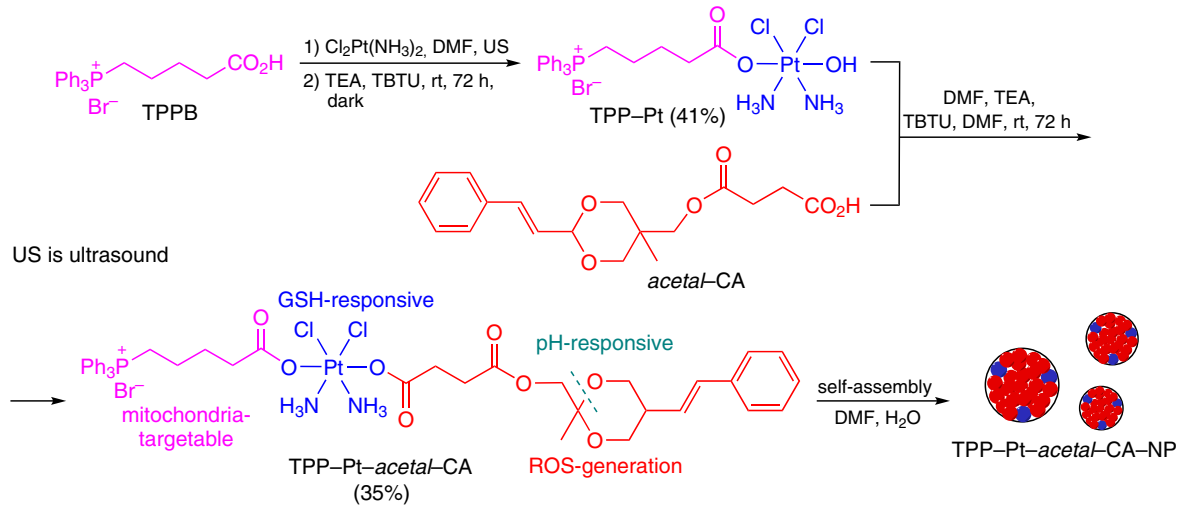

Figure 41. Synthesis of the TPP–Pt–*acetal*–CA prodrug and preparation of the prodrug nanoparticles. The Figure was created by the authors using published data.[182]

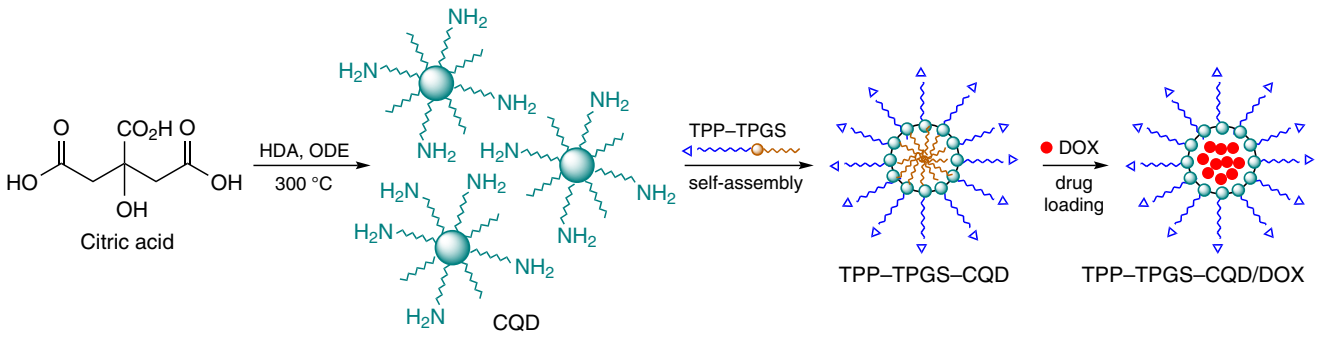

Figure 42. Preparation of the TPP–TPGS–CQD nanomicelles for the delivery of DOX. The Figure was created by the authors using published data.[183]

coupling of stearic acid with chitosan in aqueous ethanol was attached. This finally gave the C–P–CSOSA glycolipid, which was subjected to dialysis and freeze-drying.

The micelles formed from the C–P–CSOSA polymer (d = 100.4±23.1 nm, ζ-potential of +23.70±0.95 mV) were internalized by tumor cells more efficiently than by normal cells and could rapidly escape from lysosomes owing to their strong proton buffering ability. The DOX-loaded C–P–CSOSA micelles (d = 67.20±2.82 nm; 81.33% loading capacity; 10.87% encapsulation efficiency) were prepared by dialysis; they were

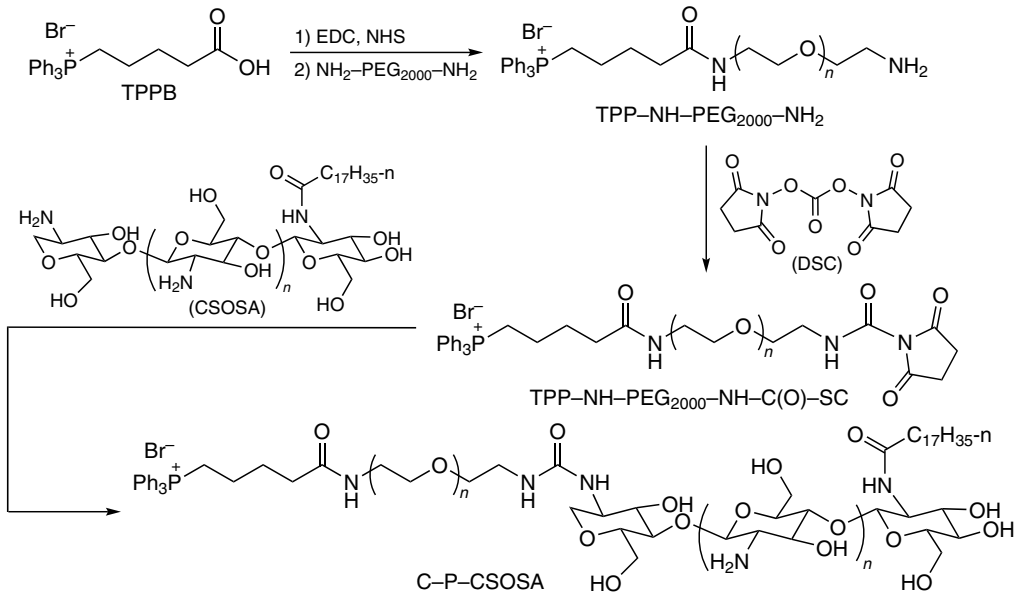

Figure 43. Synthesis of polymeric C–P–CSOSA TPP conjugate.

selectively accumulated in the mitochondria of tumor cells and efficiently activated apoptosis by the mitochondrial signaling pathway. The C–P–CSOSA/DOX composition demonstrated the highest tumor growth inhibition (75.0%) in comparison with the CSOSA/DOX system (44.8%) or DOX·HCl (55.0%). It is important that the C–P–CSOSA/DOX nanoparticles did not induce a clear-cut damage of organs and provided a good cell viability, which attests to low toxicity of the resulting polymer.

The conjugation of Pluronics PF127 and P85 — polyoxyethylene (PEO) and polyoxypropylene (PPO) block copolymers — with the TPP moiety was carried out by Wang *et al.*[185,186] The TPP-modified polymer, P85–SS–TPP (for brevity, P–S–T), had a linker containing disulfide bonds for fast release of the drug in cancer cells.[186] In addition, this polymer was modified using dimethylmaleic anhydride (DA) protective group, which can be cleaved under acidic conditions; this increased the blood circulation time of the conjugate and enhanced the endocytosis in tumor cells. The synthesis was performed by the following route: the TPP derivative of caproic acid (TPPB) reacted with the disulfide linker, NH_2–SS–NHBoc; this afforded the TPP–NH_2–SS–NHBoc salt. Then, the amino group was Boc-deprotected, which yielded TPP–SS–NH_2 (Fig. 44). Another sequence of transformations included chlorination of the HO–PEO–PPO–PEO–OH copolymer and the subsequent amination. This gave an amino group-containing polymer–NH_2–PEO–PPO–PEO–OH. The successive treatment of this compound with di-*tert*-butyl dicarbonate and maleic anhydride resulted in the formation of protected BocNH–PEO–PPO–PEO–COOH. In the final stage of assembly, the TPP–SS–NH_2 salt was conjugated with the BocNH–PEO–PPO–PEO–COOH polymer, and then the protection of the amino group was removed. The final treatment of the conjugate with dimethylmaleic anhydride gave rise to the target DA–P–SS–T copolymer.

The encapsulation of paclitaxel into DA–P–SS–T micelles was performed by the nanoprecipitation (slow addition of a PTX solution in ethanol to an aqueous solution of DA–P–SS–T followed by dialysis and freeze-drying). In water, the amphiphilic DA–P–SS–T/PTX polymer formed spherical micelles with a size of 160 nm and a ζ-potential of 8.65 mV. The DA–P–SS–T/PTX micelles demonstrated a good cellular uptake, selective mitochondria targeting at extracellular pH = 6.5, typical of a tumor, and a long blood circulation time. The TPP group helped the DA–P–SS–T/PTX nanomicelles to localize on the outer mitochondrial membrane and led to decreasing membrane potential and ATP level, which resulted in the inhibition of P-glycoprotein, overcoming of MDR and suppression of metastasis. The highest tumor growth inhibition (81.52%) was attained on the 24th day in mice that were administered with DA–P–SS–T/PTX micelles; this was 8.09, 3.87 or 2.02 times higher than the growth inhibition attained with free paclitaxel, TPP–P85/PTX micelles and P–SS–T/PTX micelles, respectively.

Shi *et al.*[187] used the method of dialysis to fabricate the TPGS/PPG2L@IONP@DOX/TPP–DOX hybrid micelles. As the starting compounds, the authors used the poly(ethylene glycol)–poly(ε-caprolactone)–polyamidoamine–lactobionic acid copolymer (mPEG–PCL–G2D–LbA, abbreviated as PPG2L, where G2D is the PAMAM dendrimer) and D-α-tocopherol poly(ethylene glycol) succinate (TPGS). Oleic acid-

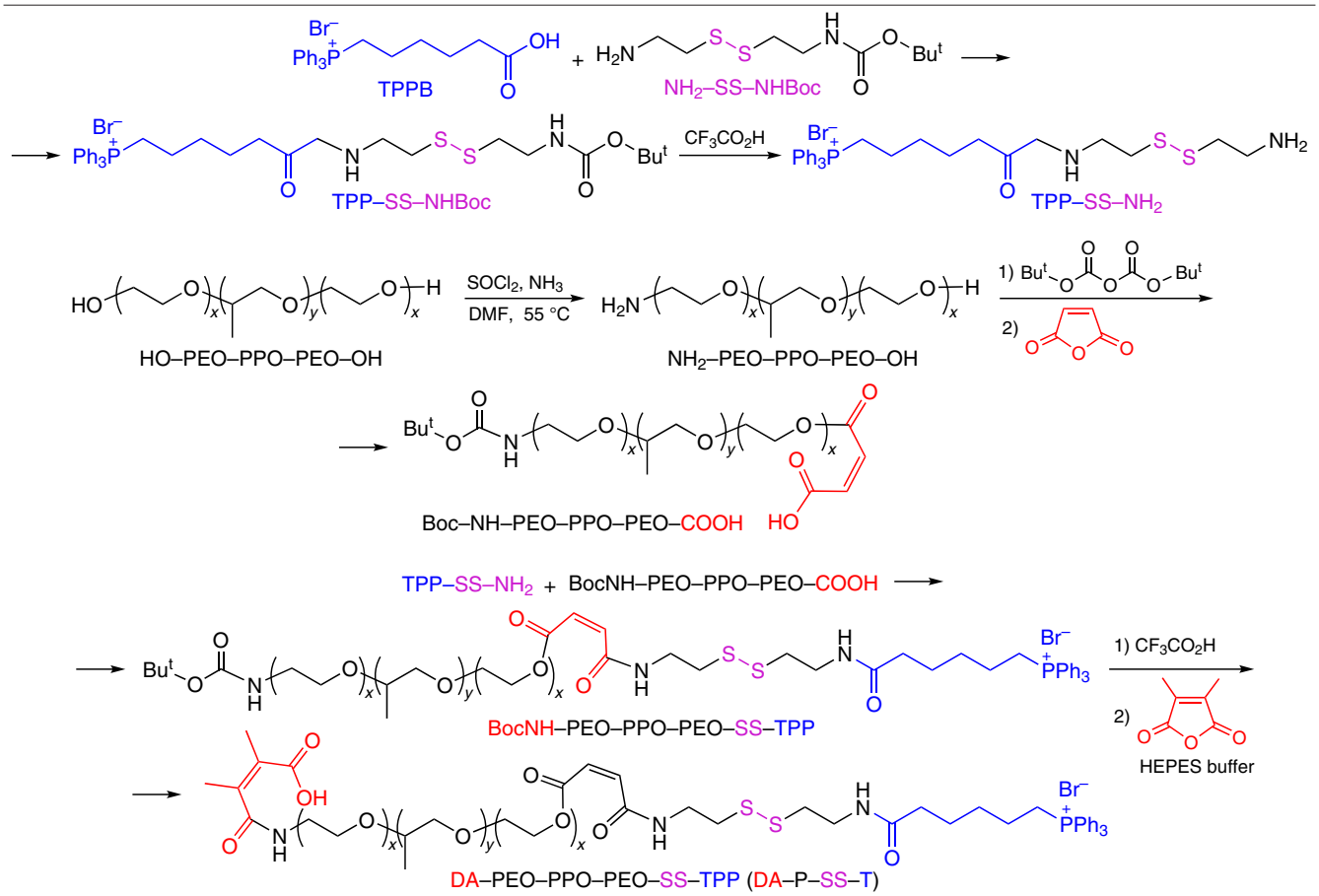

Figure 44. Synthesis of the DA–P–SS–T copolymer.

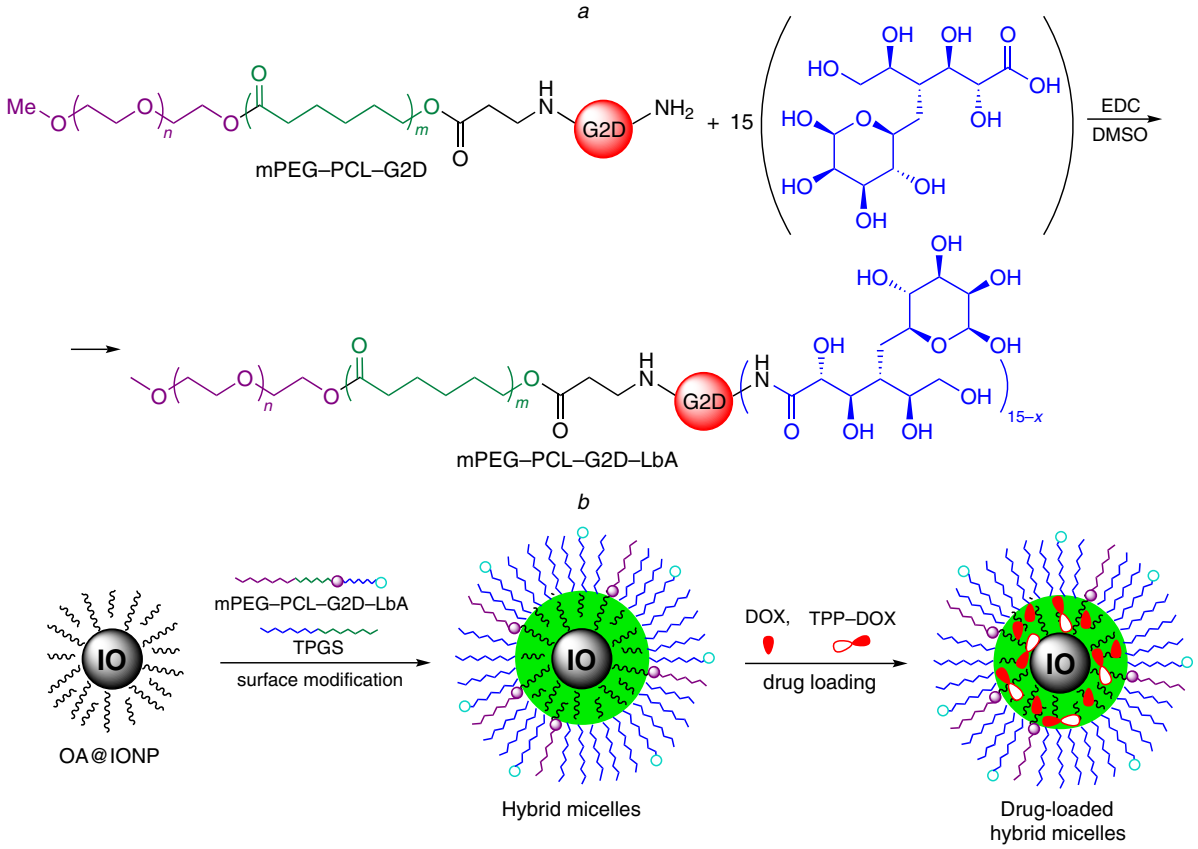

Figure 45. Synthesis of mPEG–PCL–G2D–LbA copolymer (*a*) and hybrid micelles based on this copolymer (*b*). The Figure was created by the authors using published data.[187]

coated iron oxide (IO) nanoparticles (OA@IONPs) served as the imaging agent, while the drug to be delivered was represented by anthracycline type antibiotic-loaded DOX/TPP–DOX particles with a size of 26.2±3.5 nm (Fig. 45). The authors monitored the distribution of hybrid micelles *in vivo* using MRI contrast agents (MRI is magnetic resonance imaging). These micelles showed a high anticancer activity both against usual cells (HepG2) and doxorubicin-resistant cells (HepG2/DOX).

The synthesis of amphiphilic TPP conjugate, 1,2-distearoyl-*sn*-glycero-3-phosphoethanolamine-*N*-[methoxy(polyethylene glycol)$_{2000}$] (TPP–PEG–PE), meant for the delivery of puerarin (PUE) was proposed by Li *et al.*[188] Puerarin, which has a cardioprotective action, is used in Chinese medicine for the treatment of myocardial ischemia and improving mitochondrial dysfunction. The PUE@TPP–PEG–PE micelles were prepared by hydration of a lipid film consisting of a mixture of PEG–PE and TPP–PEG–PE in 9:1 molar ratio. The particle size amounted to 17.1 nm and the ζ-potential was 6.2 mV. To monitor the cellular uptake, lysosomal escape, and mitochondria targeting, the authors also prepared micelles labeled with coumarin-6 dye, Cou6@TPP/PEG–PE, characterized by much higher cellular uptake in H9c2 cells than in normal cells, with reduced capture in lysosomes. As compared with PUE@PEG–PE micelles or free PUE, the PUE@TPP–PEG–PE nanoparticles showed an enhanced protective effect against the isoprenaline-induced apoptosis of H9c2 cells, as was indicated by decreased percentage of apoptotic cells, caspase-3 activity, ROS level and Bax expression as well as increased expression of the Bcl-2 protein. The results of *in vivo* experiments indicated that the TPP–PEG–PE micelles are capable of drug delivery to the ischemic myocardium.

Yang *et al.*[189] developed neuronal mitochondria-targeted micelles for the delivery of resveratrol (CT–NM/RES). The micelles were prepared by carbodiimide coupling of the TPP–PEG–PLA copolymer (Fig. 46) with maleimide (Mal–PEG–PLA) and methoxy derivatives (mPEG–PLA) in 1:5:4 mass ratio.

The diameter of the spherical CT–NM micelles amounted to 42.6±0.5 nm (PDI = 0.16±0.004) and their ζ-potential was +10.5±1.1 mM. The RES encapsulation efficiency and loading capacity were ~91.0 and 4.4%, respectively. The CT–NM/RES micelles, which delivered RES to brain mitochondria, efficiently reduced the consequences of oxidative stress. In addition, they restored the balance of mitochondrial fission and fusion, decreased the β-amyloid (Aβ) deposition, inhibited the hyperphosphorylation of tau protein and up-regulated the expression of the 'longevity protein' SIRT1. The administration of these micelles into an animal body mitigated the reactive gliosis and inflammation, prevented the neuronal loss and synaptic damage, and restored the function of memory in APP/PS1 transgenic mice with Alzheimer disease model.

Damrongrak *et al.*[190] described dual-purpose TPP/FA nanoparticles, which were obtained from the polyglycerol adipate (PGA) and PEG copolymer and decorated with cholesterol-conjugated folic acid (FA–PEG–PGA–Chol) and triphenylphosphonium (TPP–PEG–PGA–Chol) (Fig. 47). These particles were shown to be promising for the targeted delivery of acetogenin-enriched[j] extract from *Annona muricata* leaves to SKOV3 ovarian cancer cells with overexpression of folate receptor. The starting polymers were synthesized using Chol as the hydrophobic part for capture of the extract or hydrophobic compounds, FA as the folic receptor-targeting

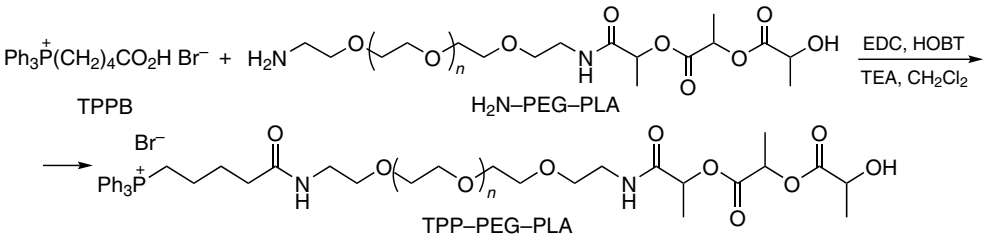

Figure 46. Preparation of the TPP–PEG–PLA polymer conjugate.

ligand, and TPPB as the mitochondria-targeted ligand penetrating into cells. The TPP–PEG–PGA–Chol conjugate was prepared by stepwise assembly: first, the modified TPP–PEG polymer was formed from PEG and TPPB; then the polymer was coupled with the PGA–Chol polymer containing ~50 mol.% cholesterol (as cholesterol succinate). According to the ^{1}H NMR spectroscopy data (acetone-d_6, 300 MHz; characteristic signals of Chol and PGA moieties were present), the TPP–PEG–PGA–Chol copolymer contained ~44.2 mol.% grafted Chol and 2.7 mol.% TPP groups. The second polymer, FA–PEG–PGA–Chol, included 3.1 mol.% folic acid, apart from an approximately equal amount of grafted Chol. The target TPP/FA-NPs were synthesized by mixing the two polymers, TPP–PEG–PGA–Chol and FA–PEG–PGA–Chol, in 1:1 mass ratio under nanoprecipitation conditions (*i.e.*, water was added with stirring to the polymer mixture in acetone, and the mixture was centrifuged and freeze-dried). The resulting nanoparticles had a size of 87±3 nm (PDI = 0.149±0.032) and ζ-potential of +34.7±4.5 mV. According to scanning electronic microscopy, the particles had an oval shape and smooth surface. The TPP/FA-NPs also showed a high loading capacity and encapsulation efficiency (14–35% and 64–83%, respectively) for the *Annona muricata* extract. The IC_{50} values for the TPP/FA-NPs loaded with the extract against SKOV3 cells

[j] Acetogenins are a class of polyketides synthesized by *Annonaceae* plants.

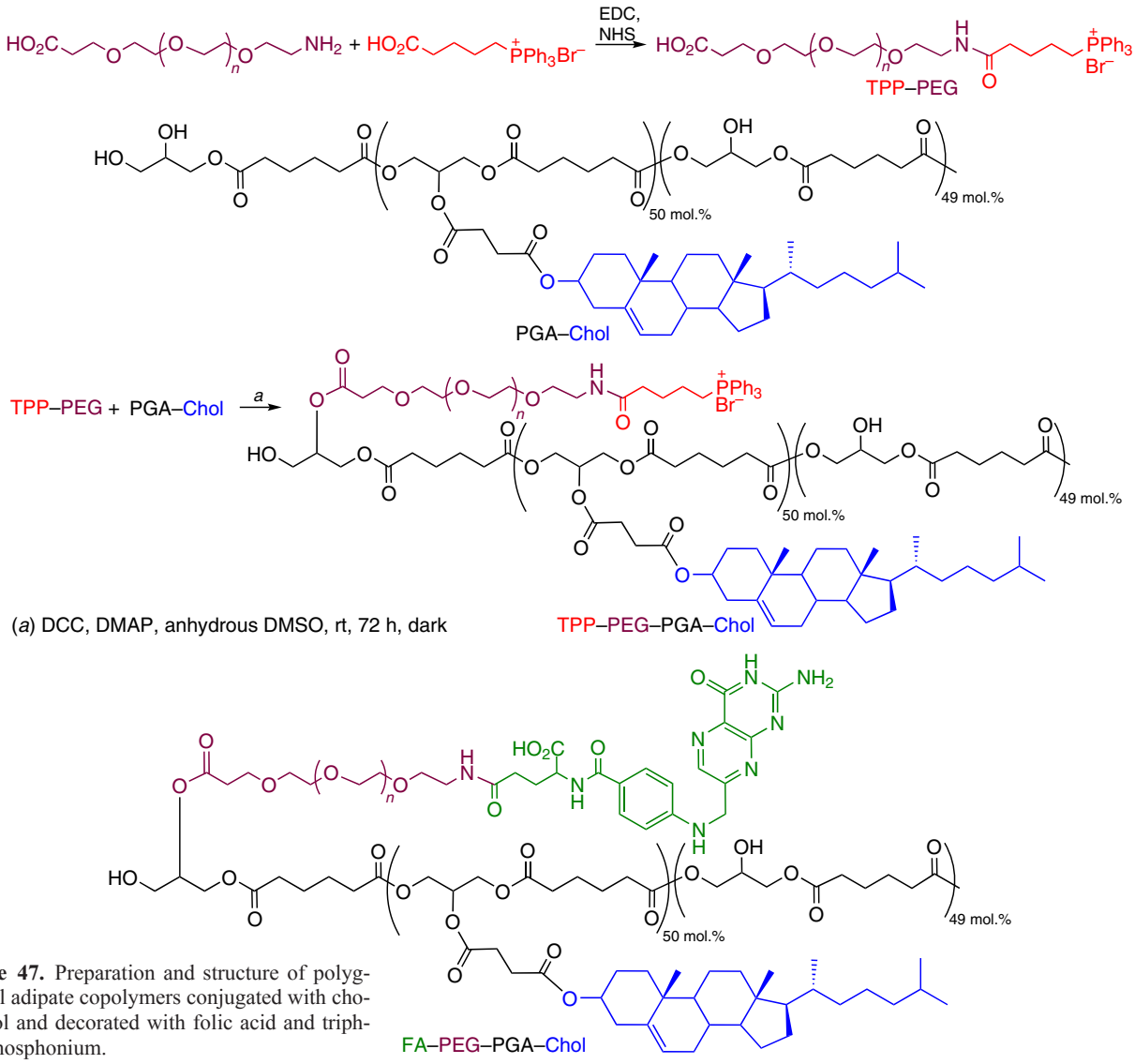

Figure 47. Preparation and structure of polyglycerol adipate copolymers conjugated with cholesterol and decorated with folic acid and triphenylphosphonium.

considerably decreased, from 25.05±8.42 to 13.72±3.68 μg mL^{-1} (*i.e.*, 2.5–3.1-fold), as the incubation time increased from 24 to 48 h. The results obtained by the authors confirm that the TPP/FA-NP system is able to deliver the mentioned extract to the mitochondria of SKOV3 cells, which induced death of the transformed cells at late apoptosis stages.

6.2. Functionalized triphenylphosphonium micelles based on prodrugs

The advantages of prodrugs over free drugs include prolonged action and noticeable EPR effects. Usually, small prodrug molecules are self-assembled into nanosized micelles when dispersed in an aqueous solution. Liu *et al.*[191,192] prepared water-soluble TPP–Cb–NA–PEG_{2000}–NA–Cb–TPP prodrug based on chlorambucil (Cb) drug substance and naphthalamide (NA) (Fig. 48). The synthesis included carbodiimide coupling of NA derivative with Cb to give the NA–Cb conjugate, which was then subjected to the click reaction with PEG diazide. The Cb–NA–PEG–NA–Cb was decorated with TPP groups also *via* the carbodiimide coupling reaction, which gave rise to the TPP–Cb–NA–PEG_{2000}–NA–Cb–TPP polymer, capable of forming spherical micelles of 200 nm size and +35.10±2.92 mV ζ-potential. These micelles had a high cytotoxicity, in addition to high selectivity and sensitivity, owing to their ability to rapidly affect mitochondria and release the drug in the alkaline medium. They were used for the targeted co-delivery of Cb and DOX to tumors in the form of DOX@TPP–Cb–NA–PEG_{2000}–NA–Cb–TPP nanoparticles for enhancement of the anticancer therapy. The TPP–Cb–NA–PEG–NA–Cb–TPP micelles showed a markedly enhanced synergistic therapeutic effect in comparison with the free drugs against MCF-7, HEPG2, HeLa, A549 and MDA-MB-231 cancer cells relative to the HL-7702 normal cells used as the control.

The synthesis of hydrophobic prodrug Platin–M was reported by Marrache *et al.*[193] (Scheme 2). First, TPPB was reacted with azadibenzocyclooctyne (DBCO) in the presence of a coupling agent to give the TPP–DBCO conjugate. The subsequent SPAAC reaction[k] of platinum(IV) diazide (Platin–Az) with TPP–DBCO resulted in the cisplatin derivative Platin–M with a high efficiency. This Pt-based prodrug releases active cisplatin in a cell at a biological pH value. For its targeted delivery, nanoparticles based on two triblock copolymers, $PLGA_{LMW}$–*b*–PEG–TPP (Fig. 49) and $PLGA_{HMW}$–*b*–PEG–TPP, were developed. Low- and high-molecular-weight copolymers (subscripts LMW and HMW, respectively) of lactic and glycolic acids, respectively, were used. The nanoparticles synthesized from two copolymers with embedded cadmium selenide quantum dots (up to 10 mass%) were located at different sites of mitochondria of human prostate carcinoma cells (PC3). The $PLGA_{LMW}$–*b*–PEG–TPP nanoparticles (d = 51.3±0.8 nm ζ-potential of +44.0±1.2 mV) were mainly accumulated in the mitochondrial matrix, whereas the $PLGA_{HMW}$–*b*–PEG–TPP nanoparticles (d = 143.2±3.2 nm, ζ-potential of +28.1±0.7 mV) were mainly in the outer mitochondrial membrane and cytosol. The Platin–M prodrug-loaded $PLGA_{LMW}$–*b*–PEG–TPP nanoparticles (abbreviated as T–Pt–M, d = 50–55 nm, ζ-potential from +28 to +37 mV) and $PLGA_{LMW}$–*b*–PEG–OH nanoparticles (abbreviated as NT–Pt–M–NP, d = 50–55 nm, ζ-potential of –22 to –34 mV) were prepared by nanoprecipitation. Analysis of mitochondrial, cytosolic and nuclear fractions, which were isolated from PC3 cells treated with cisplatin, Platin–M prodrug and NT–Pt–M and T–Pt–M nanoparticles showed that Pt concentration in the mitochondrial protein was 30 times higher than in nuclear protein fractions in the case of the Platin–M prodrug or T–Pt–M nanoparticles compared with cisplatin. The ability of these compounds to penetrate into brain, demonstrated in relation to neuroblastoma, was approximately 17 times as high as that of cisplatin.

It is known that α-TOS selectively induces apoptosis in cancer and proliferating cells by acting on mitochondrial complex II (type V mitocan) and inducing conformational changes in proapoptotic proteins (type II mitocan). A variety of block copolymers based on PEG and α-TOS methacrylic derivative (MTOS) have been described. The PEG–*b*–poly-MTOS block copolymers formed spherical nanoparticles, which exhibited selectivity and cytotoxicity against breast cancer. The triphenylphosphonium group and the GLTVSPWY (PEP) peptide ligand were successfully conjugated with the amphiphilic PEG–*b*–poly-MTOS block copolymer (see Fig. 49) to obtain modified nanoparticles for specific delivery of α-TOS to tumor cell mitochondria.[194]

Mitochondria-targeted spherical TPP–PEG–*b*–poly-MTOS nanoparticles with a size of 142 nm (PDI = 0.132) and ζ-potential of +2 mV were obtained by nanoprecipitation. The conjugation of the TPP ligands and PEG not only improved the anticancer activity of nanoparticles, but also increased the selectivity of specific delivery of α-TOS to cancer cell mitochondria *via* HER2-mediated endocytosis.[195]

[k] SPAAC is strain-promoted azide–alkyne cycloaddition.

Scheme 2

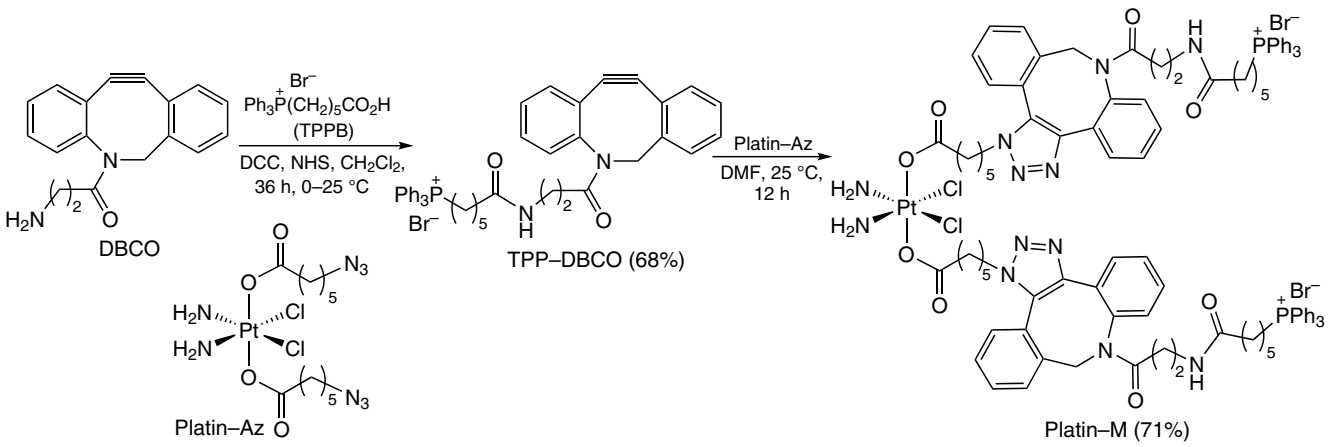

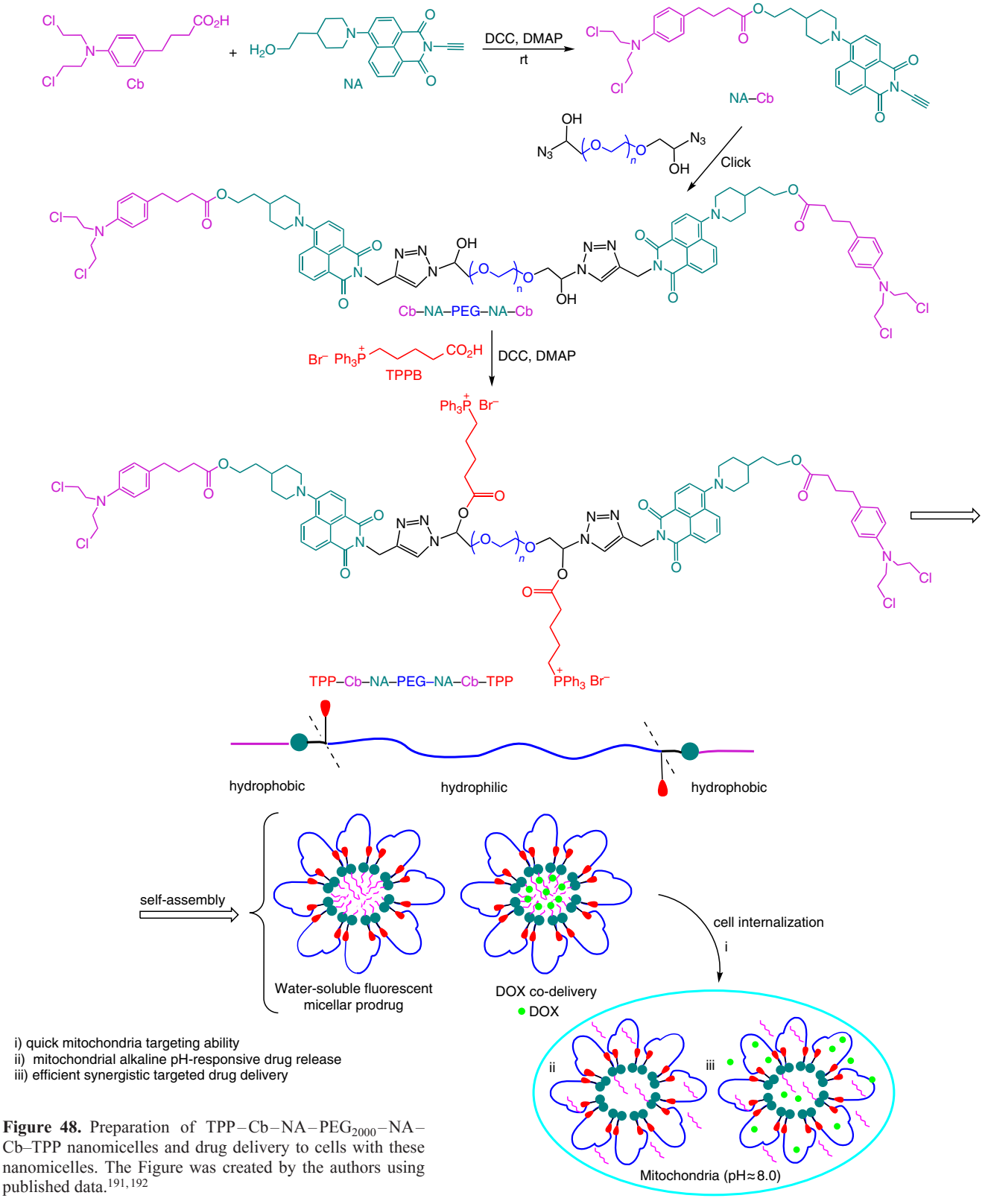

Figure 48. Preparation of TPP–Cb–NA–PEG_{2000}–NA–Cb–TPP nanomicelles and drug delivery to cells with these nanomicelles. The Figure was created by the authors using published data.[191,192]

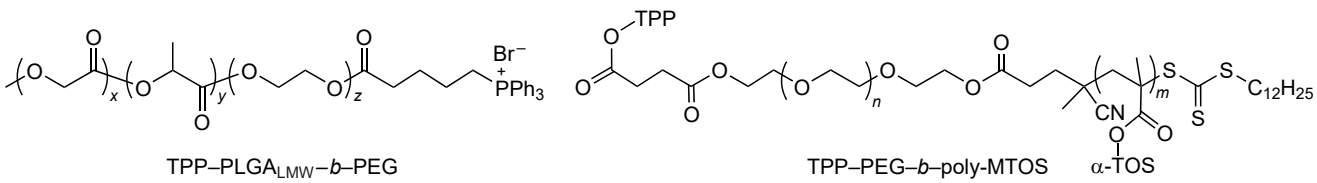

Figure 49. Structures of the PLGALMW–*b*–PEG–TPP triblock copolymer and TPP–PEG–*b*–poly-MTOS conjugate.

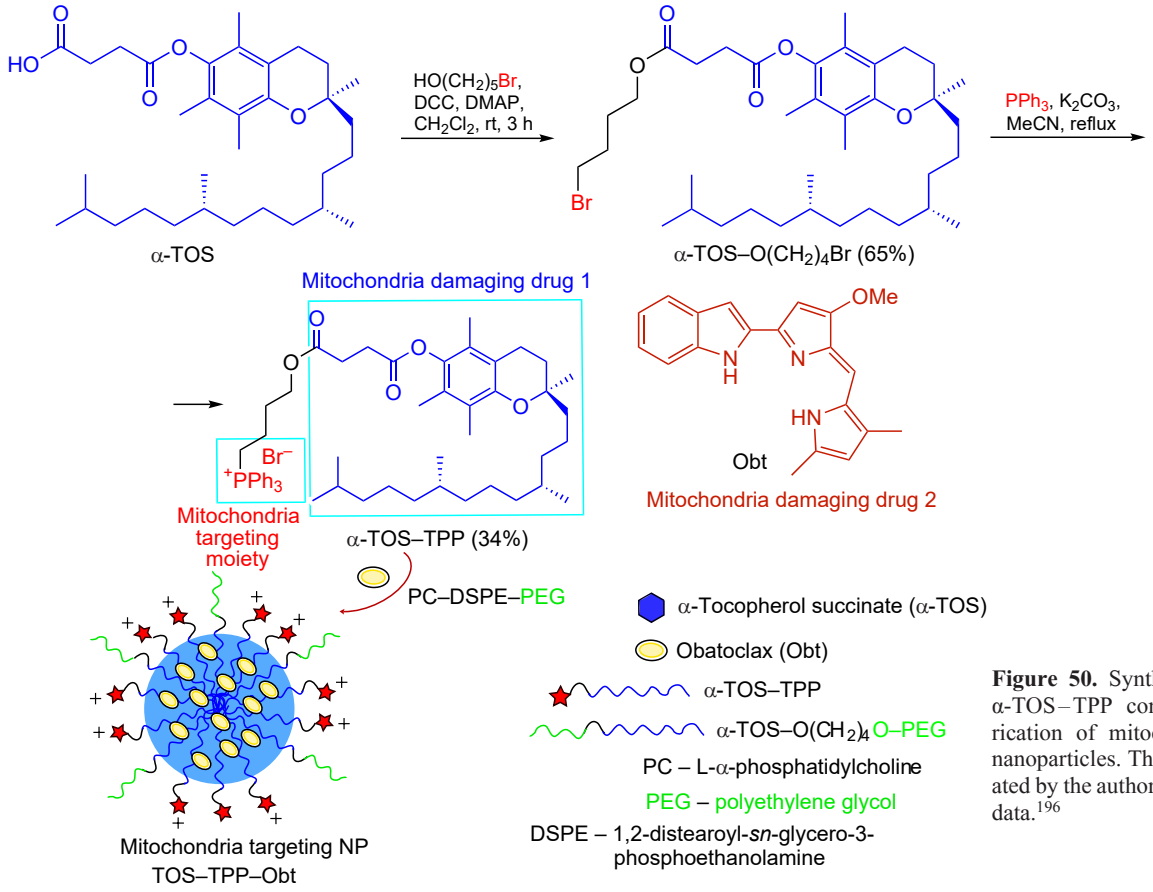

Figure 50. Synthesis of the α-TOS–TPP conjugate and fabrication of mitochondria-targeted nanoparticles. The Figure was created by the authors using published data.[196]

It is known that α-TOS damages mitochondria due to the ability to bind to mitochondrial complex II of the electron transport chain and induce apoptosis in various tumors by changing the permeability of the mitochondrial outer membrane.[196] For mitochondria targeting, α-TOS was modified by forming the bromo derivative α-TOS–$O(CH_2)_4Br$ (65% yield), which was then allowed to react with triphenylphosphine in the presence of K_2CO_3. This gave α-TOS–TPP conjugate in 34% yield (Fig. 50). The nanoparticles based on amphiphiles containing TPP-groups, α-TOS (drug 1) and obatoclax (drug 2, Obt, Bcl-2 protein inhibitor) were prepared by film hydration and extrusion; the nanoparticle size was 131.60±1.62 nm and the ζ-potential was +42.90±1.20 mV. The α-TOS–TPP–Obt nanoparticles were localized in lysosomes *via* macropinocytosis for 1 h and then escaped from lysosomes after 6 h. They got to mitochondria 24 h after being injected into cervical cancer cells (HeLa) and activated the permeabilization of the outer mitochondrial membrane by antiapoptotic inhibition of the Bcl-2 protein followed by the release of cytochrome *c*, which resulted in the release of caspase 9 and caspase 3 (Fig. 51) and induction of apoptosis.[196]

In order to increase the anticancer efficacy of 10-hydroxycamptothecin, it was reacted with (4-carboxybutyl) triphenylphosphonium bromide.[197] The TPP–HCPT conjugate (designated by TH in Fig. 52) is self-assembled into structures, with the critical aggregation concentration being 4.54 μg mL^{-1} (6.40 μM); the nanoparticle size was 203 nm (PDI = 0.27), while the ζ-potential was +0.026 mV (in deionized water at C = 1 mg mL^{-1}). The TH nanoparticles were stable in blood plasma during incubation for 12 h (at 37°C); however, they proved to be unstable in a 0.5% solution of glucose simulating gastric or intestinal fluid: after incubation for 6 h, the particle

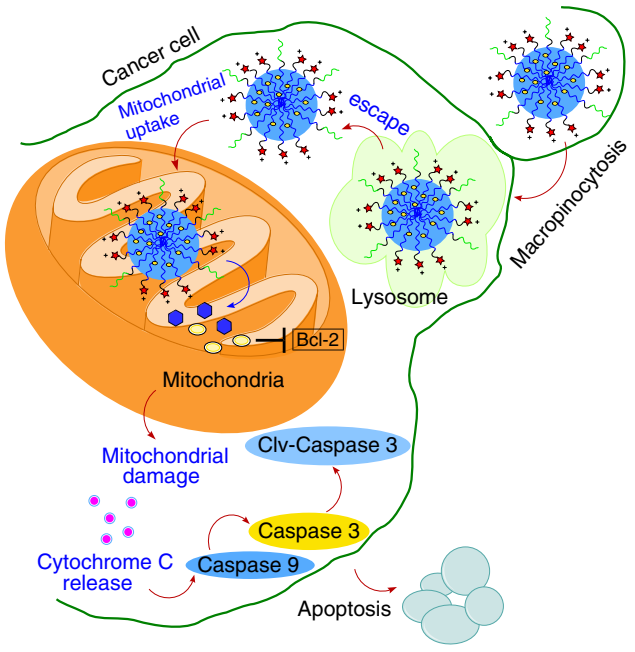

Figure 51. Schematic image of cellular internalization and mitochondria targeting of α-TOS–TPP–Obt nanoparticles leading to apoptosis. The Figure was created by the authors using published data.[196]

size increased to 1200–1600 nm. To increase the stability of this system, nanoparticles of the TH conjugate with the amphiphilic $mPEG_{3000}$–$PLGA_{5000}$ block copolymer with an optimal mass ratio of 1 : 4 were formed by the nanoprecipitation/substitution method. The nanoparticles had d = 86 nm

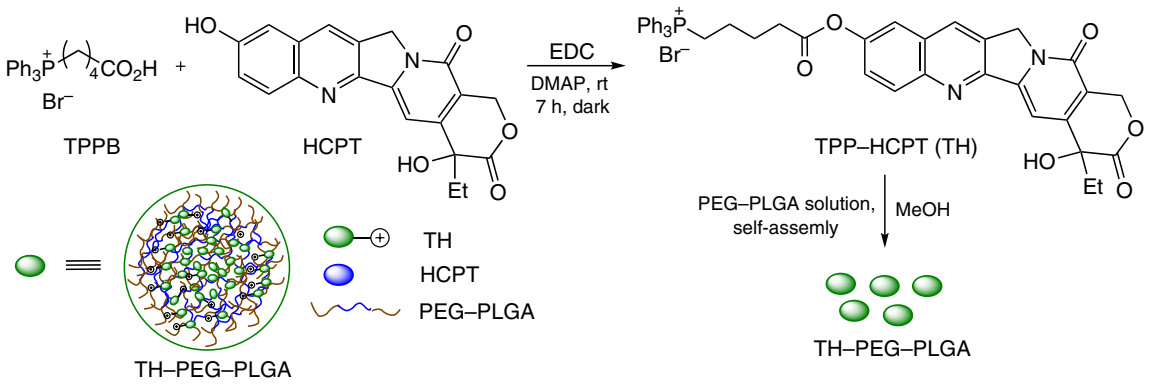

Figure 52. Synthesis of the TPP–HCPT (TH) conjugate and TH–PEG–PLGA nanoparticles.

(PDI = 0.26) and ζ-potential of +0.125 mV. Unlike the injections of HCPT, the TH aggregates showed an increased cellular uptake of the drug, obvious mitochondrial targeting and high cytotoxicity against breast cancer cells (4T1). The TH–PEG–PLGA nanoparticles were markedly more stable (they did not change after 7 days of storage at room temperature in physiological saline) and showed an even higher anticancer efficacy than TH aggregates. In *in vivo* experiments, TH aggregates also demonstrated a more pronounced anticancer effect in the 4T1 tumor-bearing mice model than HCPT injections (the tumor growth inhibition was 55.71% *vs*. 69.17%), whereas the TH–PEG–PLGA nanoparticles had an even higher activity (80.02%). The IC_{50} value for the TH–PEG–PLGA nanoparticles was 0.21 μM.

7. Functionalized triphenylphosphonium inorganic nanosystems

Inorganic nanocarriers usually exhibit physical effects such as localized surface plasmon resonance, photoluminescence, or superparamagnetism, which can be useful for many potential applications such as bioimaging and bioprobing. Most often, these carriers are carbon- or gold nanomaterials, mesoporous silica or magnetic iron oxide nanoparticles, upconversion nanoparticles, *etc*.[198]

7.1. Mesoporous silica nanoparticles

Mesoporous silica nanoparticles (MSNPs) are widely used in biomedicine owing to their large surface area, large pore volume, uniform and ordered mesopores, easy surface functionalization and good biocompatibility.[199,200] These particles are used to encapsulate drugs, genes and proteins and for their targeted delivery inside the body.[201]

Synthesis of biodegradable silica nanoparticles (BS-NPs) based on a TPP-modified monomer, bis[3-(triethoxysilyl)-propyl] disulfide (BTEPDS) and a delivery system for proteins and antibodies are depicted in Fig. 53.[202] First, the protein or antibody meant for the delivery was treated with a mixture of tetraethoxysilane and BTEPDS to give Protein@BS–NP nanoparticles, which were conjugated with the phosphonium salt TPP–APS and thus gave TPP–Protein@BS–NP nanoparticles. Treatment of Protein@BS–NP with azido-containing silane N_3–APS and phosphonium salt TPP–APS resulted in the formation of nanoparticles containing both an azide group and a phosphonium moiety (N_3/TPP–Protein@BS–NP). These particles were allowed to react with dibenzocyclooctyne-containing polyester amide TCO–PEG_{11}–DBCO to be converted to the TCO–TPP–Protein@BS–NP nanoparticles. The cycloaddition of the last-mentioned particles to functionally substituted tetrazine (Tz–CPD) afforded CPD–TPP–Protein@BS-NP nanoparticles. Successive treatment of Protein@BS–NP with the azide (N_3–APS) with TCO–PEG_{12}–DBCO and Tz–CPD conjugates yields another type of target nanoparticles–CPD–Protein@BS–NP. The synthesized nanoparticles were found to be rapidly taken up by cells with a minimum endolysosomal trapping, thus providing a sufficiently long time for effective localization in mitochondria with the subsequent glutathione-triggered biodegradation and release of native functional proteins in mitochondria.

TPP-modified MSNPs of 80 nm diameter were used for the delivery of doxorubicin to mitochondria.[203] The conjugation was performed by the reaction of the carboxyl group of TPPB with the amino group on the MSNP surface. The DOX–TPP–MSNP system in concentration from 11.3 to 180 μg mL^{-1} induced the destruction of HeLa cancer cells with high efficiency. In the case of free DOX, the cells were mainly killed upon interaction of the drug with the nuclear DNA. It was found that DOX–TPP–MSNPs were selectively accumulated in mitochondria, most likely, because of electrostatic interaction and efficient endocytosis. It also resulted in decreasing ATP production and decreasing mitochondrial membrane potential, which is indicative of mitochondrial dysfunction.

A supramolecular strategy for the preparation of TPP–MSNPs, particularly, non-covalent modification of silica gel with hexadecyltriphenylphosphonium bromide (HTPPB), which makes it possible to avoid labor-intensive chemical synthesis, was proposed by Ibragimova *et al*.[204] The MSNP@HTPPB system was prepared by template synthesis.[205] The charge of the initial and TPP-modified nanoparticles was in the range from –40 to –5 mV, while the size was 320–740 and 390–830 nm for MSNP and MSNP@HTPPB particles, respectively. The composition of MSNP@HTPPB with rhodamine B showed cellular uptake in the M-HeLa subline and improved delivery of the dye to mitochondria. The cytotoxicity against the M-HeLa cells was detected when the concentration of this composition was 0.06 μg mL^{-1}, while the activity against Chang liver normal cell line was retained in the range of 0.98–0.06 μg mL^{-1}. When the MSNP@HTPPB concentration was 30 μg mL^{-1}, hemolysis was 2%.[204]

In the last decade, there has been increasing number of nanoplatforms obtained by integration of the targeting and therapeutic components (this means drug, a gene, photosensitizer, photothermal agent, *etc*.) with fluorescent CQD with the goal of designing an ‘all-in-one’ theranostic reagent.[206] A biocompatible

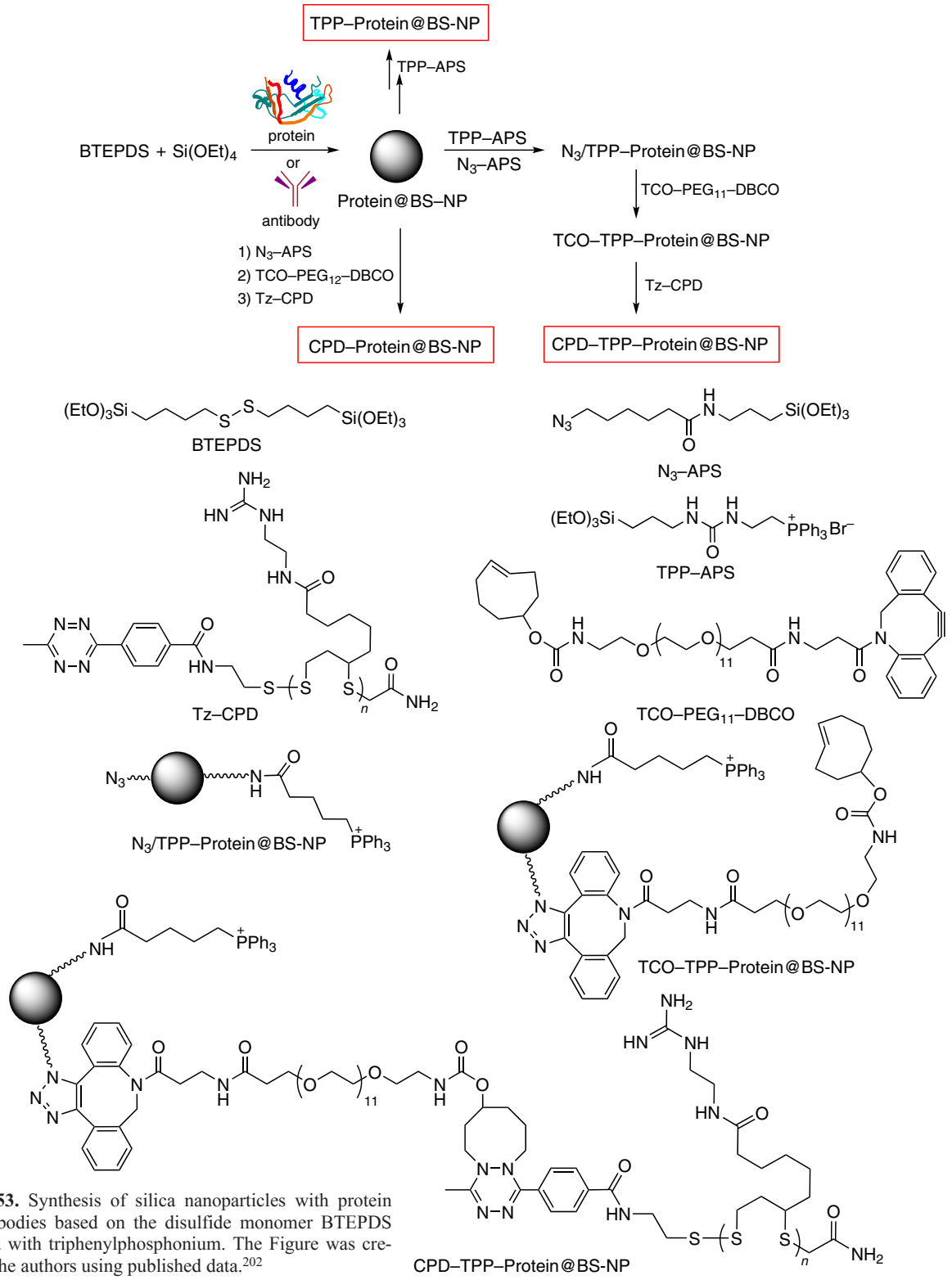

Figure 53. Synthesis of silica nanoparticles with protein and antibodies based on the disulfide monomer BTEPDS modified with triphenylphosphonium. The Figure was created by the authors using published data.[202]

nanoplatform was synthesized on the basis of magnetic mesoporous silica nanoparticles (Fe_3O_4@mSiO_2) by decorating their surface with TPP groups, which were then conjugated with fluorescent quantum dots (Fig. 54). The starting magnetic nanoparticles were obtained by the liquid–solid–solid method in the presence of cetyltrimethylammonium bromide (CTAB) and tetraethoxysilane (TEOS). Then their surface was modified with amino groups using (3-aminopropyl)triethoxysilane (APTES). The intermediate Fe_3O_4@mSiO_2–NH_2 nanoparticles were subjected to nucleophilic substitution with TPP-containing acyl chloride.[207] This process provided Fe_3O_4@mSiO_2 nanoparticles with a size of 43.30 nm. The particle surface area was 1024.42 $m^2\ g^{-1}$ and the average pore size was 5.21 nm.[208]

The resulting systems had a low cytotoxicity against A549, CHO, HeLa, SH-SY5Y, HFF and HMEC-1 cell lines at concentrations of 100 μg mL^{-1}, being even less active against HFF and HMEC-1 normal human embryonic cells (C = 200 μg mL^{-1}). The decoration of silica nanoparticles with

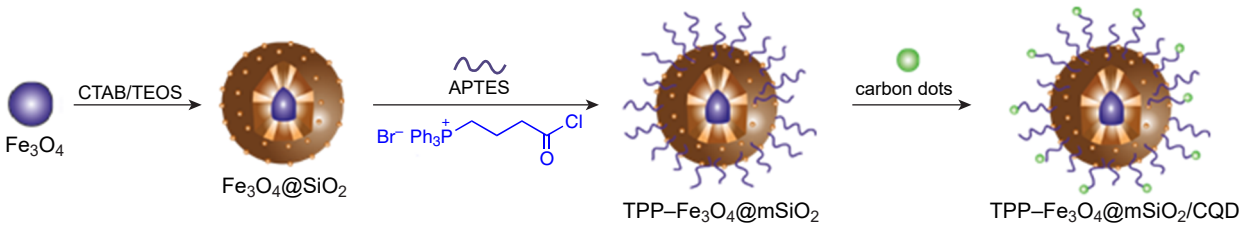

Figure 54. Synthesis of the TPP–MSNP conjugate containing quantum dots. The Figure was created by the authors using published data.[208]

TPP groups facilitates their cellular uptake and the escape from endosomes and lysosomes with the subsequent localization in mitochondria.[207]

7.2. Metal nanoparticles

Gold nanoparticles (AuNPs) of various sizes and shapes are among the nanostructures used most frequently in medicine. These nanoparticles can be decorated with drug molecules and other practically important groups and can be easily subjected to photothermal treatment. Nam *et al.*[209,210] described the synthesis of gold nanoparticles functionalized with a phosphonium group *via* the S–Au bond (Fig. 55). The authors obtained the phosphonioalkylthiosulfate zwitter ions (TPPS, FTPPS) and the TPPSA salt, which behave as latent thiolate ligands in reactions to give TPP-functionalized stable gold nanoparticles (TPPS–AuNPs).

The TPPS–AuNPs with a diameter of 3.0±1.2 nm (from TPPS) or 4.9±1.5 nm (from TPPSA) obtained by Nam *et al.*[211] were stable for several months.

Marrache and Dhar[212] decorated gold nanoparticles with TPP groups attached to polyethylene glycol and with 3-bromopyruvate (3-BP) molecules (Fig. 56). Then the NH_2–PEG–SH polymer was reacted with $Ph_3P^+(CH_2)_5CO_2H$ to give TPP–PEG–SH. Then T–AuNPs were obtained by the reduction of $HAuCl_4 \cdot 3H_2O$ with sodium borohydride in the presence of a mixture of NH_2–PEG–SH and TPP–PEG–SH polymers (in 1:1 mass ratio) meant for the nanoparticle stabilization. The synthesis was completed by modifying the T–AuNPs with 3-BP residues at the amino groups. This gave T–3-BP–AuNPs with a diameter of 20–30 nm and a narrow particle size distribution.

It is known that 3-BP inhibits HK2 as an energy blocker and can potentially endow the system with specific antitumor

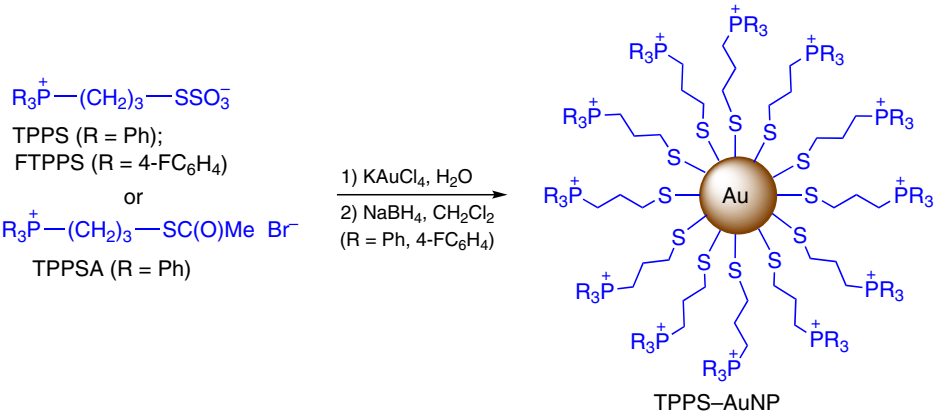

Figure 55. Preparation of stable TPP-modified TPPS–AuNPs using thiolate ligands. The Figure was created by the authors using published data.[209,210]

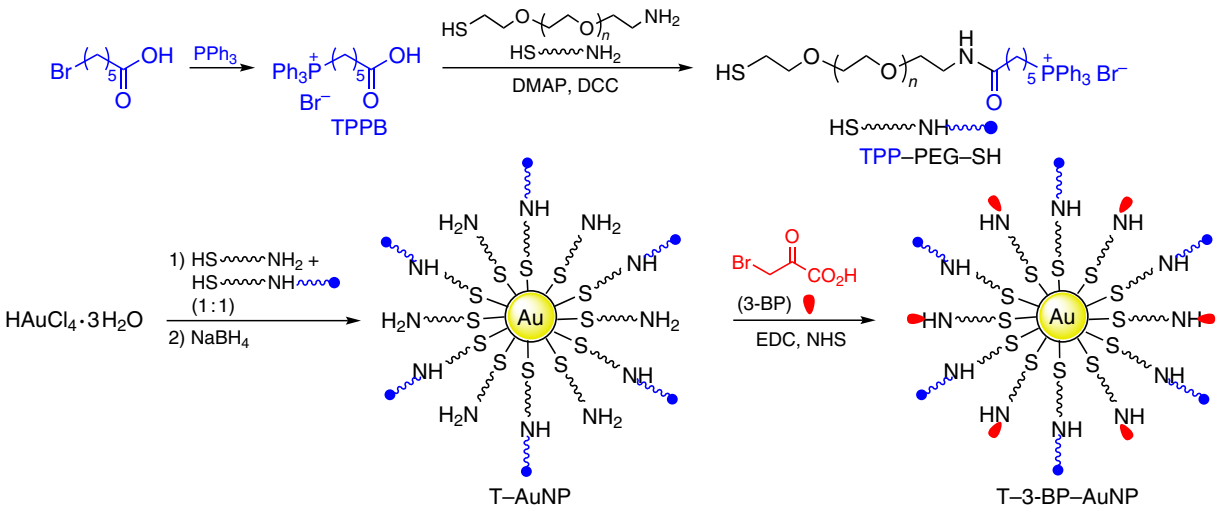

Figure 56. Synthesis of gold nanoparticles with the structure T–3-BP–AuNPs. The Figure was created by the authors using published data.[211]

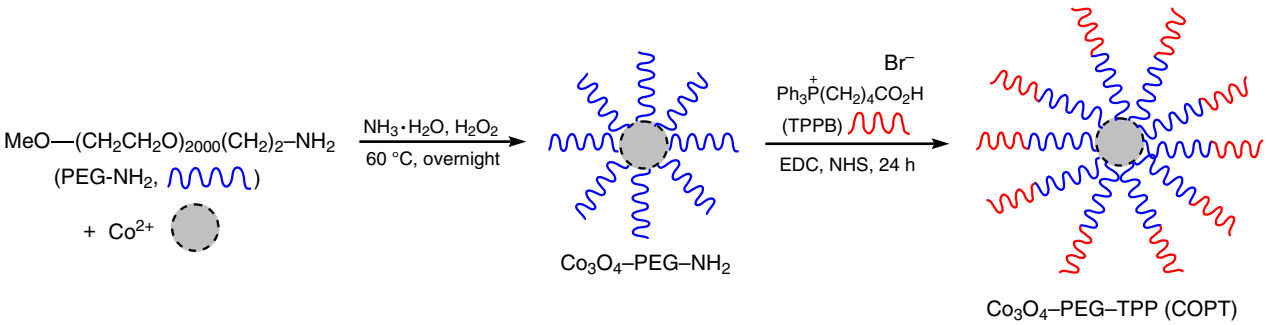

Figure 57. Synthesis of COPT nanoparticles. The Figure was created by the authors using published data.[215]

properties. The T–3-BP–AuNPs had a selective cytotoxicity against tumor cells over normal cells. In this case, TPP modification provided a targeted delivery to the cancer cell mitochondria of both the HK-inhibiting 3-BP moiety and gold nanoparticles, which exhibit a photothermal effect upon irradiation. T–3-BP–AuNPs had the highest efficiency in the inhibition of proliferation of PC3 and DU145 cells: the IC_{50} values against these cell lines were 1.3 to 28 μM.

A multifunctional polypeptide coating for gold nanoparticles was obtained on the basis of albumin. This coating includes grafted poly(ethylene oxide) chains, numerous copies of the peptide isolated from TAT protein of the human immunodeficiency virus, which provides cellular uptake, and the TPP group. The nanoparticles with this coating are promising as NIR-emitting markers for confocal microscopy and photothermal active probes in optical coherence microscopy.[213]

Vinita *et al.*[214] reported the synthesis of gold nanotriangles (AuNTs) modified with TPP groups in the presence of 5-aminolevulinic acid (5-ALA) for the use in photodynamic therapy (PDT). The starting nanoparticles were obtained by a precipitation method. In order to elucidate the role of surface charge in the efficacy of action on the cancer cells, the authors prepared particles with both positively and negatively charged surface. In the presence of cetyltrimethylammonium chloride (CTAC), positively charged CTAC©AuNTs were formed. Then these nanoparticles were used to form negatively charged PSS@CTAC©AuNTs by treatment with an anionic surfactant–polystyrene sulfonate (PSS). The resulting charged nanoparticles were modified with the phosphonium zwitter-ion compound $Ph_3P^+(CH_2)_3S^-$(TPPS). The TPPS loading capacity on the surface of CTAC©AuNTs and PSS@CTAC©AuNTs was 96.93 and 96.36%, respectively. It was shown that all particles cause a dose-dependent death of breast cancer cells (MCF-7 and MDA-MB-231). The TPP–CTAC©AuNT conjugates had a higher cytotoxicity than other particles; the following activity series was determined: TPP–PSS@CTAC©AuNTs > CTAC©AuNTs > PSS@CTAC©AuNTs > TPPS. In addition, the cytotoxicity of these particles against the normal human embryonic kidney cells (HEK-293) was lower than that against cancer cells. The positively charged particles were found to be more cytotoxic than negatively charged particles. The authors showed that in the PDT (IR light) using 5-ALA-containing nanoparticles in the presence of the TPP–CTAC©AuNT and TPP–PSS@CTAC©AuNT systems, the Pi3K/AKT apoptosis pathway is markedly inhibited, while a decrease in the Bcl-2 protein expression and an increase in the Bax protein expression lead to cytochrome *c* activation.

As noted above, the mitochondrial dysfunction is responsible for many pathologies, in particular it is a crucial factor in the pathogenesis of the acute kidney injury (AKI). Qin *et al.*[215] used mixed cobalt oxide (Co_3O_4), possessing peroxidase-like catalytic activity, as the base for the preparation of triphenylphosphonium-decorated nanoparticles coated with poly(ethylene glycol) [COPT, cobaltosic oxide poly(ethylene glycol)–triphenylphosphine]. It was found that these particles have a good biocompatibility and can have a targeted effect on mitochondria. COPT nanoparticles were obtained by mixing Co_3O_4 with methoxy-poly(ethylene glycol)-containing amino groups at the periphery (mPEG–NH_2) followed by binding to TPPB using the amide bond formation reaction (Fig. 57). The ζ-potential of the Co_3O_4–PEG nanoparticles before the deposition of the TPP coating was +15.18±1.70 mV, while after modification it increased to +19.4±2.01 mV. As shown by transmission electron microscopy, COPT particles were nearly spherical and had an average diameter of 27 nm. According to dynamic light scattering data, the average hydrodynamic diameter of COPT particles was 55.8 nm.

COPT nanoparticles were mainly accumulated in renal proximal tubule cells and considerably alleviated the ischemic AKI in mice models and gentamycin-induced AKI in zebrafish model. It was shown[215] that COPT are localized in mitochondria and reduce the hypoxia–reoxygenation-caused mitochondrial damage by enhancing BNIP3-mediated mitophagy *in vitro* and *in vivo*. It was also demonstrated that COPT particles are nontoxic to renal proximal tubules in concentrations <100 mg mL^{-1} and do not induce hemolysis.

7.3. Carbon nanomaterials

Among various types of nanomaterials, carbon nanotubes (CNTs) are becoming more and more attractive vehicles for drug delivery inside the body owing to their properties. Mention should be made of their unique shape, which promotes cellular uptake, and the set of physical characteristics that facilitates the conjugation of biologically active molecules on their surface.[216] Thus, fluorescent carbon dots have high photostability, biocompatibility and good solubility in water and are easily prepared. Carbon dots are widely used in chemical (biosensor) probing, bioimaging and in the creation of optoelectronic nanodevices. The mitochondria-targeted TPP-decorated carbon quantum dots (TPP–CQD) were fabricated for the first time for detecting mitochondrial peroxynitrite.[217] The synthesis was performed by solvothermal method based on phenylenediamines.[218] These quantum dots were monodisperse (d = 3–8 nm) and demonstrated good colloidal stability and photostability, excellent biocompatibility and low cytotoxicity (IC_{50} varied from 10 to 50 μg mL^{-1} when measured for MCF-7 cells).

A fast and inexpensive process for the synthesis of carbon nanoparticles using microwave radiation and readily available reactants (citric acid and ethylenediamine) was proposed by

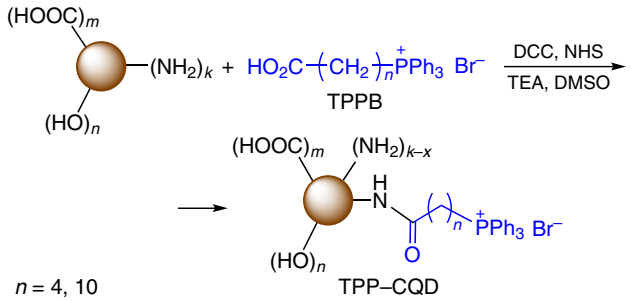

Figure 58. Synthesis of the TPP–CQD conjugate.

Kaminari *et al.*[219] Functionalization was performed by the reaction of the primary amino groups of CQD with the carboxyl groups of the (4-carboxybutyl)- or (10-carboxydecyl) triphenylphosphonium bromides (Fig. 58). The TPP–CQD represented monodispersed quasi-spherical readily separable nanoparticles with a diameter from 3 to 6 nm. The concentration ranges for TPP–CQD application for cell imaging by confocal microscopy in the absence of rhodamine B were 250–500 μg mL^{-1}. Rhodamine functionalization expanded the potential of imaging and allowed the use of these nanoparticles in lower concentrations (10 μg mL^{-1}).

Zou *et al.*[220] used biocompatible nanodiamond (ND) as the platform for drug delivery systems (Fig. 59). First, a 50 nm nanodiamond coated with polyglyceride (PG) was obtained. Then the ND–PG particles were additionally functionalized with TPP groups by esterification of the carboxyl groups in TPP-containing carboxylic acid with the hydroxyl groups located in the PG layer.

7.4. Quantum dots

Molybdenum sulfide quantum dots were functionalized with TPP groups. First, 1,2-distearoyl-*sn*-glycero-3-phosphoethanolamine-*N*-[amino(polyethylene glycol)$_{2000}$] was allowed to react with (4-carboxybutyl)triphenylphosphonium bromide in the presence of coupling agents. Then molybdenum disulfide nanoparticles were coated by the resulting polymer under microwave irradiation to give TPP–MoS_2 quantum dots (Fig. 60) designed for the targeted drug delivery to mitochondria.[221] The size of these dots was 50 nm, while the ζ-potential was negative (–0.81±0.01 mV).

It was shown that TPP–MoS_2 systems are able to penetrate the blood–brain barrier (BBB), target mitochondria, mitigate Aβ-mediated neurotoxicity and eliminate β-amyloid aggregates in mice. They act as mimics of natural enzymes (nanozymes),

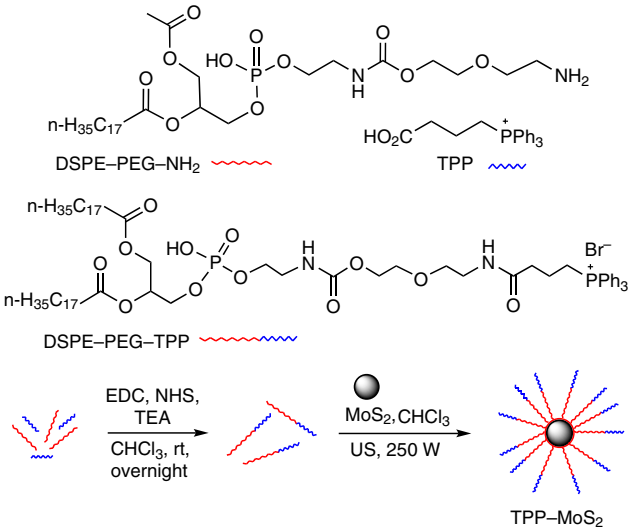

Figure 60. Synthesis of TPP–MoS_2 nanoparticles. The Figure was created by the authors using published data.[221]

inhibiting neuroinflammation and switching M1 microglia to M2 microglia.

The CdSe/ZnS quantum dots and iron oxide γ-Fe_2O_3-based particles were synthesized as systems for drug delivery to mitochondria.[222] First, a polyacrylate coating was deposited on the CdSe/ZnS hydrophobic nanoparticles (abbreviated as QD) and on γ-Fe_2O_3 (a fluorescent group was also introduced into iron oxide; it is designated as a green star); then the primary amino groups on their surface were used for binding to the aldehyde group of the TPP reagent. This gave functionalized TPP–QD and TPP–γ-Fe_2O_3 quantum dots (Fig. 61). It was established that TPP–QD and TPP–γ-Fe_2O_3 have high colloidal stability in water and in various buffer solutions. The size of the starting QD was in the range of 2–5 nm, while the size of γ-Fe_2O_3 particles was ~3–6 nm. The hydrodynamic diameter of particles with a polyacrylate shell increased to 20–40 nm, while after functionalization with TPP, it increased to 30 to 45 nm. The surface charge of the nanoparticles varied from –2 to +2 mV at pH 4.5, but greatly shifted to negative values at pH 7.4 and 9.0 (–15 to –5 mV).

8. Other types of functionalized triphenylphosphonium nanoparticles and strategies for their use

It is known that pyroptosis is accompanied by the release of immunogenic mediators and serves as an innovative strategy for

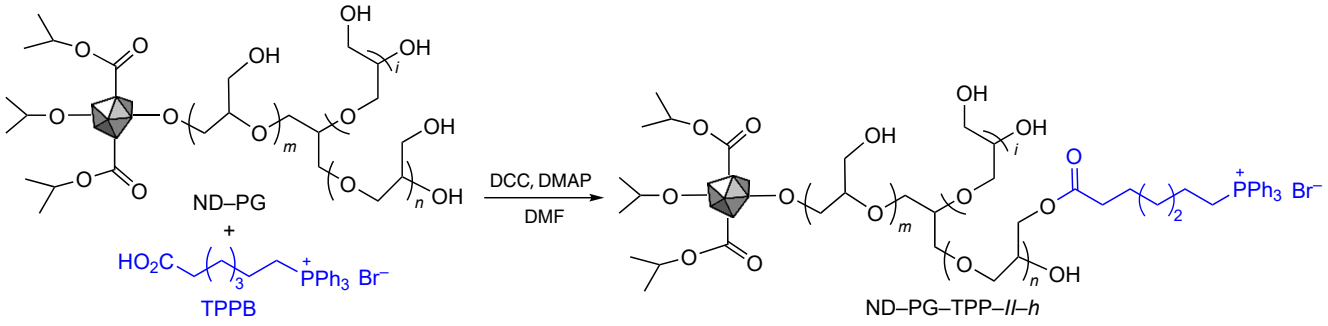

Figure 59. Synthesis of TPP nanodiamond.

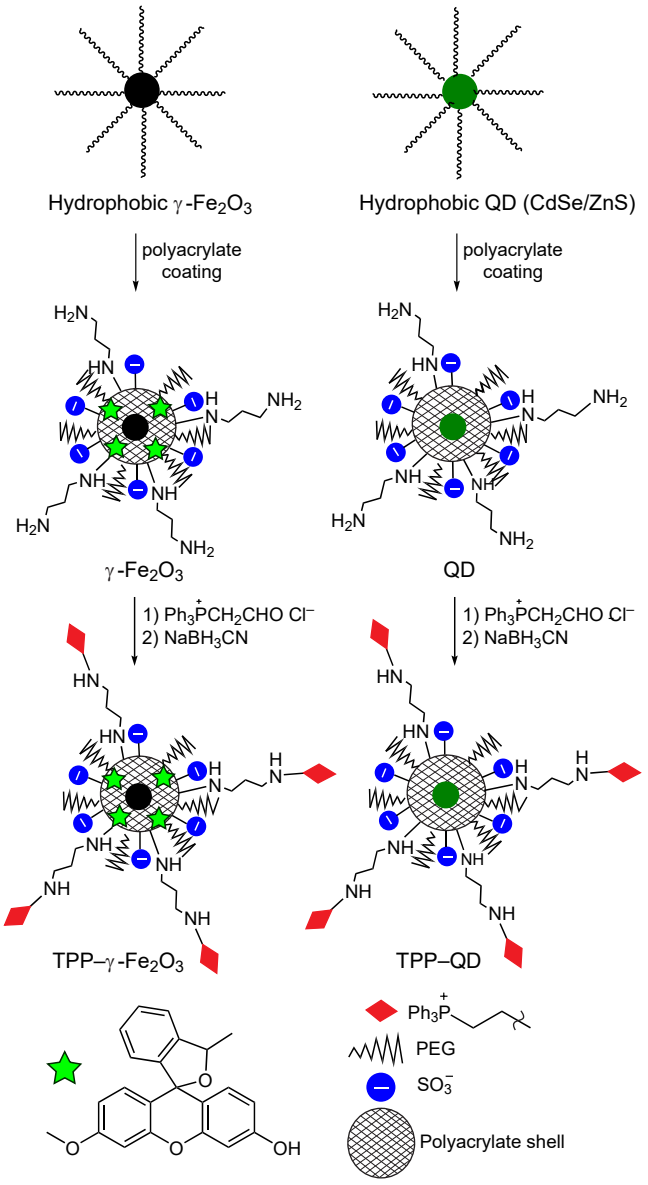

Figure 61. Synthesis of the TPP–QD and TPP–γ-Fe_2O_3. The Figure was created by the authors using published data.[222]

reprogramming of the tumor microenvironment. However, damaged mitochondria, which are the source of pyroptosis, are often destroyed by mitophagy, which considerably weakens the pyroptosis-induced immune activation. Ye *et al.*[223] used black phosphorus nanosheets (BlP-NS) as a delivery system for the pyroptosis inducer and a mitophagy blocker, since the destruction of these particles may impair the lysosome function by changing the inner pH. To facilitate pyroptosis, the lonidamine drug (an inducer of pyroptosis) was pre-coupled with a TPP agent *via* a tris(hydroxymethyl)aminomethyl spacer, which gave the compound TLD, a mitochondrial target (Fig. 62). The mitochondria-targeted LND-modified BlP sheets (TLD–BlP-NS) were additionally encapsulated into the macrophage membrane to make them able to penetrate the BBB and target the tumor. The antitumor activity of the membrane-encapsulated M@TLD–BlP-NS system (d = 230–240 nm, ζ-potential of –12.5 mV) was studied against the murine orthotopic glioblastoma model (GL261). According to the results, the M@TLD–BlP-NS system can affect mitochondria and induce pyroptosis, which is enhanced *via* mitophagy blocking, resulting in the increased release of immunoactivating factors that promote dendritic cell maturation. Generally, the system has a strong antitumor activity *in vivo*. In addition, upon NIR irradiation, the system induced mitochondrial oxidative stress, which further enhanced persistent immunogenic pyroptosis in glioblastoma cells. This example demonstrates an innovative strategy of using BlP-NS as a system for pyroptosis induction and enhancement, which activates the immunity in the tumor therapy.

Hua *et al.*[224] proposed bifunctional nanosystems targeting hepatocytes and mitochondria. The dual targeting can improve the antioxidant activity of the delivered agents such as astaxanthin and be involved in the intake of nutrients, *e.g.*, in the case of liver diseases. The TLbAC@AXT bifunctional nanosystem ($d \approx 538$ nm) containing astaxanthin targeting the hepatocyte mitochondria is formed upon self-assembly of the AXT and TPP–LbA–SA–HD conjugate (abbreviated as TLbAC) in the EtOH–H_2O system (Fig. 63). First, the conjugate of triphenylphosphonium derivative with 2-hydroxypropyl-β-cyclodextrin (HD) was obtained. Then it was treated with lactobionic acid (LbA) and sodium alginate

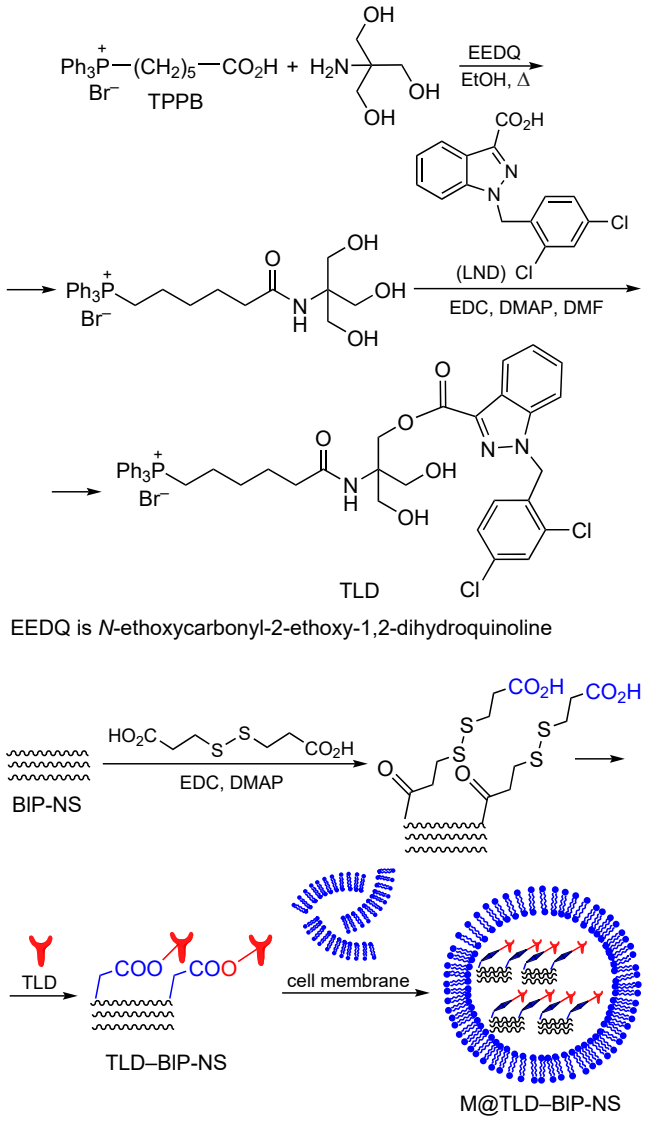

Figure 62. Synthesis of M@TLD – BlP-NS. The Figure was created by the authors using published data.[223]

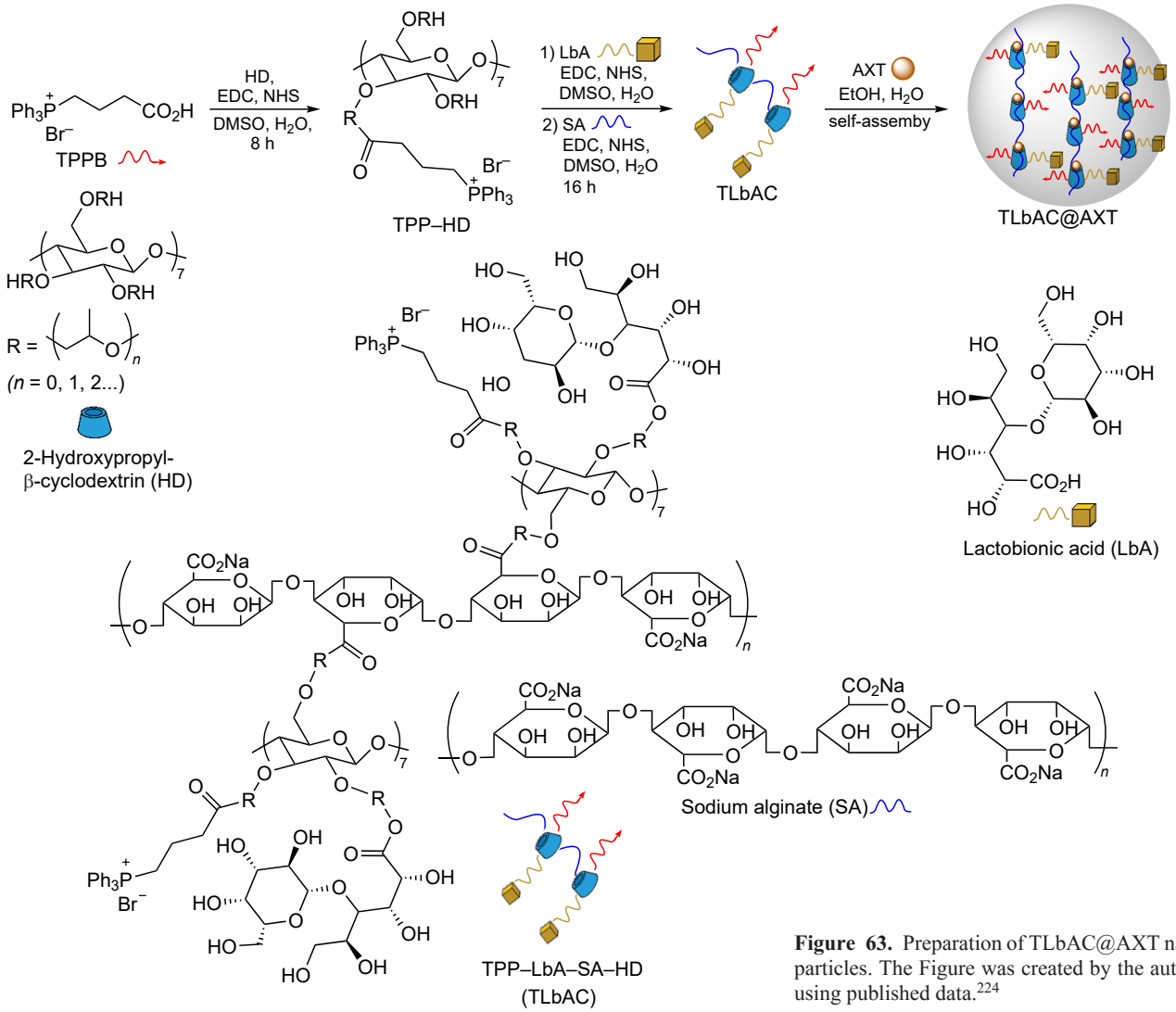

Figure 63. Preparation of TLbAC@AXT nanoparticles. The Figure was created by the authors using published data.[224]

(SA) under conditions of ester bond formation.[224] Astaxanthin has excellent antioxidant properties, which helps to prevent certain diseases and improve immune response. Lactobionic acid efficiently binds to asialoglycoprotein receptors, which are well expressed in hepatocytes, but are virtually not expressed in cells not related to liver, thus providing high accuracy of hepatocyte targeting. The decoration with TPP groups additionally promotes the penetration of the obtained nanoparticles to mitochondria.

Evaluation of the effect of the nanosystems on hepatocytes *in vivo* showed that the fluorescence intensity of HepaRG cells after the treatment with the bifunctional TLbAC@AXT system increased by 90.3%, which exceeded that for a system containing LbA in the absence of TPP groups (38.7%). The ROS level in the group of animals administered with TLbAC@AXT substantially decreased (down to 62.20%) compared to that in mice administered with only astaxanthin (84.01%) or LbA (73.83%). The mitochondrial membrane potential was 97.35% recovered for a group of subjects treated with bifunctional nanosystem and only 77.45% recovered for the group treated with only lactobionic acid. The liver uptake of the bifunctional TLbAC@AXT nanosystem increased by 31.01% compared to the control. These results indicate that the above bifunctional nanosystem is fairly effective as a delivery vehicle for astaxanthin to hepatocyte mitochondria.

The synthesis of polyfunctional peptide biopolymer[225] based on human serum albumin (HSA) is depicted in Fig. 64. In the first step, after the addition of ethylenediamine, some of carboxyl groups in the globular protein were replaced by primary amino groups. The resulting polycationic albumin (cHSA) had more active sites for the subsequent chemical modifications and also had a better adhesion to the cellular surface, which enabled cellular uptake after the initial electrostatic interaction. Upon denaturation, the cHSA polycation was converted to the dcHSA protein containing 35 accessible thiol groups out of which 27 groups were able to react with polyethylene oxide side chains, which led to decrease in non-specific interactions. This afforded the water-soluble dcHSA–PEO hybrid, the optimal base for further modification.

To increase the cellular uptake and stimulate the escape from endosomes, the TAT peptide (HS-Cys-Gly-Tyr-Gly-Arg-Lys-Lys-Arg-Arg-Gln-Arg-Arg-Arg) and *N*-hydroxysuccinimide-activated maleimide (MI–NHS) were added to the hybrid. The latter reagent reacted with the dcHSA–PEO hybrid biopolymer in the phosphate buffer at pH 7.4, and the terminal SH groups of cysteine in the peptide reacted with the maleimide moiety to give the dcHSA–PEO–TAT polymer. The attachment of the TPP groups that ensured the selective mitochondrial uptake was performed in the presence of the EDC–NHS system. The TPP–TAT–PEO–dcHSA bioconjugate thus formed was

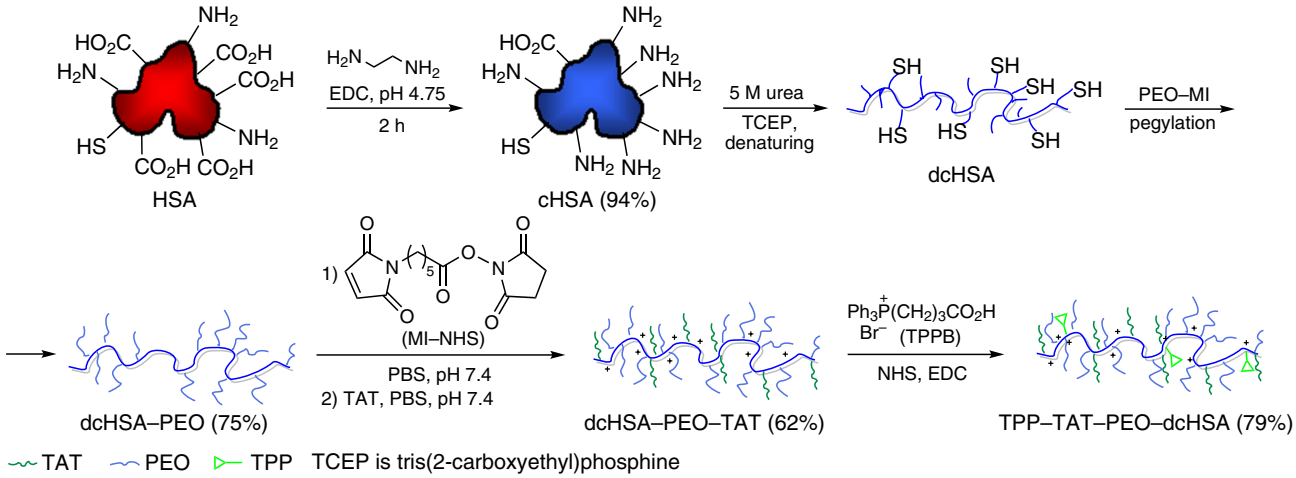

Figure 64. Synthesis of the TPP–TAT–PEO–dcHSA biopolymer. The Figure was created by the authors using published data.[225]

treated with a solution of $HAuCl_4$ and then with an aqueous solution of sodium hydroxide. This gave gold nanoparticles ($d = 2.0 \pm 0.5$ nm) coated with this bioconjugate. After treatment with an $HAuCl_4$ solution, $NaBH_4$ was added in some cases to obtain larger gold nanoparticles ($d = 4.0 \pm 1.3$ nm).

Nanohybrid cerasomes based on cerasome-forming lipid (CFL) (Fig. 65), prepared by controlled hydrolysis, were proposed as new promising drug delivery systems.[226] The polyorganosiloxane surface is known to impart high stability to cerasomes (CER) in comparison with conventional liposomes.

(3-Aminopropyl)triethoxysilane, which served as a linker, was coupled with triphenylphosphine for the introduction of the TPP moiety on the cerasome surface by the hydrolytic condensation involving the Si–OH groups.[227] The TPP modified cerasomes were formed upon self-assembly and sol–gel reaction involving amphiphilic organotrialkoxysilanes, which afforded bilayer vesicles with the siloxane surface. The CER–DOX and TPP–CER–DOX nanoparticle sizes were 226 and 220 nm, respectively, while their ζ-potentials under neutral conditions were 18.61 ± 6.41 and $+15.37 \pm 0.68$ mV, respectively. The TPP–CER–DOX particles showed better mitochondrial accumulation than cerasomes not modified with the TPP groups; this was additionally confirmed by quantitative analysis of the mitochondrial transmembrane potential.[227]

Magnetic nanoparticles (MNPs) offering the possibility of remote control and manipulation were tested for the magnetomechanical destruction of cancer cells.[228–230] It is known that MNPs can convert the magnetic field energy into mechanical force due to the remote interaction between the nanoparticles and applied magnetic fields, and in this state, they are able to damage tumor cells. Chen *et al.*[231] considered a magnetomechanical approach to the treatment of deep-seated tumors using mitochondria-targeted zinc-doped iron oxide nanoparticles modified with TPP-groups (TPP–MNPs). These nanoparticles can move under the action of rotating magnetic field at 15 Hz frequency and 40 mT strength. TPP–MNPs synthesized by thermal decomposition had a size of 22.6 ± 1.5 nm and ζ-potential of $+35.4 \pm 0.8$ mV. They mechanically affected

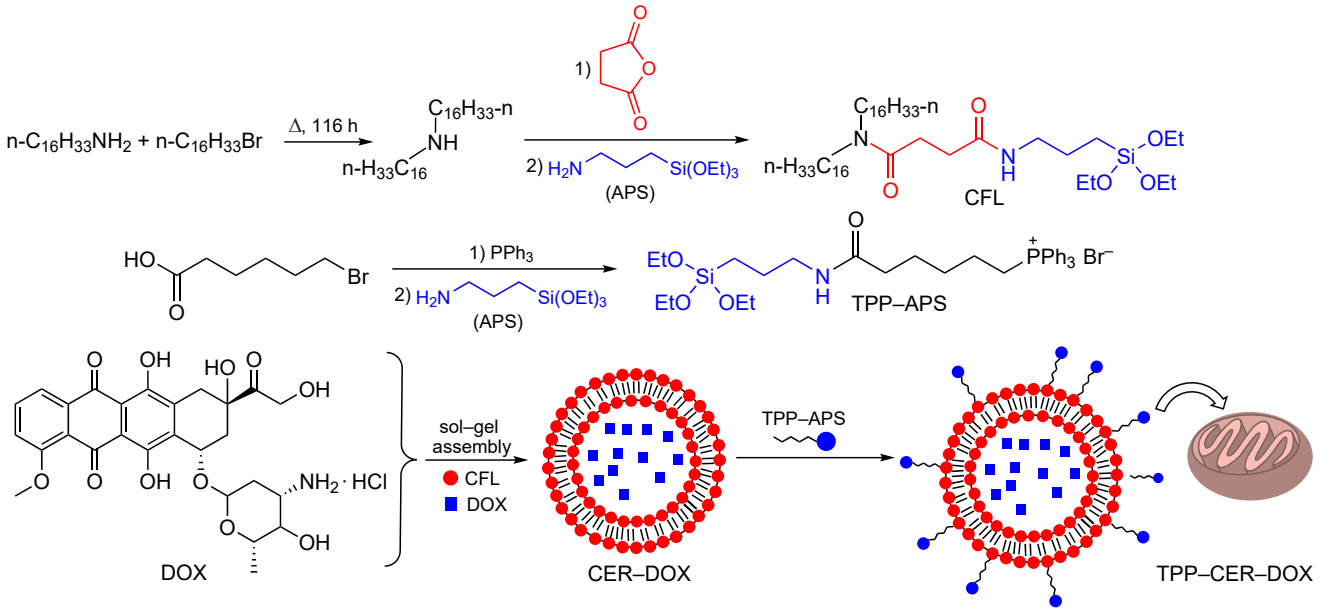

Figure 65. Preparation of cerasome-forming lipids and TPP cerasomes for DOX delivery to mitochondria. The Figure was created by the authors using published data.[226,227]

the mitochondria of brain cancer cells, resulting in effective cell damage, initiation of apoptosis and decrease in the tumor growth rate.

The generation of high doses of ROS, which can damage mitochondria and activate apoptosis, is a promising *in situ* strategy, as this enhances the therapeutic effect in cancer treatment.[232] Zhang *et al*.[233] synthesized dual targeted polyprodrug nanoparticles (DT-PNs) (Fig. 66), in which covalently bound camptothecin (CPT) repeated units released the free drug in the presence of endogenous mitochondrial ROS. Camptothecin is a cytotoxic quinoline alkaloid, which was isolated from the 'happy tree' (*Camptotheca acuminata*), often used in the treatment of cancer in traditional Chinese medicine. This drug was chosen as a model for the developed nanoreactors, because, apart from inhibition of DNA topoisomerase I, it also inhibits the cellular respiration thus inducing the activation of mitochondrial ROS. After being released from the nanoreactor, CPT provides the generation of ROS and induces long-term high oxidative stress, which causes the cancer cell apoptosis. The average diameter of spherical DT-PNs was ~55 nm. The ROS-sensitive block of this reactor included the CPT–SM conjugate containing a dithioketal moiety and was located in the hydrophobic core, while the hydrophilic corona was decorated with the cRGD groups.[1] This peptide is specific to integrins that are expressed during tumor-associated angiogenesis and selectively interacts with $a_v\beta_3$ receptors and triphenylphosphonium.

It was found that the peak value of ROS burst occurred for cancer cells approximately 10 h after the treatment with DT-PNs. In addition, the most significant tumor inhibition was observed, and the treatment did not cause infections or inflammation in treated mice.

9. Synergistic nanosystems for photodynamic and photothermal therapy

[1] cRGD is the Arg-Gly-Asp-D-Phe-N-Me-Lys cyclic peptide containing arginylglycylaspartic acid (RGD).

Mitochondria are widely studied as the targets for photodynamic therapy. In order to improve the transport of photosensitizers (PS) and enhance the therapeutic effect, TPP derivatives are often used as mitochondria-targeted systems. It is known[234] that the attachment of folic acid and a photosensitizer to the graphene oxide (GO) surface improves the transport characteristics of the nanocomplex for the delivery to cancer cells and decreases their toxicity. To enhance the effect of PDT, Yang *et al*.[235] developed a system based on GO, which combined groups for cellular [*meso*-tetrakis(4-carboxyphenyl)porphyrin (TCPP)] and mitochondria [(3-aminopropyl)triphenylphosphonium bromide] targeting, which were connected *via* the amide bond. It is noteworthy that in this case, one of the four carboxyl groups of the porphyrin derivative remained free. Then the TPP–TCPP conjugate was introduced into the GO–FA complex by physical mixing, which gave rise to the layered nano-sized TPP–TCPP@GF complex (Fig. 67). This complex demonstrated low toxicity, good mitochondria targeting, water solubility and photoluminescent properties. It was shown that TPP–TCPP@GF can be localized in the mitochondria of HeLa cell cytoplasm and inhibit the cell viability. The IC_{50} values under irradiation were 11.91±1.10 and 83.15±4.25 μg mL^{-1} for the TPP–TCPP conjugate and for free TCPP complex, respectively.

The PDT effect can be enhanced by simultaneous encapsulation of chlorin e6 (Ce6) and IR780 dye into liposomes. Chlorin generates oxygen and is responsible for fluorescence, while the dye-induced hyperthermia leads to tumor cell damage (photothermal therapy).[236] These delivery systems were called theranosomes (TNS) owing to a combination of the multimodal therapeutic properties and the possibility of dual imaging. The TPP ligand was added to theranosomes by direct chemical conjugation with a PEG chain to give TPP/IR780/Ce6-TNS nanoparticles (TICT). The theranosomes were obtained by film hydration. The theranosome size increased upon conjugation from 132 to 256 nm. The mice bearing 100–200 mm^3 tumors were treated by intravenous injections of physiological saline containing free IR780 and Ce6 or TICT conjugate (the dye concentration was 0.5 mg kg^{-1}). Evaluation of the antitumor

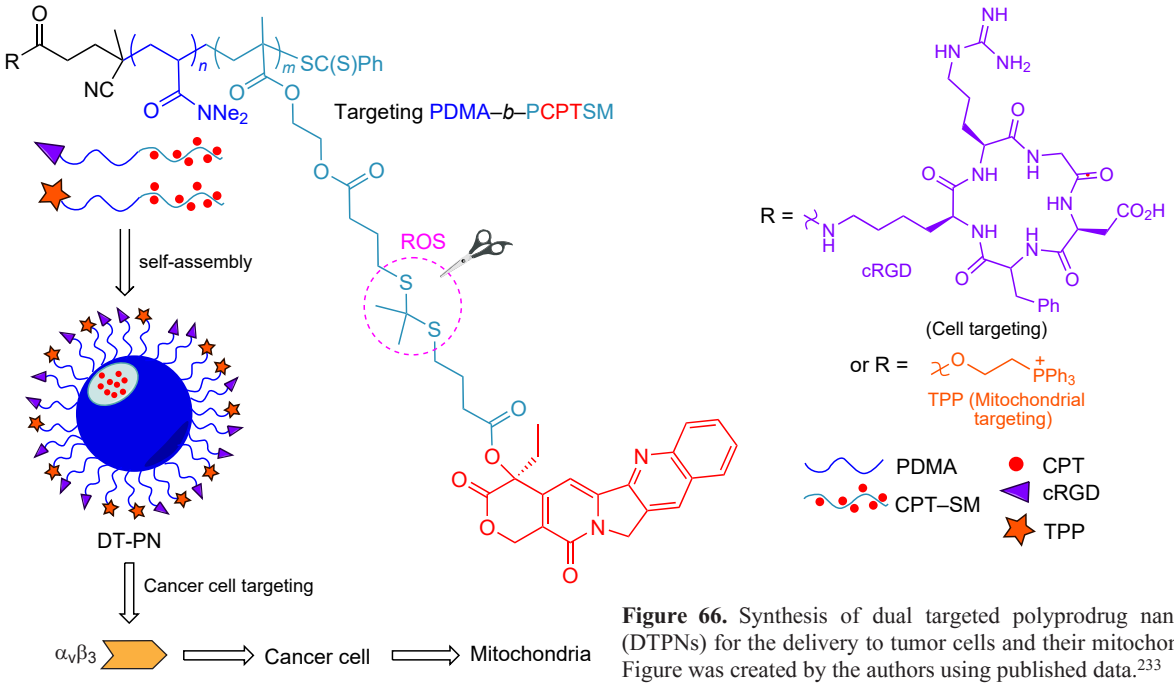

Figure 66. Synthesis of dual targeted polyprodrug nanoparticles (DTPNs) for the delivery to tumor cells and their mitochondria. The Figure was created by the authors using published data.[233]

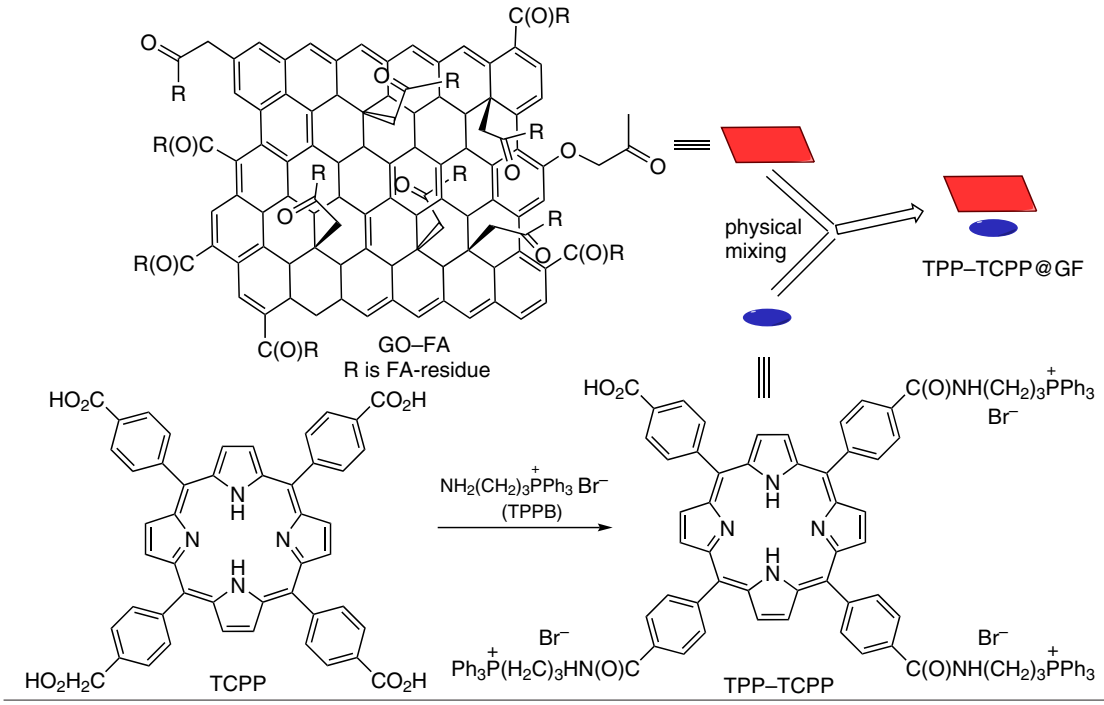

Figure 67. Synthesis of TPP–TCPP@GF.

properties of the agents *in vitro* and *in vivo* attested to good prospects of using theranosomes for the multimodal tumor therapy both regarding the imaging and strongly enhanced PDT effect. The dye-induced hyperthermia led to the destruction of tumor cells, while lysosome destruction during PTT improved chlorin delivery into cytoplasm and promoted the release and accumulation of chlorin in mitochondria, which enhanced its photodynamic activity.

The biological theranostics induced by NIR light (λ = 808 nm) is gradually becoming a popular method for the treatment of cancer. The $AgBiS_2$ nanodots (d = 3–12 nm), which had photothermal properties, were coated by the PEI layer (MW = 25 kDa). The resulting $AgBiS_2$–PEI nanoparticles were then allowed to react with (3-carboxypropyl)triphenylphosphonium bromide in DMF in the HBTU–HOBT–DIPEA system (Fig. 68).[237] The decoration of the particles with TPP groups improved their targeting of tumor cells, which contain more mitochondria than normal cells for energy generation providing fast growth and increase in the population. Then the $AgBiS_2$–PEI–TPP conjugates were treated with the FITC–APTES composition; this gave $AgBiS_2$–TPP–FITC nanoparticles coated by silicon-containing oligomers. The photothermal effect of the $AgBiS_2$–PEI–TPP particles (ζ-potential of ~20 mV) was confirmed by chemical probes (mito-Traker Red, Hoechst 33342, *etc.*) and by detection of intracellular ROS. In the resulting structure, $AgBiS_2$ nanodots exhibited photothermal properties both *in vitro* and *in vivo* in mice bearing HeLa tumor; furthermore, the nanoparticles had low toxicity. The presence of TPP groups somewhat improved the photothermal properties of $AgBiS_2$ nanodots through targeted delivery to the mitochondria of cancer cells, which makes the $AgBiS_2$–PEI–TPP nanocomposite an effective PTT agent. In addition, the $AgBiS_2$–PEI–TPP showed excellent results as an agent for computed tomography in the tumor diagnosis.

It is believed that breast cancer stem cells are responsible for tumor initiation, invasion, metastasis and recurrence, which lead to treatment failure.[238] Hence, the development of effective strategies targeted at CSC has a crucial importance for increasing the efficiency of anticancer therapy. Pan *et al.*[239] decorated gold nanostars (AuNSt) simultaneously with several agents: 3-bromopyruvate [hexokinase 2 (HK2) inhibitor], (4-carboxybutyl)triphenylphosphonium bromide (mitochondria targeting group) and hyaluronic acid (CSC targeting group) and thus obtained AuNSt–dPG/3-BP/TPP/HA nanocomposite particles coated by dendritic polyglycerol (dPG) (Fig. 69). These particles have a good biocompatibility and demonstrate an excellent ability to bind to HK2 into mitochondria *via* interaction with 3-BP, thus inhibiting metabolism and further inducing cell apoptosis by releasing cytochrome *c*. The use of the nanocomposite enhanced the therapeutic efficacy of targeted PTT involving gold nanoparticles specific to CSC an provided a

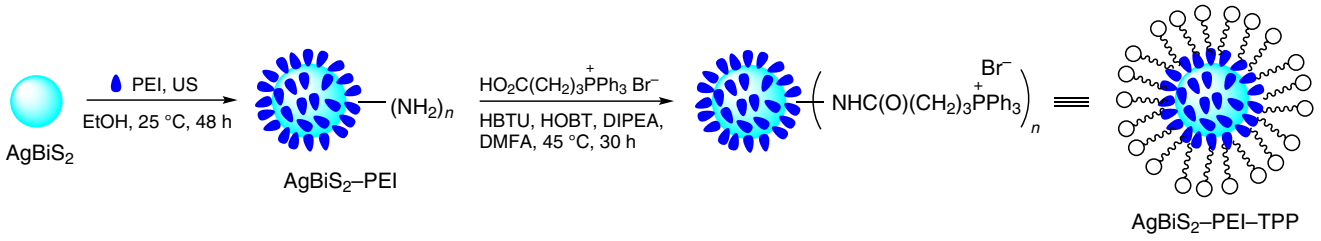

Figure 68. Preparation of the $AgBiS_2$–PEI–TPP nanocomposite. The Figure was created by the authors using published data.[237]

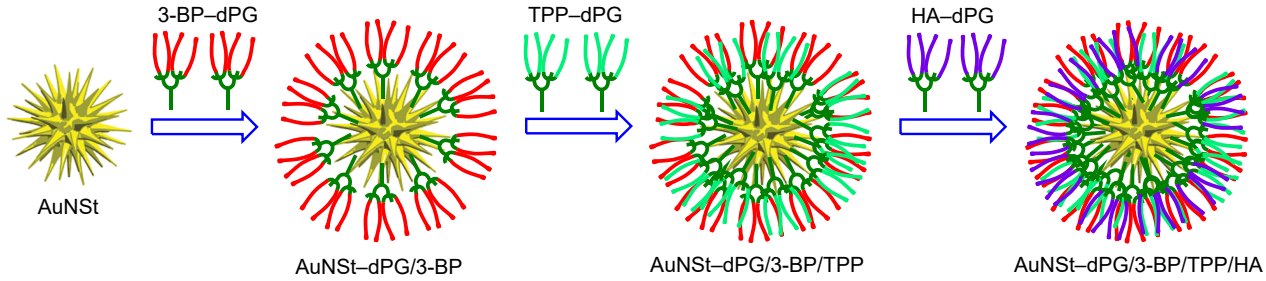

Figure 69. Synthesis of GNS–dPG/3-BP/TPP/HA nanocomposite. The Figure was created by the authors using published data.[239]

synergistic effect in eradication of these cells. After treatment, the self-renewal of the breast CSC and stemness gene expression are suppressed, CSC-driven mammosphere formation diminishes, the tumor growth is effectively inhibited and CSC are killed Thus, the developed AuNSt–dPG/3-BP/TPP/HA nanocomposites demonstrate a new strategy for targeted, precise and highly effective destruction of CSC.

In order to attain synergism of the chemodynamic therapy (CDT) and PTT, Li *et al.*[240] synthesized MoS2@PDA–Fe@PEG–TPP nanosheets (abbreviated as MPFPT), which acted as mitochondria-targeted delivery agent. As the starting compounds, the authors used TPP-modified PEG and MoS_2 nanoparticles coated by the polydopamine complex with Fe^{3+} ions. The results of *in vitro* experiments showed that MPFPT nanosheets were more active against cancer cells than similar agents based on MoS_2 without mitochondria-targeted groups. An enhanced therapeutic efficacy of a combination of PTT and CDT using this nanosystem was demonstrated.

Currently, a considerable progress has been made in the antitumor therapy related to cancer cell hypoxia. However, the treatment with only hypoxia-activated prodrugs has a low efficiency due to the difficulty of their targeted delivery. The HCuS–TH302–PDA–Ce6/TPP nanoparticles combining the properties of PDT and PTT agents and mitochondria-targeted hypoxia-activated chemotherapy agents have been developed for synergistic treatment of cancer.[241] Hollow copper sulfide nanoparticles coated by polydopamine (HCuS–PDA) were used as photothermal nanoagents and thermoresponsive carriers for (1-methyl-2-nitro-1*H*-imidazol-5-yl)methyl-*N*,*N*-bis(2-bromoethyl)phosphpdiamidate, hypoxia-activated prodrug encoded as TH302. The Ce6 moieties and TPP groups were attached to the surface of the HCuS–PDA particles (Fig. 70) in the presence of EDC and NHS for carboxyl group activation. The HCuS–TH302–PDA–Ce6/TPP nanoparticles were mainly accumulated in mitochondria. The use of a laser at 660 nm wavelength for the excitation of Ce6 may result in ROS generation and simultaneously aggravate the cellular hypoxia. Upon laser irradiation at $\lambda = 808$ nm, the HCuS–TH302–PDA–Ce6/TPP nanoparticles generated local heat by increasing the release of the TH302 agent in tumor cells, promoting cell death and increasing the tumor hypoxia level. Under these conditions, the antitumor activity of the released drug was significantly enhanced. The *in vitro* and *in vivo* assays carried out by the authors demonstrated a high efficacy of the combined use of hypoxia-activated chemotherapy, PDT and PTT compared to conventional cancer therapy.

Liu *et al.*[242] synthesized a material with antioxidant and anti-inflammatory properties (encoded as TPCD) by conjugation of 4-hydroxy-2,2,6,6-tetramethylpiperidin-1-oxyl (Tempol) and phenylboronic acid pinacol ester (PBAP) moiety with β-cyclodextrin. TPCD nanoparticles were obtained by the modified nanoprecipitation–self-assembly of the conjugate in the presence of the DSPE–PEG polymer. The obtained nanoparticles had a core–shell structure with a hydrophobic core coated by this polymer; they had a narrow size distribution ($d = 101$ nm) and a ζ-potential of -29.4 ± 1.7 mV. *In vivo*

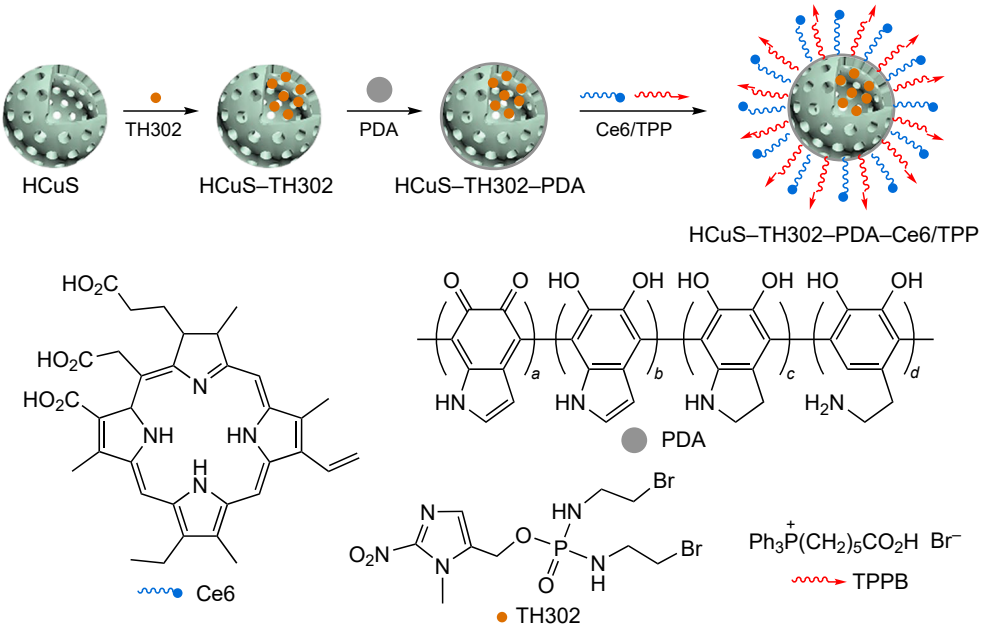

Figure 70. Synthesis of HCuS–TH302–PDA–Ce6/TPP nanoparticles. The Figure was created by the authors using published data.[241]

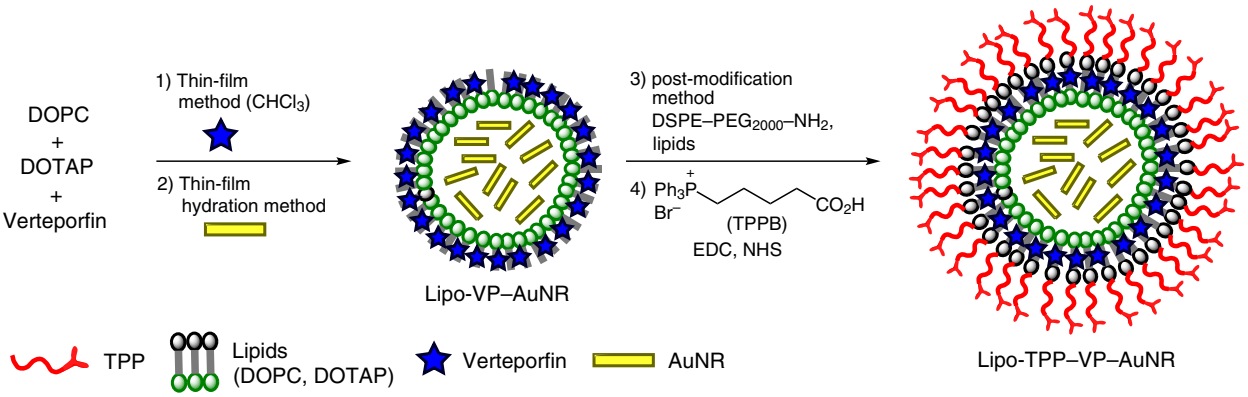

Figure 71. Preparation of liposomes containing gold nanorods and decorated with the TPP–NH–PEG_{2000}–DSPE polymers. The Figure was created by the authors using published data.[243]

experiments involving TPCD were carried out on a mouse model of heart failure. It was found that these nanoparticles can accumulate in the heart (*via* the transport across the lung epithelial and endothelial barriers to pulmonary circulation) and efficiently prevent heart failure.

Gu *et al.*[243] created a mitochondria-targeted nanomaterial intended for neoadjuvant PDT of rectal cancer (HCT116). As a photosensitizer, the authors used verteporfin (VP), which induces the conversion of inactive oxygen to cytotoxic singlet oxygen ($^1O_2$) under the action of X-ray radiation. This biodegradable nanomaterial was obtained in several stages. First, DOPS (1,2-dioleoyl-*sn*-glycero-3-phospho-*L*-serine) and DOTAP lipids and verteporfin were dissolved in chloroform (Fig. 71). Then, the solution was evaporated until a thin film formed, the film was hydrated with an aqueous dispersion containing gold nanorods (AuNRs) of 10 nm size; and Lipo-VP–AuNR nanoparticles (d = 143.5 nm, PDI = 0.222, ζ-potential of +42.7 mV) were formed. According to thermogravimetry data, these particles contained 1.1% AuNRs in the aqueous core. The nanoparticles were then successively treated with a micellar solution obtained from a mixture of the lipids and the DSPE–PEG_{2000}–NH_2 polymer and the TPPB–EDC–NHS system (see Fig. 71), which gave rise to Lipo-TPP–VP–AuNR nanoparticles ($d \approx$ 150 nm). They had a lipid bilayer with a thickness of 8 nm, according to transmission electron microscopy data. In the author's opinion, this method of synthesis was more efficient than the pre-decoration of the initial polymer with TPP groups in the presence of coupling agents (EDC and NHS) to form the TPP–NH–PEG_{2000}–DSPE conjugate. Owing to the synergistic effect of X-rays, combined action of gold nanorods and verteporfin, and the presence of TPP-modified liposomal carriers, these nanoconjugates generated a relatively high amount of $^1O_2$ in the mitochondria, thus decreasing the membrane potential and inducing mitochondrial-mediated apoptosis of cancer cells.

10. Conclusion

Mitochondria perform many important functions in eukaryotic cells: they accomplish oxidative phosphorylation processes, produce ATP, participate in various metabolic processes such as pyruvate conversion to acetyl-CoA or cleavage of fatty acids *via* β-oxidation, and promote the deposition of calcium ions and the synthesis of steroid hormones from precursors. Mitochondria are involved in the biosynthesis of urea and pyrimidine nucleotides, apoptosis regulation and ferroptosis. Mitochondrial dysfunctions disrupt cellular homeostasis, which leads to serious diseases such as neurological and cardiovascular pathologies, metabolic disorders, diabetes mellitus, cancer and others. For this reason, mitochondria are a promising potential target for diagnostic and therapeutic interventions. However, the delivery of drugs to mitochondria requires overcoming a number of cellular and mitochondrial barriers such as the plasma membrane and mitochondrial membranes, lysosomal uptake, blood–brain barrier (for brain cells), *etc*. Often, pharmaceutical agents cannot pass these barriers without assistance and show poor biodistribution and non-optimal pharmacokinetics. Nanoparticles are able to eliminate these drawbacks by providing cell targeting, controlled release to specific subcellular organelles and long blood circulation times. Nanoparticles based on liposomes, liposome-like vesicles, biodegradable polymer particles, metals, quantum dots, *etc*., help in drug delivery to mitochondria. Some of them (drug substances, metal particles, quantum dots) induce mechanical destruction of cells under the action of physical stimuli such as heating or radiation, some other induce metabolic damage, thus leading to the death of the transformed cells.

An important achievement of the targeted delivery is effective decoration of nanoparticles with groups or ligands capable of targeted delivery of 'useful load' to mitochondria. Among these groups, charged lipophilic phosphonium cations, which easily overcome both cellular and mitochondrial barriers, deserve special mention.

In this report, we demonstrated various methods and techniques used for modification of nanoparticles with triarylphosphonium (most often, triphenylphosphonium) cation. A special place belongs to the covalent coupling of derivatives of TPP salts with the corresponding functional groups of nanoparticles and incorporation of hydrophobic substituents present in the phosphonium moiety into the nanoparticle surface layer. There are quite numerous commercially available phosphonium salts containing carboxyl groups. These reagents can be easily conjugated by traditional organic reactions, in particular carbodiimide coupling, which enables quantitative linking of the phosphonium group to the hydroxyl or amino group under mild conditions, which could further serve for structure optimization. Nanoparticles are fabricated using a broad range of both natural (albumin, *etc*.) and synthetic polymers [poly(ethylene oxide), its copolymers, *etc*.]. It was shown using numerous examples that nanoparticles are promising nanoplatforms for the integration with other diagnostic and therapeutic components for subsequent

biomedical applications. These TPP-decorated nanoparticles loaded with various drug substances show high efficiency in the targeted drug delivery to mitochondria and enhance the biological action of drugs in comparison with their free forms.

Table 1 summarizes data on the TPP derivatives used for decoration of mitochondria-targeted nanoparticles in *in vivo* assays that approximately correspond to the criteria imposed on preclinical trials in animals (GLP). The Table includes data on the particles used for modification, drug substances that are used for delivery, *in vivo* models, types of tumors, applied doses and therapeutic effects.

The targeted delivery and manifestation of biological effects are greatly affected by both the physicochemical characteristics of TPP-containing nanoparticles (composition, size, polydispersity index, shape, ζ-potential, chemical composition of the surface, drug loading capacity, encapsulation efficiency, stability in acidic or alkaline medium) and their diverse interactions with biological membranes. These factors play an important role in determining not only the transport functions of nanoparticles, but also their biomedical applications, biomolecular signaling, biological kinetics and toxicity *in vivo* and *in vitro*.

Of considerable interest are TPP-nanoparticles with drug substances coated by hyaluronic acid for neutralization of the positive charge and recognition by the receptor systems of tumor cells. They have good biocompatibility, enhanced cellular uptake *via* endocytosis and efficiently deliver the drug to mitochondria with the subsequent degradation by hyaluronidase in endosomes, thus markedly increasing the anticancer activity of the drug. Thus, the combination of mitochondriotropic strategies with the preparation of dosage forms based on nanotechnologies can give rise to new methods of treatment of a wide range of socially significant diseases, such as cancer and cardiovascular, age-related neurodegenerative and autoimmune diseases.

Meanwhile, it is necessary to note a number of unsolved problems that hinder the development of this promising scientific area at the boundary between molecular biology and various fields of chemistry, *i.e.*, inorganic, organic, pharmaceutical, colloid and polymer chemistry. The problems are associated, first of all, with elucidation of the relationship between nanoparticle characteristics and biological properties and between the physicochemical and transport properties of nanoparticles. In addition to other properties, the size of TPP-nanoparticles is an important parameter for the development of effective drug delivery systems, which determines both the way of internalization and the mechanism of intracellular targeting. The targeting strategies for TPP nanoparticles with a modified surface to transformed cells also await further development. The release of drug-carrying TPP nanoparticles from internalized endosomes to avoid lysosomal degradation is also a key task, which has to be solved for a design of efficient systems for drug delivery to mitochondria. In addition, an essential trend of research is the creation of TPP-modified nanosystems that withstand acidic conditions of lysosomes and then escape from lysosomes to mitochondria. Studies of the effect of TPP nanoforms on the toxicity of both the carriers and drug substances they transport and on the cell metabolism and drug pharmacokinetics are also important today.

11. List of abbreviations and symbols

The following abbreviations and symbols are used in the review:

ADR — Adriamycin,
AKI — acute kidney injury,
AMI — acute myocardial infarction,
ATP — adenosine triphosphate,
ATM — serine threonine protein kinase with a mutation in ataxia/telangiectasia
AXT — astaxanthin,
3-BP — 3-bromopuryvate,
BlP-NS — black phosphorus nanosheets,
Cb — chlorambucil,
CDT — chemodynamic therapy,
Cela — celastrol,
CE — casein,
CER — cerasome,
Chol — cholesterol,
COPT — cobaltosic oxide poly(ethylene glycol) triphenylphosphine,
CQ — chloroquine,
CQD — carbon quantum dots,
CS — chitosan,
CSC — cancer stem cells,
CTAC — cetyltrimethylammoinum chloride,
Cou6 — 3-(2-benzothiazolyl)-7-(diethylamino)coumarin,
Cur — curcumin,
d — average hydrodynamic diameter,
DA — dimethylmaleic anhydride,
DCC — dicyclohexylcarbodiimide,
DCM — dichloromethane,
DIPEA — diisopropylethylamine,
DMPE — dimyristoyl phosphatidylethanolamine,
DOTAP — *N*-[1-(2,3-dioleoyloxy)propyl]-*N*,*N*,*N*-trimethylammonium,
DOPE — dioleoyl phosphatidylethanolamine,
DOX — doxorubicin,
DPPE — dipalmitoyl phosphatidylethanolamine,
DPPC — 1,2-dipalmitoyl-*sn*-glycero-3-phosphatidylcholine,
DTPN — polyprodrug nanoreactors,
DTPP — 2-distearoyl-*sn*-glycero-3-phosphatidylethanolamine-3-carboxypropyltriphenylphosphonium,
DS — drug substance,
DTX — docetaxel,
DS — distearoyl,
EDC — 3-ethyl-1-(3-dimethylaminopropyl)-3-carbodiimide,
EPR — enhanced permeability and retention,
FA — folic acid,
FITC — fluorescein isothiocyanate,
G(n) — dendrimer with the generation number n,
G2R-DA — dendritic amino acids,
GO — graphene oxide,
GS — genistein,
GSH — glutathione,
HA — hyaluronic acid,
HAS — human serum albumin,
HBTU — *N*,*N*,*N*′,*N*′-tetramethyl-*O*-(1*H*-benzotriazol-1-yl)-uronium hexafluorophosphate,
HCPT — 10-hydroxycamptothecin,
hydChol — hydrogenated cholesterol,
HK2 — hexokinase 2,
HOBt — 1-hydroxybenzotriazole,
HTPPB — hexadecyltriphenylphosphonium bromide,
IC_{50} — half-maximal inhibitory concentration,
IO — iron oxide,
LbA — lactobionic acid,
LND — lonidamine [1-(2,4-dichlorobenzyl)-1*H*-indazole-3-carboxylic acid],
LPT — lapatinib,
Luc — D-luciferin,

Table 1. Mitochondria-targeted nanoparticles in *in vivo* assays.

Particle type	TPP conjugate	Drug substance	Animals (sex, age)	Type of tumor	Way of administration	DS dose, mg per kg (see [a])	Therapeutic effect	Ref.
Liposomes	Stearyltriphenylphosphonium bromide (STPPB)	Ceramide	Immunodeficient BALB mice (females)	4T1 human breast cancer xenograft model	s/c	6 (6)	Tumor growth inhibition	94
Liposomes	TPP–Cholesterol (TPP–Chol)	Celastrol, Nile Red (NR)	Immunodeficient mice	HepG2 human hepatocellular carcinoma xenograft	i/v	2 (for Cela) and 0.2 (for NR) in 5% solution of glucose	Tumor growth inhibition	107
Liposomes	TPP–poly(ethylene glycol)–phosphatidyl-ethanolamine (TPP–PEG_{2000}–PE)	Paclitaxel	Immunodeficient BALB mice (6–8 weeks)	4T1 human breast cancer xenograft model	i/v	1	Tumor growth inhibition	109
Liposomes	TPP–1,2-Distearoyl-*sn*-glycero-3-phosphoethanol-amine–*N*-aminopoly(ethy-lenglycol)$_{2000}$ succinate (TPP–DSPE–PEG_{2000})	Lonidamine, IR-780	Immunodeficient BALB mice (females, 5 weeks)	LL/2 Lewis lung carcinoma xenograft	i/v	9 (for LND) and 1.5 (for IR-780)	Complete tumor eradication of LL/2 tumor, no recurrence for 50 days	111
Liposomes	PEGylated TPP–Cholesterol (TPP–Chol)	Doxorubicin, lonidamine	Kunming mice	Glioma model *in situ* (C6 cells)	i/v	5	Decrease in the tumor volume, decrease in toxicity	115
Liposomes	MitoPBN prodrug	MitoPBN	HFD:C57BL/6J mice (4 weeks)	Diabetes model *in situ*	i/p	2.5 per day (8 weeks)	Decrease in the mitochondrial oxidative stress and ROS production in liver, decrease in the blood glucose level	121
Liposomes	TPP–D-α-Tocopherol poly(ethylene glycol) succinate (TPP–$TPGS_{1000}$)	Paclitaxel	Immunodeficient BALB mice (females)	A549/CDDDP human lung adeno-carcinoma xenograft	i/v	10	Tumor growth inhibition	122
Liposomes	TPP–docetaxel	Docetaxel	Immunodeficient BALB mice (females)	MCF-7 human breast adenocarcinoma xenograft	i/v	5 (see [b])	Decrease in the tumor growth rate; higher dose kills the animals	123
Solid lipid nanoparticles	TPP–DSPE–PEG	Genistein	APP/PS1 mice	–	i/v	2 (every other day, 30 days)	Decrease in brain inflammation; memory and cognitive function improvement	126
Dendrimer	TPP–PAMAM	*N*-Acetyl-cysteine	White rabbits (from New Zealand)	Brain injury model (TBI)	i/v	55	Accumulation in brain mitochondria	133
Polymer nanoparticles	PEI–TPP–CQ, PEI–TPP–DOX	Chloroquine, doxorubicin	SCID mice (6 weeks)	DU145 human prostate cancer xenograft	i/p	4.5 (for CQ) and 0.75 (for DOX)	Tumor growth inhibition without side effects	139
Polymer nanoparticles	TPP–TOS–PDA–PEG	α-Tocopherol succinate	Immunodeficient BALB/c mice (6 weeks)	Lung cancer cell xenograft	i/v	–	Tumor growth inhibition without signs of toxicity or side effects	155
Hybrid lipid–polymer nanoparticles, PLGA/CPT/DSSP	TPP–C18–PEG_{2000}	Paclitaxel	Immunodeficient BALB/c mice (females)	MCF-7 human breast adenocarcinoma xenograft	i/v	7.5	Accumulation in mitochondria, activation of apoptosis	161

Table 1 (continued).

Particle type	TPP conjugate	Drug substance	Animals (sex, age)	Type of tumor	Way of administration	DS dose, mg per kg (see[a])	Therapeutic effect	Ref.
Hybrid lipid–polymer nanoparticles, PLGA/AA–PEG–hydChol/TPP–Chol	TPP–Chol	Doxorubicin	Immunodeficient BALB/c mice	A549 human lung adenocarcinoma	i/v	10 (7)[b]	Tumor growth inhibition, no systemic toxicity	163
Hybrid nanoparticles, HCPT/TPP–PLGA–PEG_{2000}	TPP–PEG_{2000}	10-Hydroxy-camptothecin	Immunodeficient mice	SW620 human colon adenocarcinoma xenograft	i/v	4	Histopathological changes in tumor tissue without changes in normal tissues	164
CS-FA/TT/PLGA@Cela nanoparticles	TPP-tocopherol poly(ethylene glycol) succinate (TPP–TPGS)	Celastrol	Immunodeficient BALB/c mice	4T1 human breast cancer xenograft model	i/v	2	Antitumor effect, induction of mitochondrial damage, increase in the level of proapoptotic proteins, no toxicity	165
Chitosan-based polymer particles	TPP-Chitosan		Immunodeficient BALB/c mice	H22 hepatoma xenograft	i/v	5 and 50	Tumor growth inhibition at high doses	167
Polymer particles based on electrostatic complexes of modified chitosan with sodium alginate	ТФФ-Chitosan (MW = 100–300 kDa)	Doxorubicin	CD mice (males)	Hepatocellular carcinoma xenograft	i/p	2.5	Reduced cardiotoxicity, restoration of normal liver function and structure	168
Chitosan-based polymer particles	TPP–DOX	Doxorubicin	Mice	Ehrlich ascites carcinoma xenograft	–	7	Induction of apoptosis	169
Hyaluronic acid-based polymer particles	TPP–DOX	Doxorubicin	Immunodeficient mice	MCF-7/ADR human breast adenocarcinoma xenograft	i/v	5	Tumor growth inhibition	170
Hyaluronic acid-based polymer particles, HA–*hydra*–DOX–TPP	TPP–DOX	Doxorubicin	Immunodeficient BALB/c mice (females, 4 weeks)	MCF-7/ADR human breast adenocarcinoma xenograft	i/v	5	Tumor growth inhibition, no side effects	171
Hyaluronic acid-based polymer particles, HA–TS–TPP	TPP–TS	Lapatinib	Mice	MDA-MB-231 human breast adenocarcinoma xenograft	i/v	20	Tumor growth inhibition	172
Supamolecular assemblies	Alkylated TPP derivatives of cyanostilbene	Doxorubicin	Immunodeficient BALB/c mice (5 weeks)	HeLa human cervical cancer xenograft	s/c (see[c])		Decrease in the tumor growth rate	180
Supramolecular assemblies TPP–DTX@FA–Chol–BSA	TPP–DTX	Doxorubicin	Immunodeficient BALB/c mice (males)	MCF7 human breast adenocarcinoma xenograft	i/v	5	Decrease in the tumor growth rate for 14 days	181

Table 1 (continued).

Particle type	TPP conjugate	Drug substance	Animals (sex, age)	Type of tumor	Way of administration	DS dose, mg per kg (see [a])	Therapeutic effect	Ref.
Polymer micelles	Polycationic glycolipid TPP-modified polymer	Doxorubicin	Immunodeficient mice (females, 6–8 weeks)	MCF7 human breast adenocarcinoma xenograft	i/v	2	Tumor growth inhibition, increase in the survival rate	184
Polymer micelles	Pluronic TPP-conjugates	Paclitaxel	Mice	A549/ADR human lung cancer xenograft	i/v	15	Decrease in the tumor growth rate	186
Hybrid micelles	TPP–DOX	Doxorubicin	Mice	H22 hepatoma xenograft	i/v	15	Good contrast properties for MRI (see [d])	187
Polymer micelles	TPP–PEG–PE	DiR-puerarin [e]	Immunodeficient BALB/c mice (females)	ISO-Induced myocardial ischemia	i/v	–	TPP-Conjugate provides preferential drug accumulation and retention in the ischemic myocardium	188
Polymer micelles	TPP–PEG–PLA	Resveratrol	Immunodeficient mice, ICR–mice and SD rats		i/v	10	Improvement of cognitive function and memory	189
PEG–PLA polymer nanoparticles	TPP–HCPH	–	Immunodeficient BALB/c mice (females, 6–8 weeks)	4T1 murine breast cancer xenograft	i/v	5	Decrease in the tumor growth rate without visible side effects	197
TPP–MNP–QD magnetic nanoparticles in 15 Hz magnetic field	TPP–PLL	–	Immunodeficient mice	U87 glioma xenograft at a brain site	–	2	Decrease in the tumor growth rate and increase in the life span	231
TPP–PDMA–*b*–PCPTSM nanoreactor	TPP–PDMA–*b*–PCPTSM	Camptothecin	Immunodeficient BALB/c mice (females, 5 weeks)	4T1 murine breast cancer xenograft	i/v	80 [f]	Complete tumor regression without side effects	233
Theranosomes	TPP–DSPE–PEG	Chlorin 6 and IR780	Immunodeficient BALB/c mice (females, 6–8 weeks)	HeLa human cervical cancer xenograft	i/v	1.5 (for IR780)	Tumor growth inhibition	236
Polymer-modified nanodots	TPP–$AgBiS_2$–PEI		Kunming mice (females)	U14 murine cervical carcinoma xenograft	i/v	See [g]	Recommended for tumor diagnosis	237

Note. The ways of administration are designated as follows: i/v is intravenous, i/p is intraperitoneal, s/c is subcutaneous. [a] The number of doses or duration of treatment is indicated in parentheses; [b] in μM kg^{-1}; [c] injected directly into the tumor as a solution with $C = 1$ μg mL^{-1}; [d] MRI is magnetic resonance imaging; [e] puerarin labeled with 1,1′-dioctadecyl-3,3,3′,3′-tetramethylindotricarbocyanine iodide (DiR); [f] in μg mL^{-1}; [g] 100 μL with $C = 1$ μg mL^{-1}.

MA — macrophages,
MDR — multiple drug resistance,
MET — metformin hydrochloride,
MitoQ — mitoquinone mesylate,
MMP — metalloproteinase,
MNP — magnetic nanoparticles,
mPTP — mitochondrial permeability transition pore
MRI — magnetic resonance imaging,
MSNP — mesoporous silica nanoparticles,
MW — molecular weight,
NAC — *N*-acetylcysteine,
ND — nanodiamond,
NHS — *N*-hydroxysuccinimide,
NIR — near IR range,
NP — nanoparticles,
NS — nanosheets,
NSt — nanostars,
NR — nanorods,
OA — oleic acid,
OXPHOS — oxidative phosphorylation,
PAMAM — polyamidoamine,
PBS — phosphate buffered saline,
PC — phosphatidylcholine,
PCL — poly(ε-caprolactone),
PDA — polydopamine,
PDI — polydispersity index,
PDT — photodynamic therapy,
PE — phosphatidylethanolamine,
PEG — poly(ethylene glycol),
PEI — polyethyleneimine,
PEO — poly(ethylene oxide),
PG — polyglyceride,
PGA — polyglyceroadipate,
Phc — phthalocyanine,
PISA — polymerization-induced self-assembly,
PL — poly(L-lysine),
PLGA — copolymer of lactic and glycolic acids,
PPO — polypropylene oxide,
PS — photosensitizer,
PSS — polystyrene sulfonate,
PTT — photothermal therapy,
PTX — paclitaxel,
PUE — puerarin [8-(β-D-glucopyranosyl)-4′,7-dihydroxy-isoflavone],
QD — quantum dots,
RAW264.7 — leukemia virus-transformed murine macrophages,
RES — resveratrol,
Rhd — rhodamine B,
ROS — reactive oxygen species,
rt — room temperature,
RT — X-ray therapy,
RVG29 — rabies virus glycoprotein,
SA — sodium alginate,
SGP — chondroitin sulfate,
STPP — stearyltriphenylphosphonium,
SPC — soy phosphatidylcholine,
SLN — solid lipid nanoparticles,
TCPP — *meso*-tetrakis(4-carboxyphenyl)porphyrin,
α-TOS — α-tocopherol succinate,
TPGS — D-α-tocopherol poly(ethylene glycol) succinate,
TPP — triphenylphosphonium,
US — ultrasound,
VP — verteporfin.

Cell lines:
A549 — lung adenocarcinoma,
A2780 — ovarian cancer,
B16F10 — C57BL/6J murine melanoma,
BT-20 — breast cancer,
Chang liver — normal liver cells,
DU145 — human prostate carcinoma,
H69AR — lung cancer,
H9c2 — myoblasts used as a cell model of cardiomyocytes,
HCT116 — rectal cancer,
HepG2 — human hepatocellular carcinoma,
HeLa — cervical cancer,
MCF-7 — breast cancer,
MCF-7/ADR — adriamycin-resistant MCF-7 cells,
MDA-MB-231 — breast cancer,
N27 — mesencephalic neurons of rats,
NRK — normal rat kidney cells,
Ovcar-3 — human ovarian cancer,
PANC-1 — ductal carcinoma of the pancreas,
PC3 — human pancreatic carcinoma,
SK-BR-3 — breast cancer,
4T1 — breast cancer.

12. References

1. W.G.Bottje. In *Sturkie's Avian Physiology*. (7th Edn). (Eds C.G.Scanes, S.Dridi). (New York: Academic Press, 2022). P. 65
2. R.Keshet, P.Szlosarek, A.Carracedo, A.Erez. *Nat. Rev. Cancer*, **18**, 634 (2018); https://doi.org/10.1038/s41568-018-0054-z
3. S.Matsumoto, J.Häberle, J.Kido, H.Mitsubuchi, F.Endo, K.Nakamura. *J. Hum. Genet.*, **64**, 83 (2019); https://doi.org/10.1038/s10038-019-0614-4
4. I.B.Zavodnik. *Biomed. Khim.*, **62**, 311 (2016)
5. J.F.Garbincius, J.W.Elrod. *Physiol. Rev.*, **102**, 893 (2022); https://doi.org/10.1152/physrev.00041.2020
6. M.B.Rone, J.Fan, V.Papadopoulos. *Biochim. Biophys. Acta*, **1791**, 646 (2009); https://doi.org/10.1016/j.bbalip.2009.03.001
7. V.Papadopoulos, W.L.Miller. *Best Pr. Res. Clin. Endocrinol. Metab.*, **26**, 771 (2012); https://doi.org/10.1016/j.beem.2012.05.002
8. W.L.Miller. *Mol. Cell. Endocrinol.*, **379**, 62 (2013); https://doi.org/10.1016/j.mce.2013.04.014
9. G.Bassi, S.K.Sidhu, S.Mishra. *Cells*, **10**, 1851 (2021); https://doi.org/10.3390/cells10081851
10. L.Wang. *Nucleosides Nucleotides Nucleic Acids*, **35**, 578 (2016); https://doi.org/10.1080/15257770.2015.1125001
11. M.Löffler, E.A.Carrey, W.Knecht. *Nucleosides Nucleotides Nucleic Acids*, **39**, 1281 (2020); https://doi.org/10.1080/15257770.2020.1723625
12. H.Vakifahmetoglu-Norberg, A.T.Ouchida, E.Norberg. *Biochem. Biophys. Res. Commun.*, **482**, 426 (2017); https://doi.org/10.1016/j.bbrc.2016.11.088
13. F.J.Bock, S.W.G.Tait. *Nat. Rev. Mol. Cell Biol.*, **21**, 85 (2020); https://doi.org/10.1038/s41580-019-0173-8
14. M.Abate, A.Festa, M.Falco, A.Lombardi, A.Luce, A.Grimaldi, S.Zappavigna, P.Sperlongano, C.Irace, M.Caraglia, G.Misso. *Semin. Cell Dev. Biol.*, **98**, 139 (2020); https://doi.org/10.1016/j.semcdb.2019.05.022
15. S.Dadsena, L.E.King, A.J.García-Sáez. *Biochim. Biophys. Acta — Biomembranes*, **1863**, 183716 (2021); https://doi.org/10.1016/j.bbamem.2021.183716
16. S.Javadov. *Curr. Opin. Physiol.*, **25**, 100483 (2022); https://doi.org/10.1016/j.cophys.2022.100483
17. J.B.Spinelli, M.C.Haigis. *Nat. Cell Biol.*, **20**, 74 (2018); https://doi.org/10.1038/s41556-018-0124-1
18. C.-H.Wang, Y.-H.Wei. *Int. J. Mol. Sci.*, **21**, 5266 (2020); https://doi.org/10.3390/ijms21155266

19. L.A.Videla, A.Marimán, B.Ramos, M.José Silva, A.del Campo. *Mitochondrion*, **63**, 9 (2022); https://doi.org/10.1016/j.mito.2021.12.006
20. L.R.Rodríguez, T.Lapeña-Luzón, N.Benetó, V.Beltran-Beltran, F.V.Pallardó, P.Gonzalez-Cabo, J.A.Navarro. *Antioxidants*, **11**, 165 (2022); https://doi.org/10.3390/antiox11010165
21. M.Verma, B.N.Lizama, C.T.Chu. *Transl. Neurodegener.*, **11**, 3 (2022); https://doi.org/10.1186/s40035-021-00278-7
22. E.Trushina, S.Trushin, M.F.Hasan. *Acta Pharm. Sin. B*, **12**, 483 (2022); https://doi.org/10.1016/j.apsb.2021.11.003
23. S.Ozgen, J.Krigman, R.Zhang, N.Sun. *Neural Regen. Res.*, **17**, 741 (2022); https://doi.org/10.4103/1673-5374.322429
24. K.Zambrano, D.Barba, K.Castillo, P.Robayo, D.Argueta-Zamora, S.Sanon, E.Arizaga, A.Caicedo, A.W.D.Gavilanes. *Mitochondrion*, **64**, 125 (2022); https://doi.org/10.1016/j.mito.2022.03.003
25. I.V.Shemarova, S.M.Korotkov, V.P.Nesterov. *J. Evol. Biochem. Physiol*., **56**, 304 (2020); https://doi.org/10.1134/S002209302004002X
26. R.K.Sharma, A.Chafik, G.Bertolin. *Am. J. Physiol. Physiol.*, **322**, 311 (2022); https://doi.org/10.1152/ajpcell.00256.2021
27. H.Tian, X.Chen, J.Liao, T.Yang, S.Cheng, Z.Mei, J.Ge. *J. Cell. Mol. Med.*, **26**, 1000 (2022); https://doi.org/10.1111%2Fjcmm.17189
28. A.Ludhiadch, R.Sharma, A.Muriki, A.Munshi. *CNS Neurol. Disord. Drug Targets*, **21**, 52 (2022); https://doi.org/10.2174/1871527320666210212141232
29. S.A.Dabravolski, V.A.Khotina, V.N.Sukhorukov, V.A.Kalmykov, L.M.Mikhaleva, A.N.Orekhov. *Int. J. Mol. Sci.*, **23**, 952 (2022); https://doi.org/10.3390/ijms23020952
30. J.A. Amorim, G.Coppotelli, A.P.Rolo, C.M.Palmeira, J.M.Ross, D.A.Sinclair. *Nat. Rev. Endocrinol.*, **18**, 243 (2022); https://doi.org/10.1038/s41574-021-00626-7
31. A.Ravindranath, M.SenSarma. *World J. Hepatol.*, **14**, 180 (2022); https://doi.org/10.4254/wjh.v14.i1.180
32. Y.Yoon, C.A.Galloway, B.S.Jhun, T.Yu. *Antioxid. Redox Signal.*, **14**, 439 (2011); https://doi.org/10.1089/ars.2010.3286
33. J.Gollmer, A.Zirlik, H.Bugger. *Diabetes Metab. J.*, **44**, 33 (2020); https://doi.org/10.4093/dmj.2019.0185
34. S.Demir, P.P.Nawroth, S.Herzig, B.E.Üstünel. *Adv. Sci.*, **8**, e2100275 (2021); https://doi.org/10.1002/advs.202100275
35. L.Yao, X.Liang, Y.Qiao, B.Chen, P.Wang, Z.Liu. *Metabolism*, **131**, 155195 (2022); https://doi.org/10.1016/j.metabol.2022.155195
36. W.Dai, H.Lu, Y.Chen, D.Yang, L.Sun, L.He. *Front. Cell Dev. Biol.*, **9**, 706832 (2021); https://doi.org/10.3389/fcell.2021.706832
37. M.Ito, M.Z.Gurumani, S.Merscher, A.Fornoni. *Biomolecules*, **12**, 351 (2022); https://doi.org/10.3390/biom12030351
38. S.Mani, G.Swargiary, S.J.Ralph. *Mitochondrion*, **62**, 50 (2022); https://doi.org/10.1016/j.mito.2021.11.002
39. P.J.Burke. *Trends Cancer*, **3**, 857 (2017); https://doi.org/10.1016/j.trecan.2017.10.006
40. B.A.Carneiro, W.S.El-Deiry. *Nat. Rev. Clin. Oncol.*, **17**, 395 (2020); https://doi.org/10.1038/s41571-020-0341-y
41. C.Garcia-Ruiz, L.Conde de la Rosa, V.Ribas, J.C.Fernandez-Checa. *Semin. Cancer Biol.*, **73**, 76 (2021); https://doi.org/10.1016/j.semcancer.2020.07.014
42. E.Hajaj, M.Sciacovelli, C.Frezza, A.Erez. *Mol. Cell*, **81**, 3749 (2021); https://doi.org/10.1016/j.molcel.2021.08.005
43. S.Vyas, E.Zaganjor, M.C.Haigis. *Cell*, **166**, 555 (2016); https://doi.org/10.1016/j.cell.2016.07.002
44. D.Grasso, L.X.Zampieri, T.Capelôa, J.A.VandeVelde, P.Sonveaux. *Cell Stress*, **4**, 114 (2020); https://doi.org/10.15698/cst2020.06.221
45. M.van der Merwe, G.van Niekerk, C.Fourie, M.du Plessis, A.-M.Engelbrecht. *Cell. Oncol.* **44**, 983 (2021); https://doi.org/10.1007/s13402-021-00623-y
46. X.Guo, N.Yang, W.Ji, H.Zhang, X.Dong, Z.Zhou, L.Li, H.Shen, S.Q.Yao, W.Huang. *Adv. Mater.*, **33**, e2007778 (2021); https://doi.org/10.1002/adma.202007778
47. J.Patel, B.A.Baptiste, E.Kim, M.Hussain, D.L.Croteau, V.A.Bohr. *Carcinogenesis*, **41**, 1625 (2020); https://doi.org/10.1093/carcin/bgaa114
48. E.E.Newton, L.E.Mueller, S.M.Treadwell, C.A.Morris, H.L.Machado. *Cancers (Basel)*, **14**, 482 (2022); https://doi.org/10.3390/cancers14030482
49. N.M.Almansour. *Front. Mol. Biosci.*, **9**, 836417 (2022); https://doi.org/10.3389/fmolb.2022.836417
50. J.W.Smithy, E.M.O'Reilly. *J. Surg. Oncol.*, **123**, 1475 (2021); https://doi.org/10.1002/jso.26359
51. J.Xu, J.G.Shamul, E.A.Kwizera, X.He. *Nanomaterials*, **12**, 743 (2022); https://doi.org/10.3390/nano12050743
52. T.A.Tabish, M.R.Hamblin. *Biomater. Biosyst.*, **3**, 100023 (2021); https://doi.org/10.1016/j.bbiosy.2021.100023
53. Z.He, Y.Zhang, A.R.Khan, J.Ji, A.Yu, G.Zhai. *J. Drug Target.*, **29**, 12 (2021); https://doi.org/10.1080/1061186X.2020.1797051
54. S.Mani, G.Swargiary, S.Tyagi, M.Singh, N.K.Jha, K.K.Singh. *Life Sci.*, **281**, 119773 (2021); https://doi.org/10.1016/j.lfs.2021.119773
55. J.Qin, N.Gong, Z.Liao, S.Zhang, P.Timashev, S.Huo, X.-J.Liang. *Nanoscale*, **13**, 7108 (2021); https://doi.org/10.1039/D1NR01068A
56. D.Choudhary, H.Goykar, T.Karanwad, S.Kannaujia, V.Gadekar, M.Misra. *Asian J. Pharm. Sci.*, **16**, 397 (2021); https://doi.org/10.1016/j.ajps.2020.10.002
57. L.Huang, Z.Sun, Q.Shen, Z.Huang, S.Wang, N.Yang, G.Li, Q.Wu, W.Wang, L.Li, C.Yu. *Chin. Chem. Lett.*, **33**, 4146 (2022); https://doi.org/10.1016/j.cclet.2022.02.047
58. T.I.Rokitskaya, E.V.Aleksandrova, G.A.Korshunova, L.S.Khailova, V.N.Tashlitsky, V.B.Luzhkov, Y.N.Antonenko. *J. Phys. Chem. B*, **126**, 412 (2022); https://doi.org/10.1021/acs.jpcb.1c08135
59. X.Fu, Y.Shi, T.Qi, S.Qiu, Y.Huang, X.Zhao, Q.Sun, G.Lin. *Signal Transduct. Target. Ther.*, **5**, 262 (2020); https://doi.org/10.1038/s41392-020-00342-0
60. C.A.Kulkarni, B.D.Fink, B.E.Gibbs, P.R.Chheda, M.Wu, W.I.Sivitz, R.J.Kerns. *J. Med. Chem.*, **64**, 662 (2021); https://doi.org/10.1021/acs.jmedchem.0c01671
61. V.F.Mironov, A.V.Nemtarev, O.V.Tsepaeva, M.N.Dimukhametov, I.A.Litvinov, A.D.Voloshina, T.N.Pashirova, E.A.Titov, A.P.Lyubina, S.K.Amerhanova, A.T.Gubaidullin, D.R. Islamov. *Molecules*, **26**, 6350 (2021); https://doi.org/10.3390/molecules26216350
62. R.John, B.Dalal, A.Shankarkumar, P.V.Devarajan. *Int. J. Pharm.*, **600**, 120511 (2021); https://doi.org/10.1016/j.ijpharm.2021.120511
63. O.V.Tsepaeva, A.V.Nemtarev, T.I.Salikhova, T.I.Abdullin, L.R.Grigor`eva, S.A.Khozyainova, V.F.Mironov. *Anticancer. Agents Med. Chem.*, **20**, 286 (2020); https://doi.org/10.2174/1871520619666191014153554
64. O.V.Tsepaeva, T.I.Salikhova, L.R.Grigor'eva, D.V.Ponomaryov, T.Dang, R.A.Ishkaeva, T.I.Abdullin, A.V.Nemtarev, V.F. Mironov. *Med. Chem. Res.*, **30**, 925 (2021); https://doi.org/10.1007/s00044-020-02674-6
65. G.Xu, X.Xu, J.Liu, Q.Jia, C.Ke, H.Zhang, C.Xu, E.Ou, W.Tan, Y.Zhao. *ChemMedChem*, 17, e202100659 (2022); https://doi.org/10.1002/cmdc.202100659
66. L.Wang, M.Yao, Y.Hu, C.Chen, L.Jin, X.Ma, H.Yang. *ACS Med. Chem. Lett.*, **13**, 786 (2022); https://doi.org/10.1021/acsmedchemlett.1c00581
67. D.V.Tsyganov, A.V.Samet, E.A.Silyanova, V.I.Ushkarov, A.E.Varakutin, N.B.Chernysheva, R.N.Chuprov-Netochin, A.A.Khomutov, A.S.Volkova, S.V.Leonov, M.N.Semenova, V.V. Semenov. *ACS Omega*, **7**, 3369 (2022); https://doi.org/10.1021/acsomega.1c05515
68. J.S.Armstrong. *Br. J. Pharmacol.*, **151**, 1154 (2007); https://doi.org/10.1038/sj.bjp.0707288
69. M.Edeas, V.Weissig. *Mitochondrion*, **13**, 389 (2013); https://doi.org/10.1016/j.mito.2013.03.009

70. L.Milane, S.Dolare, T.Jahan, M.Amiji. *Nanomed.: Nanotechnol. Biol. Med.*, **37**, 102422 (2021); https://doi.org/10.1016/j.nano.2021.102422
71. *Organelle-Specific Pharmaceutical Nanotechnology.* (Eds V.Weissig, G.G.M.D'Souza). (Hoboken: Wiley, 2010)
72. R.W.Horobin, S.Trapp, V.Weissig. *J. Control. Release*, **121**, 125 (2007); https://doi.org/10.1016/j.jconrel.2007.05.040
73. M.J.Rossman, J.R.Santos-Parker, C.A.C.Steward, N.Z.Bispham, L.M.Cuevas, H.L.Rosenberg, K.A.Woodward, M.Chonchol, R.A.Gioscia-Ryan, M.P.Murphy, D.R.Seals. *Hypertension*, **71**, 1056 (2018); https://doi.org/10.1161/HYPERTENSIONAHA.117.10787
74. S.-Y.Park, E.J.Pekas, R.J.Headid, W.-M.Son, T.K.Wooden, J.Song, G.Layec, S.K.Yadav, P.K.Mishra, I.I.Pipinos. *Am. J. Physiol. Circ. Physiol.*, **319**, H456 (2020); https://doi.org/10.1152/ajpheart.00235.2020
75. V.Weissig, S.V.Boddapati, S.-M.Cheng, G.G.M.D'Souza. *J. Liposome Res.*, **16**, 249 (2006); https://doi.org/10.1080/08982100600851169
76. A.T.Hoye, J.E.Davoren, P.Wipf, M.P.Fink, V.E.Kagan. *Acc. Chem. Res.*, **41**, 87 (2008); https://doi.org/10.1021/ar700135m
77. C.M.Paleos, D.Tsiourvas, Z.Sideratou. *Mol. Pharm.*, **13**, 2233 (2016); https://doi.org/10.1021/acs.molpharmaceut.6b00237
78. S.S.Liew, X.Qin, J.Zhou, L.Li, W.Huang, S.Q.Yao. *Angew. Chem., Int. Ed.*, **60**, 2232 (2021); https://doi.org/10.1002/anie.201915826
79. K.S.Allemailem, A.Almatroudi, M.A.Alsahli, A.Aljaghwani, A.MEl-Kady, A.H.Rahmani, A.A.Khan. *Int. J. Nanomed.*, **16**, 3907 (2021); https://doi.org/10.2147/IJN.S303832
80. Y.Yamada, Satrialdi, M.Hibino, D.Sasaki, J.Abe, H.Harashima. *Adv. Drug Deliv. Rev.*, **154**–**155**, 187 (2020); https://doi.org/10.1016/j.addr.2020.09.010
81. C.Wang, F.Li, T.Zhang, M.Yu, Y.Sun. *Drug Deliv.*, **29**, 1684 (2022); https://doi.org/10.1080/10717544.2022.2079771
82. S.Buchke, M.Sharma, A.Bora, M.Relekar, P.Bhanu, J.Kumar. *Life*, **12**, 657 (2022); https://doi.org/10.3390/life12050657
83. P.Mi, H.Cabral, K.Kataoka. *Adv. Mater.*, **32**, 1902604 (2020); https://doi.org/10.1002/adma.201902604
84. S.Tran, P.J.De Giovanni, B.Piel, P.Rai. *Clin. Transl. Med.*, **6**, 44 (2017); https://doi.org/10.1186/s40169-017-0175-0
85. A.A.Khan, K.S.Allemailem, A.Almatroudi, S.A.Almatroodi, M.A.Alsahli, A.H.Rahmani. *J. Drug Deliv. Sci. Technol.*, **61**, 102315 (2021); https://doi.org/10.1016/j.jddst.2020.102315
86. J.Zielonka, J.Joseph, A.Sikora, M.Hardy, O.Ouari, J.Vasquez-Vivar, G.Cheng, M.Lopez, B.Kalyanaraman. *Chem. Rev.*, **117**, 10043 (2017); https://doi.org/10.1021/acs.chemrev.7b00042
87. N.R.Khasiyatullina, V.F.Mironov, S.K.Gumerova, A.D.Voloshina, A.S.Sapunova. *Mendeleev Commun.*, **29**, 435 (2019); https://doi.org/10.1016/j.mencom.2019.07.027
88. N.R.Khasiyatullina, V.F.Mironov, A.D.Voloshina, A.S.Sapunova. *Chem. Biodiv.*, **16**, e1900039 (2019); https://doi.org/10.1002/cbdv.201900039
89. M.E.Shemakhina, A.V.Nemtarev, R.R.Fayzullin, N.R.Khasiyatullina, L.R.Grigor'eva, V.F.Mironov. *Mendeleev Commun.*, **30**, 700 (2020); https://doi.org/10.1016/j.mencom.2020.11.003
90. C.Larpent, H.Patin. *Tetrahedron*, **44**, 6107 (1988); https://doi.org/10.1016/S0040-4020(01)89800-8
91. C.Lim. *Adv. Drug Deliv. Rev.*, **59(8)**, 697 (2007); https://doi.org/10.1016/j.addr.2007.06.001
92. Y.Shi, Z.Luo, J.You. *WIREs Nanomed. Nanobiotechnol.*, **14**, e1803 (2022); https://doi.org/10.1002/wnan.1803
93. S.V.Boddapati, P.Tongcharoensirikul, R.N.Hanson, G.G.M.D'Souza, V.P.Torchilin, V.Weissig. *J. Liposome Res.*, **15**, 49 (2005); https://doi.org/10.1081/LPR-200064958
94. S.V.Boddapati, G.G.M.D'Souza, S.Erdogan, V.P.Torchilin, V.Weissig. *Nano Lett.*, **8**, 2559 (2008); https://doi.org/10.1021/nl801908y
95. N.R.Patel, S.Hatziantoniou, A.Georgopoulos, C.Demetzos, V.P.Torchilin, V.Weissig, G.G.M.D'Souza. *J. Liposome Res.*, **20**, 244 (2010); https://doi.org/10.3109/08982100903347931
96. M.A.Solomon, A.A.Shah, G.G.M.D'Souza. *Mitochondrion*, **13**, 464 (2013); https://doi.org/10.1016/j.mito.2012.10.013
97. J.Alizadeh, S.C.da Silva Rosa, X.Weng, J.Jacobs, S.Lorzadeh, A.Ravandi, R.Vitorino, S.Pecic, A.Zivkovic, H.Stark, S.Shojaei, S.Ghavami. *Eur. J. Cell Biol.*, **102**, 151337 (2023); https://doi.org/10.1016/j.ejcb.2023.151337
98. D.A.Kuznetsova, G.A.Gaynanova, L.A.Vasileva, G.V.Sibgatullina, D.V.Samigullin, A.S.Sapunova, A.D.Voloshina, I.V.Galkina, K.A.Petrov, L.Y.Zakharova. *J. Mater. Chem. B*, **7**, 7351 (2019); https://doi.org/10.1039/C9TB01853K
99. D.A.Kuznetsova, L.A.Vasileva, G.A.Gaynanova, R.V.Pavlov, A.S.Sapunova, A.D.Voloshina, G.V.Sibgatullina, D.V.Samigullin, K.A.Petrov, L.Y.Zakharova, O.G.Sinyashin. *J. Mol. Liq.*, **330**, 115703 (2021); https://doi.org/10.1016/j.molliq.2021.115703
100. V.P. Torchilin. *Nat. Rev. Drug Discov.*, **13**, 813 (2014); https://doi.org/10.1038/nrd4333
101. S.Shah, M.Ouellette, G.G.M.D'Souza. *4open*, **5**, 6 (2022); https://doi.org/10.1051/fopen/2022003
102. J.Di Gregorio, S.Petricca, R.Iorio, E.Toniato, V.Flati. *Eur. J. Cell Biol.*, **101**, 151225 (2022); https://doi.org/10.1016/j.ejcb.2022.151225
103. P.Benein, M.A.Almuteri, A S.Mehanna, G.G.M.D'Souza. In *Mitochondrial Medicine. Manipulating Mitochondrial Function.* Vol. II. (Eds V.Weissig, M.Edeas). (New York: Springer Humana, 2015). P. 51
104. P.Benien, M.A.Solomon, P.Nguyen, E.M.Sheehan, A.S.Mehanna, G.G.M.D'Souza. *J. Liposome Res.*, **26**, 21 (2016); https://doi.org/10.3109/08982104.2015.1022557
105. L.Jiang, S.Zhou, X.Zhang, C.Li, S.Ji, H.Mao, X.Jiang. *Nat. Commun.*, **12**, 2390 (2021); https://doi.org/10.1038/s41467-021-22594-2
106. J.Pendhari, H.Savla, D.Bethala, S.Vaidya, U.Shinde, M.Menon. *J. Drug Deliv. Sci. Technol.*, **76**, 103795 (2022); https://doi.org/10.1016/j.jddst.2022.103795
107. S.Xiao, S.Huang, X.Yang, Y.Lei, M.Chang, J.Hu, Y.Meng, G.Zheng, X.Chen. *Drug Deliv.*, **30**, 2162156 (2023); https://doi.org/10.1080/10717544.2022.2162156
108. P.-W.Shueng, L.-Y.Yu, H.-H.Hou, H.-C.Chiu, C.-L.Lo. *Int. J. Mol. Sci.*, **23**, 3080 (2022); https://doi.org/10.3390/ijms23063080
109. S.Biswas, N.S.Dodwadkar, P.P.Deshpande, V.P.Torchilin. *J. Control. Release*, **159**, 393 (2012); https://doi.org/10.1016/j.jconrel.2012.01.009
110. J.H.Kang, Y.T.Ko. *Pharmaceutics*, **11**, 423 (2019); https://doi.org/10.3390/pharmaceutics11080423
111. C.Yue, Y.Yang, J.Song, G.Alfranca, C.Zhang, Q.Zhang, T.Yin, F.Pan, J.M.de la Fuente, D.Cui. *Nanoscale*, **9**, 11103 (2017); https://doi.org/10.1039/C7NR02193C
112. J.He, D.Liu, L.Zhao, D.Zhou, J.Rong, L.Zhang, Z.Xia. *Exp. Ther. Med.*, **23**, 430 (2022); https://doi.org/10.3892/etm.2022.11357
113. F.Li, Y.Wang, W.Li, J.Wu, S.Li, X.Hu, T.Tang, X.Liu. *J. Liposome Res.*, **33**, 1 (2023). https://doi.org/10.1080/08982104.2023.2193845
114. L.Kennedy, J.K.Sandhu, M.E.Harper, M. Cuperlovic-Culf. *Biomolecules*, 10, 1429 (2020); https://doi.org/10.3390/biom10101429
115. Y.Peng, J.Lu, R.Li, Y.Zhao, L.Hai, L.Guo, Y.Wu. *ACS Appl. Mater. Interfaces*, **13**, 26682 (2021); https://doi.org/10.1021/acsami.1c02404
116. B.Kapoor, R.Gupta, S.K.Singh, M.Gulati, S.Singh. *Adv. Colloid Interface Sci.*, **253**, 35 (2018); https://doi.org/10.1016/j.cis.2018.01.003
117. H.M.Cochemé, G.F.Kelso, A.M.James, M.F.Ross, J.Trnka, T.Mahendiran, J.AsinCayuela, F.H.Blaikie, A.R.B.Manas, C.M.Porteous, V.J.Adlam, R.A.J.Smith, M.P.Murphy. *Mitochondrion*, **7**, 94 (2007); https://doi.org/10.1016/j.mito.2007.02.007

118. R.A.J.Smith, M.P.Murphy. *Ann. N.Y. Acad. Sci.*, **1201**, 96 (2010); https://doi.org/10.1111/j.1749-6632.2010.05627.x
119. K.J.Botting, K.L.Skeffington, Y.Niu, B.J.Allison, K.L.Brain, N.Itani, C.Beck, A.Logan, A.J.Murray, M.P.Murphy, D.A.Giussani. *Sci. Adv.*, **6**, eabb1929 (2020); https://doi.org/10.1126/sciadv.abb1929
120. R.J.Perry, T.Kim, X.-M.Zhang, H.-Y.Lee, D.Pesta, V.B.Popov, D.Zhang, Y.Rahimi, M.J.Jurczak, G.W.Cline, D.A.Spiegel, G.I.Shulman. *Cell Metab.*, **18**, 740 (2013); https://doi.org/10.1016/j.cmet.2013.10.004
121. M.Wu, L.Liao, L.Jiang, C.Zhang, H.Gao, L.Qiao, S.Liu, D.Shi. *Biomaterials*, **222**, 119457 (2019); https://doi.org/10.1016/j.biomaterials.2019.119457
122. J.Zhou, W.-Y.Zhao, X.Ma, R.-J.Ju, X.-Y.Li, N.Li, M.-G.Sun, J.-F.Shi, C.-X.Zhang, W.-L.Lu. *Biomaterials*, **34**, 3626 (2013); https://doi.org/10.1080/10717544.2018.1446475
123. J.Zhang, C.Yang, S.Pan, M.Shi, J.Li, H.Hu, M.Qiao, D.Chen, X.Zhao. *Drug Deliv.*, **25**, 723 (2018); https://doi.org/10.1080/10717544.2018.1446475
124. S.Wang, Z.Zhou, R.Hu, M.Dong, X.Zhou, S.Ren, Y.Zhang, C.Chen, R.Huang, M.Zhu, W.Xie, L.Han, J.Shen, C.Xie. *Adv. Sci.*, **10**, 2207608 (2023); https://doi.org/10.1002/advs.202370075
125. X.Wang, H.Cai, X.Huang, Z.Lu, L.Zhang, J.Hu, D.Tian, J.Fu, G.Zhang, Y.Meng, G.Zheng, C.Chang. *J. Biomater. Sci., Polym. Ed.*, (2023) (in the press); https://doi.org/10.1080/09205063.2023.2201815
126. Y.Han, C.Gao, H.Wang, J.Sun, M.Liang, Y.Feng, Q.Liu, S.Fu, L.Cui, C.Gao, Y.Li, Y.Yang, B.Sun. *Bioact. Mater.*, **6**, 529 (2021); https://doi.org/10.1016/j.bioactmat.2021.06.002
127. P.Karunanidhi, N.Verma, D.N.Kumar, A.K.Agrawal, S.Singh. *AAPS PharmSciTech*, **22**, 158 (2021); https://doi.org/10.1208/s12249-021-02016-8
128. X.Zhang, X.Zhao, S.Tie, H.Wang, M.Tan, *J. Agric. Food Chem.*, **69**, 2719 (2021); https://doi.org/10.1021/acs.jafc.0c05983
129. Y.Sun, Q.Yang, X.Xia, X.Li, W.Ruan, M.Zheng, Y.Zou, B.Shi. *Front. Bioeng. Biotechnol.*, **9**. 755727 (2021); https://doi.org/10.3389/fbioe.2021.755727
130. P.Laskar, C.Dufès. *Nanoscale Adv.*, **3**, 6007 (2021); https://doi.org/10.1039/D1NA00536G
131. S.Biswas, N.S.Dodwadkar, A.Piroyan, V.P.Torchilin. *Biomaterials*, **33**, 4773 (2012); https://doi.org/10.1016/j.biomaterials.2012.03.032
132. E.R.Bielski, Q.Zhong, M.Brown, S.R.P.daRocha. *Mol. Pharm.*, **12**, 3043 (2015); https://doi.org/10.1021/acs.molpharmaceut.5b00320
133. A.Sharma, K.Liaw, R.Sharma, Z.Zhang, S.Kannan, R.M. Kannan. *Theranostics*, **8**, 5529 (2018); https://doi.org/10.7150/thno.29039
134. A.H.Hunter. *Adv. Drug Deliv. Rev.*, **58**, 1523 (2006); https://doi.org/10.1016/j.addr.2006.09.008
135. K.Osada, H.Oshima, D.Kobayashi, M.Doi, M.Enoki, Y.Yamasaki, K.Kataoka. *J. Am. Chem. Soc.*, **132**, 12343 (2010); https://doi.org/10.1021/ja102739b
136. T.A.Theodossiou, Z.Sideratou, D.Tsiourvas, C.M.Paleos. *Mitochondrion*, **11**, 982 (2011); https://doi.org/10.1016/j.mito.2011.08.004
137. X.-H.Wang, H.-S.Peng, L.Yang, F.-T.You, F.Teng, A.-W.Tang, F.-J.Zhang, X.-H.Li. *J. Mater. Chem. B*, **1**, 5143 (2013); https://doi.org/10.1039/c3tb20884b
138. T.A.Theodossiou, Z.Sideratou, M.E.Katsarou, D.Tsiourvas. *Pharm. Res.*, **30**, 2832 (2013); https://doi.org/10.1007/s11095-013-1111-7
139. K.Panagiotaki, Z.Sideratou, S.Vlahopoulos, M.Paravatou-Petsotas, M.Zachariadis, N.Khoury, V.Zoumpourlis, D.Tsiourvas. *Pharmaceuticals*, **10**, 91 (2017); https://doi.org/10.3390/ph10040091
140. V.Stagni, A.Kaminari, Z.Sideratou, E.Sakellis, S.A.Vlahopoulos, D.Tsiourvas. *Int. J. Pharm.*, **585**, 119465 (2020); https://doi.org/10.1016/j.ijpharm.2020.119465
141. K.Stakyte, M.Rotheneder, K.Lammens, J.D.Bartho, U.Grädler, T.Fuchß, U.Pehl, A.Alt, van de E.Logt, K.P.Hopfner. *Nat. Struct. Mol. Biol.*, **28**, 789 (2021); https://doi.org/10.1038/s41594-021-00654-x
142. V.Stagni, A.Kaminari, C.Contadini, D.Barilà, R.L.Sessa, Z.Sideratou, S.A.Vlahopoulos, D.Tsiourvas. *Cancers (Basel)*, **15**, 1474 (2023); https://doi.org/10.3390/cancers15051474
143. D.Y.Cho, H.Cho, K.Kwon, M.Yu, E.Lee, K.M.Huh, D.H.Lee, H.C. Kang. *Adv. Funct. Mater.*, **25**, 5479 (2015); https://doi.org/10.1002/adfm.201501422
144. A.Sharma, G.M.Soliman, N.Al-Hajaj, R.Sharma, D.Maysinger, A.Kakkar. *Biomacromolecules*, **13**, 239 (2012); https://doi.org/10.1021/bm201538j
145. Y.Xu, S.Wang, H.F.Chan, Y.Liu, H.Li, C.He, Z.Li, M.Chen. *Int. J. Pharm.*, **522**, 21 (2017); https://doi.org/10.1016/j.ijpharm.2017.01.064
146. N.Kumar, R.S.Langer, A.J.Domb. *Adv. Drug Deliv. Rev.*, **54**, 889 (2002); https://doi.org/10.1016/S0169-409X(02)00050-9
147. D.Katti, S.Lakshmi, R.Langer, C.Laurencin. *Adv. Drug Deliv. Rev.*, **54**, 933 (2002); https://doi.org/10.1016/S0169-409X(02)00052-2
148. B.W.Schlichtmann, B.Kalyanaraman, R.L.Schlichtmann, M.G.Panthani, V.Anantharam, A.G.Kanthasamy, S.K.Mallapragada, B.Narasimhan. *J. Biomed. Mater. Res., Part B: Appl. Biomater.*, **110**, 450 (2022); https://doi.org/10.1002/jbm.b.34922
149. A.Ghosh, M.R.Langley, D.S.Harischandra, M.L.Neal, H.Jin, V.Anantharam, J.Joseph, T.Brenza, B.Narasimhan, A.Kanthasamy, B.Kalyanaraman, A.G.Kanthasamy. *J. Neuroimmune Pharmacol.*, **11**, 259 (2016); https://doi.org/10.1007/s11481-016-9650-4
150. T.M.Brenza, S.Ghaisas, J.E.V.Ramirez, D.Harischandra, V.Anantharam, B.Kalyanaraman, A.G.Kanthasamy, B.Narasimhan. *Nanomed.: Nanotechnol. Biol. Med.*, **13**, 809 (2017); https://doi.org/10.1016/j.nano.2016.10.004
151. Y.Liu, K.Ai, L.Lu. *Chem. Rev.*, **114**, 5057 (2014); https://doi.org/10.1021/cr400407a
152. X.Zhong, K.Yang, Z.Dong, X.Yi, Y.Wang, C.Ge, Y.Zhao, Z.Liu. *Adv. Funct. Mater.*, **25**, 7327 (2015); https://doi.org/10.1002/adfm.201503587
153. W.-Q.Li, Z.Wang, S.Hao, H.He, Y.Wan, C.Zhu, L.-P.Sun, G.Cheng, S.-Y.Zheng. *ACS Appl. Mater. Interfaces*, **9**, 16793 (2017); https://doi.org/10.1021/acsami.7b01540
154. F.Liu, X.He, J.Zhang, H.Chen, H.Zhang, Z.Wang. *J. Mater. Chem. B*, **3**, 6731 (2015); https://doi.org/10.1039/C5TB01159K
155. Z.Meng, B.Wang, Y.Liu, Y.Wan, Q.Liu, H.Xu, R.Liang, Y.Shi, P.Tu, H.Wu, C.Xu. *Regen. Biomater.*, **9**, rbac051 (2022); https://doi.org/10.1093/rb/rbac051
156. Y.Lu, D.Cheng, B.Niu, X.Wang, X.Wu, A.Wang. *Pharmaceuticals*, **16**, 454 (2023); https://doi.org/10.3390/ph16030454
157. A.Narmani, R.Jahedi, E.Bakhshian-Dehkordi, S.Ganji, M.Nemati, R.Ghahramani-Asl, K.Moloudi, S.M.Hosseini, H.Bagheri, P.Kesharwani, A.Khani, B.Farhood, A.Sahebkar. *Expert Opin. Drug Deliv.,* **20**, 937 (2023); https://doi.org/10.1080/17425247.2023.2223941
158. S.Marrache, S.Dhar. *Proc. Natl. Acad. Sci. USA*, **109**, 16288 (2012); https://doi.org/10.1073/pnas.1210096109
159. S.Marrache, S.Tundup, D.A.Harn, S.Dhar. *ACS Nano*, **7**, 7392 (2013); https://doi.org/10.1021/nn403158n
160. M.Velichkovska, B.Surnar, M.Nair, S.Dhar, M.Toborek. *Mol. Pharm.*, **16**, 724 (2019); https://doi.org/10.1021/acs.molpharmaceut.8b01014
161. W.Zhou, H.Yu, L.-J.Zhang, B.Wu, C.-X.Wang, Q.Wang, K.Deng, R.-X.Zhuo, S.-W.Huang. *Nanoscale*, **9**, 17044 (2017); https://doi.org/10.1039/C7NR06130G
162. L.Zhang, J.M.Chan, F.X.Gu, J.-W.Rhee, A.Z.Wang, A.F.Radovic-Moreno, F.Alexis, R.Langer, O.C.Farokhzad. *ACS Nano*, **2**, 1696 (2008); https://doi.org/10.1021/nn800275r

163. Y.Song, D.Liu, Y.Cheng, Z.Teng, H.Cui, M.Liu, B.Zhang, Q.Mei, S.Zhou. *Mol. Pharm.*, **15**, 1296 (2018); https://doi.org/10.1021/acs.molpharmaceut.7b01109
164. H.Li, W.Ye, M.Huan, Y.Cheng, D.Liu, H.Cui, M.Liu, B.Zhang, Q.Mei, S.Zhou. *Nanomedicine (Lond.)*, **14**, 1011 (2019); https://doi.org/10.2217/nnm-2018-0227
165. Y.Qin, Z.Wang, X.Wang, T.Zhang, Y.Hu, D.Wang, H.Sun, L.Zhang, Y.Zhu. *Mater. Today Adv.*, **17**, 100328 (2023); https://doi.org/10.1016/j.mtadv.2022.100328
166. R.Jha, R. A.Mayanovic. *Nanomaterials*, **13**, 1302 (2023); https://doi.org/10.3390/nano13081302
167. H.Huang, H.Wu, Y.Huang, S.Zhang, Y.Lam, N.Ao. *J. Mater. Res.*, **33**, 2586 (2018); https://doi.org/10.1557/jmr.2018.255
168. K.K.Arafa, M.A.Hamzawy, S.A.Mousa, I.M.El-Sherbiny. *RSC Adv.*, **12**, 21690 (2022); https://doi.org/10.1039/D2RA03240F
169. K.K.Arafa, H.D.C.Smyth, I.M.El-Sherbiny. *Int. J. Pharm.*, **606**, 120936 (2021); https://doi.org/10.1016/j.ijpharm.2021.120936
170. H.Liu, N.Guo, W.Guo, M.Huang-Fu, M.R.Vakili, J.Chen, W.Xu, Q.Wei, M.Han, A.Lavasanifar, J.Gao. *Acta Pharmacol. Sin.*, **39**, 1681 (2018); https://doi.org/10.1038/aps.2018.9
171. H.-N.Liu, N.-N.Guo, T.-T.Wang, W.-W.Guo, M.-T.Lin, M.-Y.Huang-Fu, M.R.Vakili, W.-H.Xu, J.-J.Chen, Q.-C.Wei, M.Han, A.Lavasanifar, J.-Q.Gao. *Mol. Pharm.*, **15**, 882 (2018); https://doi.org/10.1080/17425247.2023.2223941
172. S.Y.Lee, H.-J.Cho. *Biomacromolecules*, **20**, 835 (2019); https://doi.org/10.1021/acs.biomac.8b01449
173. K.Wang, M.Qi, C.Guo, Y.Yu, B.Wang, L.Fang, M.Liu, Z.Wang, X.Fan, D.Chen. *Nanoscale Res. Lett.*, **13**, 32 (2018); https://doi.org/10.1186%2Fs11671-018-2445-1
174. A.V.Kabanov, V.Y.Alakhov. *Crit. Rev. Ther. Drug Carrier Syst.*, **19**, 1 (2002); https://doi.org/10.1615/CritRevTherDrugCarrierSyst.v19.i1.10
175. R.Savić, L.Luo, A.Eisenberg, D.Maysinger. *Science*, **300**, 615 (2003); https://doi.org/10.1126/science.1078192
176. Q.Zhang, M.R.Vakili, X.-F.Li, A.Lavasanifar, X.C.Le. *Biomaterials*, **35**, 7088 (2014); https://doi.org/10.1016/j.biomaterials.2014.04.072
177. J.-M.Noy, F.Chen, M.Stenzel. *Beilstein J. Org. Chem.*, **17**, 2302 (2021); https://doi.org/10.3762/bjoc.17.148
178. F.Ceccacci, S.Sennato, E.Rossi, R.Proroga, S.Sarti, M.Diociaiuti, S.Casciardi, V.Mussi, A.Ciogli, F.Bordi, G.Mancini, C.Bombelli. In *Mitochondrial Medicine.* Vol. 1. (New York: Springer, 2021). P. 27
179. F.Ceccacci, S.Sennato, E.Rossi, R.Proroga, S.Sarti, M.Diociaiuti, S.Casciardi, V.Mussi, A.Ciogli, F.Bordi, G.Mancini, C.Bombelli. *J. Colloid Interface Sci.*, **531**, 451 (2018); https://doi.org/10.1016/j.jcis.2018.07.067
180. K.Y.Kim, H.Jin, J.Park, S.H.Jung, J.H.Lee, H.Park, S.K.Kim, J.Bae, J.H.Jung. *Nano Res.*, **11**, 1082 (2018); https://doi.org/10.1007/s12274-017-1728-7
181. G.Battogtokh, O.Gotov, J. H.Kang, J.Cho, T.H.Jeong, G.Chimed, Y.T.Ko. *Nanomedicine*, **13**, 325 (2018); https://doi.org/10.2217/nnm-2017-0274
182. Y.Liu, D.Wang, H.Liu, L.Liu, S.Li, Z.Zhou, L.Lu, X.Liu, L.He, D.He, C.-Y.Yu, H.Wei. *J. Med. Chem*., **66**, 4045 (2023); https://doi.org/10.1021/acs.jmedchem.2c01924
183. Y.Zhang, C.Zhang, J.Chen, L.Liu, M.Hu, J.Li, H.Bi. *ACS Appl. Mater. Interfaces*, **9**, 25152 (2017); https://doi.org/10.1021/acsami.7b07219
184. Y.Tan, X.Yang, S.Dai, K.Lian, L.Wen, Y.Zhu, T.Meng, X.Liu, H.Yuan, F.Hu. *Polym. Chem.*, **10**, 512 (2019); https://doi.org/10.1039/C8PY01504J
185. H.Wang, F.Zhang, H.Wen, W.Shi, Q.Huang, Y.Huang, J.Xie, P.Li, J.Chen, L.Qin, Y.Zhou. *J. Nanobiotechnol.*, **18**, 98 (2020); https://doi.org/10.1186/s12951-020-00657-8
186. H.Wang, W.Shi, D.Zeng, Q.Huang, J.Xie, H.Wen, J.Li, X.Yu, L.Qin, Y.Zhou. *J. Nanobiotechnol.*, **19**, 152 (2021); https://doi.org/10.1186/s12951-021-01005-0
187. X.Shi, G.Lv, X.Sun, D.Cao, G.Wang, Y.Chang. *RSC Adv.*, **7**, 25694 (2017); https://doi.org/10.1039/C7RA00597K
188. W.Li, J.Wu, D.Xiang, S.Luo, X.Hu, T.Tang, T.Sun, X.Liu. *Int. J. Nanomed.*, **14**, 8345 (2019); https://doi.org/10.2217/nnm-2019-0278
189. P.Yang, D.Sheng, Q.Guo, P.Wang, S.Xu, K.Qian, Y.Li, Y.Cheng, L.Wang, W.Lu, Q.Zhang. *Biomaterials*, **238**, 119844 (2020); https://doi.org/10.1016/j.biomaterials.2020.119844
190. K.Damrongrak, K.Kloysawat, S.Bunsupa, K.Sakchasri, A.Wongrakpanich, V.Taresco, V.CuzzucoliCrucitti, M.C.Garnett, J.Suksiriworapong. *Int. J. Pharm.*, **618**, 121636 (2022); https://doi.org/10.1016/j.ijpharm.2022.121636
191. X.-Q.Yu, B.-Y.Liu, W.-X.Wu, Y.-H.Liu, C.Jia, X.-L.Yang, J.Li, N.Wang. *Polym. Chem*., **8**, 5982 (2017); https://doi.org/10.1039/C7PY01138E
192. B.-Y.Liu, X.-L.Yang, X.Xing, J.Li, Y.-H.Liu, N.Wang, X.-Q.Yu. *ACS Macro Lett.*, **8**, 719 (2019); https://doi.org/10.1021/acsmacrolett.9b00121
193. S.Marrache, R.K.Pathak, S.Dhar. *Proc. Natl. Acad. Sci. USA*, **111**, 10444 (2014); https://doi.org/10.1073/pnas.1405244111
194. R.Palao-Suay, M.R.Aguilar, F.J.Parra-Ruiz, S.Martín-Saldaña, N.A.Rohner, S.N.Thomas, J. San Román. *J. Mater. Sci. Mater. Med.*, **28**, 152 (2017); https://doi.org/10.1007/s10856-017-5963-y
195. H.Yabu. *Bull. Chem. Soc. Jpn.*, **85**, 265 (2012); https://doi.org/10.1246/bcsj.20110197
196. A.Mallick, P.More, M.M.K.Syed, S.Basu. *ACS Appl. Mater. Interfaces*, **8**, 13218 (2016); https://doi.org/10.1021/acsami.6b00263
197. K.Zhang, J.Fu, X.Liu, Y.Guo, M.Han, M.Liu, X.Wang. *Pharmaceutics*, **15**, 388 (2023); https://doi.org/10.3390/pharmaceutics15020388
198. Z.Xu, X.Chen, Z.Sun, C.Li, B.Jiang. *Mater. Today Chem.*, **12**, 240 (2019); https://doi.org/10.1016/j.mtchem.2019.02.004
199. X.Li, Q.He, J.Shi. *ACS Nano*, **8**, 1309 (2014); https://doi.org/10.1021/nn4046985
200. J.Zhang, Z.-F.Yuan, Y.Wang, W.-H.Chen, G.-F.Luo, S.-X.Cheng, R.-X.Zhuo, X.-Z.Zhang. *J. Am. Chem. Soc.*, **135**, 5068 (2013); https://doi.org/10.1021/ja312004m
201. B.Yang, Y.Chen, J.Shi. *Mater. Sci. Eng. R Rep.*, **137**, 66 (2019); https://doi.org/10.1016/j.mser.2019.01.001
202. P.Yuan, X.Mao, X.Wu, S.S.Liew, L.Li, S.Q.Yao. *Angew. Chem., Int. Ed.*, **58**, 7657 (2019); https://doi.org/10.1002/anie.201901699
203. Q.Qu, X.Ma, Y.Zhao. *Nanoscale*, **7**, 16677 (2015); https://doi.org/10.1039/C5NR05139H
204. A.R.Ibragimova, D.R.Gabdrakhmanov, F.G.Valeeva, L.A.Vasileva, A.S.Sapunova, A.D.Voloshina, A.F.Saifina, A.T.Gubaidullin, M.P.Danilaev, S.R.Egorova, A.A.Tyryshkina, A.A.Lamberov, A.R.Khamatgalimov, G.V.Sibgatullina, D.V.Samigullin, K.A.Petrov, L.Y.Zakharova, O.G.Sinyashin. *Int. J. Pharm.*, **604**, 120776 (2021); https://doi.org/10.1016/j.ijpharm.2021.120776
205. Q.Cai, W.-Y.Lin, F.-S.Xiao, W.-Q.Pang, X.-H.Chen, B.-S.Zou. *Microporous Mesoporous Mater.*, **32**, 1 (1999); https://doi.org/10.1016/S1387-1811(99)00082-7
206. J.Du, N.Xu, J.Fan, W.Sun, X.Peng. *Small*, **15**, 1805087 (2019); https://doi.org/10.1002/smll.201805087
207. Y.Zhang, Y.Shen, X.Teng, M.Yan, H.Bi, P.C.Morais. *ACS Appl. Mater. Interfaces*, **7**, 10201 (2015); https://doi.org/10.1021/acsami.5b00405
208. X.Liang, X.Wang, J.Zhuang, Y.Chen, D.Wang, Y.Li. *Adv. Funct. Mater.*, **16**, 1805 (2006); https://doi.org/10.1002/adfm.200500884
209. Y.Ju-Nam, N.Bricklebank, D.W.Allen, P.H.E.Gardiner, M.E.Light, M.B.Hursthouse. *Org. Biomol. Chem.*, **4**, 4345 (2006); https://doi.org/10.1039/B610480K
210. Y.Ju-Nam, D.W.Allen, P.H.E.Gardiner, N.Bricklebank. *J. Organomet. Chem.*, **693**, 3504 (2008); https://doi.org/10.1016/j.jorganchem.2008.08.009
211. Y.Ju-Nam, Y.S.Chen, J.J.Ojeda, D.W.Allen, N.A.Cross, P.H.Gardiner, N.Bricklebank. *RSC Adv.*, **2**, 10345 (2012); https://doi.org/10.1039/C2RA21421K

212. S.Marrache, S.Dhar. *Chem. Sci.*, **6**, 1832 (2015); https://doi.org/10.1039/C4SC01963F
213. S.Chakrabortty, M.Sison, Y.Wu, A.Ladenburger, G.Pramanik, J.Biskupek, J.Extermann, U.Kaiser, T.Lasser, T.Weil. *Biomater. Sci.*, **5**, 966 (2017); https://doi.org/10.1039/C6BM00951D
214. N.M.Vinita, U.Devan, S.Durgadevi, S.Anitha, D.Prabhu, S.Rajamanikandan, M.Govarthanan, A.Yuvaraj, M.Biruntha, A.A.J.Velanganni, J.Jeyakanthan, P.A.Prakash, M.S.M.Jaabir, P.Kumar. *Sci. Rep.*, **13**, 2230 (2023); https://doi.org/10.1038/s41598-023-28678-x
215. S.Qin, C.Liu, Y.Chen, M.Yao, S.Liao, W.Xin, S.Gong, X.Guan, Y.Li, J.Xiong, J.Chen, Y.Shen, Y.Liu, J.Zhao, Y.Huang. *Kidney Int.*, **103**, 903 (2023); https://doi.org/10.1016/j.kint.2023.01.025
216. X.-Y.Zhang, P.-Y.Zhang. *Oncol. Lett.*, **12**, 4887 (2016); https://doi.org/10.3892/ol.2016.5302
217. X.Wu, S.Sun, Y.Wang, J.Zhu, K.Jiang, Y.Leng, Q.Shu, H. Lin. *Biosens. Bioelectron.*, **90**, 501 (2017); https://doi.org/10.1016/j.bios.2016.10.060
218. K.Jiang, S.Sun, L.Zhang, Y.Lu, A.Wu, C.Cai, H.Lin. *Angew. Chem., Int. Ed.*, **54**, 5360 (2015); https://doi.org/10.1002/anie.201501193
219. A.Kaminari, E.Nikoli, A.Athanasopoulos, E.Sakellis, Z.Sideratou, D.Tsiourvas. *Pharmaceuticals*, **14**, 932 (2021); https://doi.org/10.3390/ph14090932
220. Y.Zou, M.Nishikawa, H.G.Kang, G.Cheng, W.Wang, Y.Wang, N.Komatsu. *Mol. Pharm.*, **18**, 2823 (2021); https://doi.org/10.1021/acs.molpharmaceut.1c00188
221. C.Ren, D.Li, Q.Zhou, X.Hu. *Biomaterials*, **232**, 119752 (2020); https://doi.org/10.1016/j.biomaterials.2019.119752
222. A.Chakraborty, N.R.Jana. *J. Phys. Chem. C*, **119**, 2888 (2015); https://doi.org/10.1021/jp511870e
223. Y.Ye, K.Ren, Y.Dong, L.Yang, D.Zhang, Z.Yuan, N.Ma, Y.Song, X.Huang, H.Qiao. *ACS Appl. Mater. Interfaces*, **15**, 26285 (2023); https://doi.org/10.1021/acsami.3c01559
224. Z.Hua, X.Zhang, Y.Chen, R.Liu, Y.Li, J.Li, D.Liu, M.Tan. *Food Chem.*, **424**, 136439 (2023); https://doi.org/10.1016/j.foodchem.2023.136439
225. Y.Wu, G.Pramanik, K.Eisele, T.Weil. *Biomacromolecules*, **13**, 1890 (2012); https://doi.org/10.1021/bm300418r
226. K.Katagiri, K.Ariga, J.Kikuchi. *Chem. Lett.*, **28**, 661 (1999); https://doi.org/10.1246/cl.1999.661
227. Y.Wang, B.Wang, H.Liao, X.Song, H.Wu, H.Wang, H.Shen, X.Ma, M.Tan. *J. Mater. Chem. B*, **3**, 7291 (2015); https://doi.org/10.1039/C5TB01197C
228. D.-H.Kim, E.A.Rozhkova, I.V.Ulasov, S.D.Bader, T.Rajh, M.S.Lesniak, V.Novosad. *Nat. Mater.*, **9**, 165 (2010); https://doi.org/10.1038/nmat2591
229. Y.Cheng, M.E.Muroski, D.C.M.C.Petit, R.Mansell, T.Vemulkar, R.A.Morshed, Y.Han, I.V.Balyasnikova, C.M.Horbinski, X.Huang, L.Zhang, R.P.Cowburn, M.S.Lesniak. *J. Control. Release*, **223**, 75 (2016); https://doi.org/10.1016/j.jconrel.2015.12.028
230. E.Zhang, M.F.Kircher, M.Koch, L.Eliasson, S.N.Goldberg, E.Renström. *ACS Nano*, **8**, 3192 (2014); https://doi.org/10.1021/nn406302j
231. M.Chen, J.Wu, P.Ning, J.Wang, Z.Ma, L.Huang, G.R.Plaza, Y.Shen, C.Xu, Y.Han, M.S.Lesniak, Z.Liu, Y.Cheng. *Small*, **16**, 1905424 (2020); https://doi.org/10.1002/smll.201905424
232. X.Hu, J.Hu, J.Tian, Z.Ge, G.Zhang, K.Luo, S.Liu. *J. Am. Chem. Soc.*, **135**, 17617 (2013); https://doi.org/10.1021/ja409686x
233. W.Zhang, X.Hu, Q.Shen, D.Xing. *Nat. Commun.*, **10**, 1704 (2019); https://doi.org/10.1038/s41467-019-09566-3
234. W.Zhuang, L.He, K.Wang, B.Ma, L.Ge, Z.Wang, H.Ying. *ACS Omega*, **3**, 2396 (2018); https://doi.org/10.1021/acsomega.7b02022
235. C.Yang, H.Zhang, Z.Wang, X.Wu, Y.Jin. *J. Porphyrins Phthalocyanines*, **23**, 1028 (2019); https://doi.org/10.1142/S1088424619500779
236. S.Wang, F.Guo, Y.Ji, M.Yu, J.Wang, N.Li. *Mol. Pharm.*, **15**, 3318 (2018); https://doi.org/10.1021/acs.molpharmaceut.8b00351
237. M.Sun, D.Yang, C.Wang, H.Bi, Y.Zhou, X.Wang, J.Xu, F.He, S.Gai, P.Yang. *Biomater. Sci.*, **7**, 4769 (2019); https://doi.org/10.1039/C9BM01077G
238. Y.Huang, W.Mo, X.Ding, Y.Ding. *Med. Oncol.*, **40**, 177 (2023); https://doi.org/10.1007/s12032-023-02046-1
239. Y.Pan, S.Zhou, C.Liu, X.Ma, J.Xing, B.Parshad, W.Li, A.Wu, R.Haag. *Adv. Healthc. Mater.*, **11** (8), e2102272 (2022);
240. X.Li, H.Xiao, W.Xiu, K.Yang, Y.Zhang, L.Yuwen, D.Yang, L.Weng, L.Wang. *ACS Appl. Mater. Interfaces*, **13**, 55928 (2021); https://doi.org/10.1021/acsami.1c18311
241. J.Lv, S.Wang, D.Qiao, Y.Lin, S.Hu, M.Li. *J. Nanobiotechnol.*, **20**, 42 (2022); https://jnanobiotechnology.biomedcentral.com/articles/10.1186/s12951-022-01244-9
242. C.Liu, L.Chen, Y.Ma, K.Hu, P.Wu, L.Pan, H.Chen, L.Li, H.Hu, J.Zhang. *Theranostics*, **11**, 8550 (2021); https://doi.org/10.7150/thno.61875
243. X.Gu, T.Shu, W.Deng, C.Shen, Y.Wu. *J. Mater. Chem. B*, **11**, 4539 (2023); https://doi.org/10.1039/D3TB00608E